

Lecture 20 121219

- Il pdf delle lezioni puo' essere scaricato da
- http://www.fisgeo.unipg.it/~fiandrin/didattica_fisica/cosmic_rays1920/

Counting rate

- What is measured in any CR experiment is the counting rate dN_i/dt , not the flux J_i
- Practically, in any experiment, data are collected for a time T during which N_i particles (crossing the detector volume and interacting with its active materials) are identified and counted
- The relationship between dN_i/dt and J_i must be found, i.e. the Instrument Response Function (IRF) must be known

Counting rate

The **coincidence counting rate C** of any particle telescope depends upon the effective dimensions and relative positions, i.e. **the geometry**, of the telescope sensors as well as the **intensity of radiation in the surrounding space and the sensor efficiencies**.

The experimentalist's task is to compute the intensity of radiation given the coincidence counting rate and the parameters (e.g. sensor dimensions) of his telescope. This is the task not only of the space scientist with instruments in an unknown radiation environment but also of the nuclear physicist with his collimated beams.

For an ideal telescope the factor of proportionality relating the counting rate C to the intensity I is defined as the ***gathering power Γ*** of the telescope.

When the intensity is isotropic, i.e., $I = I_0$, the factor of proportionality is called the ***geometrical factor G*** . *That is $C = G I_0$.*

Also called geometrical acceptance.

Detector Response function

The $C(x,t)$ in a time period T in a detector is given by

J.D. Sullivan,
GEOMETRICAL FACTOR AND DIRECTIONAL RESPONSE OF
SINGLE AND MULTI-ELEMENT PARTICLE TELESCOPES,
NUCLEAR INSTRUMENTS AND METHODS 95 (1971) pp. 5-11

$$C(x, t_0) = (1/T) \int_{t_0}^{t_0+T} dt \int_S d\sigma \cdot \hat{r} \int_{\Omega} d\omega \int_0^{\infty} dE \times \\ \times \sum_{\alpha} \varepsilon_{\alpha}(E, \sigma, \omega, t) J_{\alpha}(E, \omega, x, t),$$

where

- C = coincidence counting rate (sec^{-1}),
- α = label for kind of particle,
- J_{α} = spectral intensity of the α th kind of particle ($\text{sec}^{-1} \text{cm}^{-2} \text{sr}^{-1} E^{-1}$),
- ε_{α} = detection efficiency for the α th kind of particle,
- t = time,
- t_0 = time at start of observation,
- T = total observation time,
- $d\sigma$ = element of surface area of the last telescope sensor to be penetrated,
- S = total area of the last telescope sensor,
- $d\omega = d\phi d\cos\theta$ = element of solid angle (θ polar angle, ϕ azimuth),
- Ω = domain of ω , this is limited by the other telescope sensors,
- x = spatial coordinate of the telescope,
- r = unit vector in direction ω , and
- $\hat{r} d\sigma$ = effective element of area looking into ω .

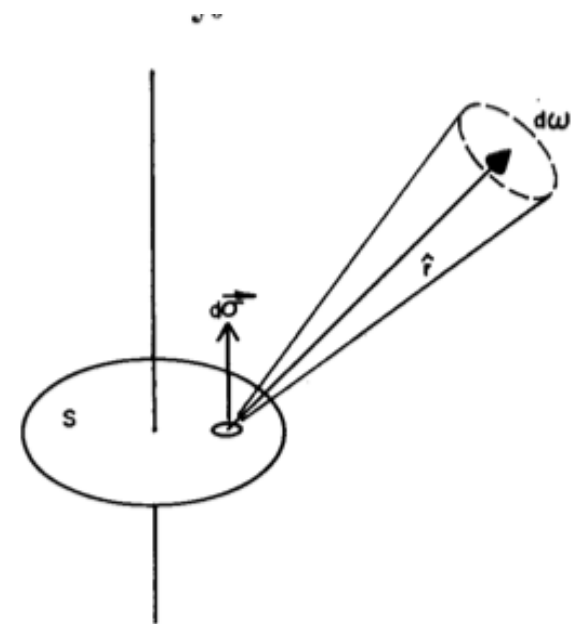


Fig. 1. A telescope with a single plane detector viewing one hemisphere.

article

Semplifichiamo assumendo che:

il flusso incidente sia indipendente da x ,
 fattorizzabile come $J(E, \omega, t) = J_0(E, t)F(\omega)$,
 ci sia una sola specie di particelle $\alpha = 1 \rightarrow$
 il # di particelle con E fra E e $E+dE$ contate nel tempo T e'

$$C(\mathbf{x}, t_0) = (1/T) \int_{t_0}^{t_0+T} dt \int_S d\vec{\sigma} \cdot \hat{\mathbf{r}} \int_{\Omega} d\omega \int_0^{\infty} dE \times \\ \times \sum_{\alpha} \varepsilon_{\alpha}(E, \sigma, \omega, t) J_{\alpha}(E, \omega, \mathbf{x}, t),$$

$$\frac{dN}{dE} = \int_t^{t+T} dt \underbrace{\int_{\Omega} d\omega \int_S d\vec{\sigma} \cdot \hat{\mathbf{r}} F(\omega) \varepsilon(E, t) J_0(E, t)}_{\text{fattore di accettazione geometrica}}$$

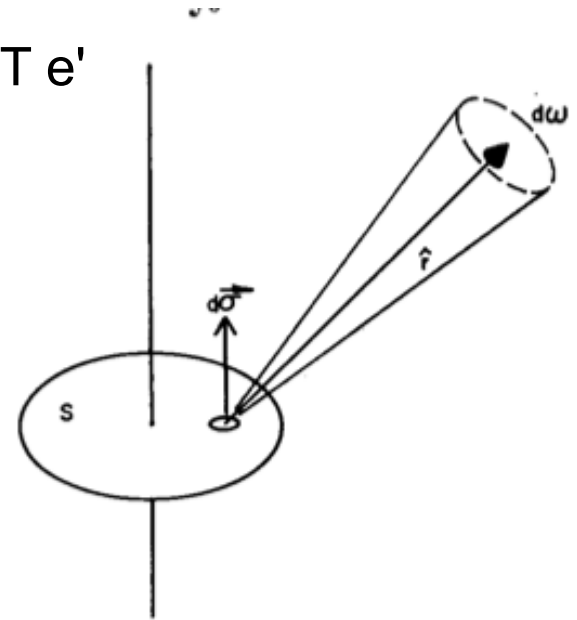
e' il fattore o accettazione geometrica del rivelatore $G(E, t)$ in unita' di area x sr

La funzione di risposta direzionale del rivelatore e' definita da

$$A(\omega, E) = \int_S d\vec{\sigma} \cdot \hat{\mathbf{r}}$$

il term.nell'integrale e' l'area "vista" da una particella che arriva da θ, ϕ

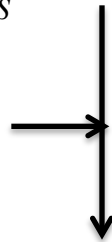
Nel caso di distribuzione isotropa, $F(\omega)d\omega = d\omega/4\pi$



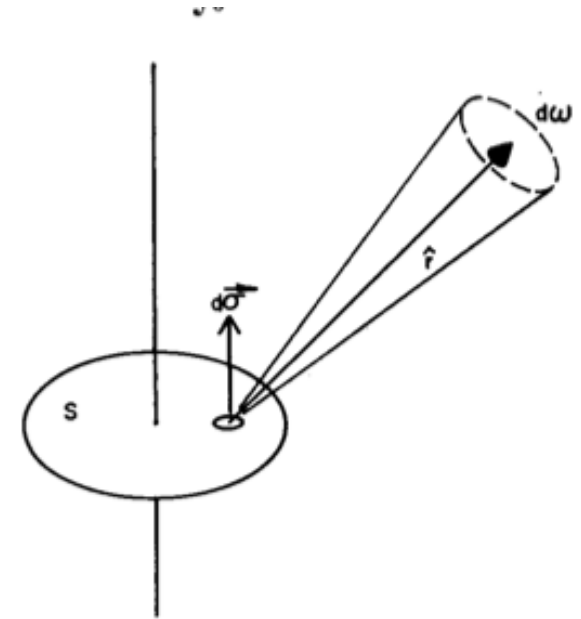
Detector Response function

$$\frac{dN}{dE} = \int_t^{t+T} dt \int_{\Omega} d\omega \int_S d\vec{\sigma} \cdot \hat{r} F(\omega) \varepsilon(E, t) J_o(E, t)$$

$$A(\omega, E) = \int_S d\vec{\sigma} \cdot \hat{r}$$



$$\frac{dN}{dE} = \int_t^{t+T} dt \int_{\Omega} d\omega A(\omega, E) F(\omega) \varepsilon(E, t) J_o(E, t)$$



Nel caso di distribuzione isotropa, $F(\omega)d\omega = d\omega/4\pi$

$$\frac{dN}{dE} = \int_t^{t+T} dt \underbrace{\left[\int_{\Omega} d\omega \frac{A(\omega, E)}{4\pi} \right]}_{=G(E)} \varepsilon(E, t) J_o(E, t)$$

→ nel caso di flusso isotropo l'accettanza dipende solo dalla geometria del rivelatore e dall'energia della particella

Detector Response function

Nel caso semplice di un telescopio a singolo piano di un rivelatore qualsiasi su cui incide un flusso isotropo di particelle e' semplice calcolare i fattori geometrici del rivelatore

$$A(\omega, E) = \int_S d\vec{\sigma} \cdot \hat{r} = \int_S \cos\theta d\sigma = S \cos\theta$$

$$G(E) = \int_{\Omega} A(E, \omega) d\omega = 2\pi S \int_0^1 \cos\theta d\cos\theta = \pi S$$

E' l'accettanza geometrica di un rivelatore a singolo piano: non e' l'area S ma πS perche' "raccoglie" particelle con dir di incidenza fra 0 e $\pi/2$, cioe' con accettanza differenziale $S \cos\theta$

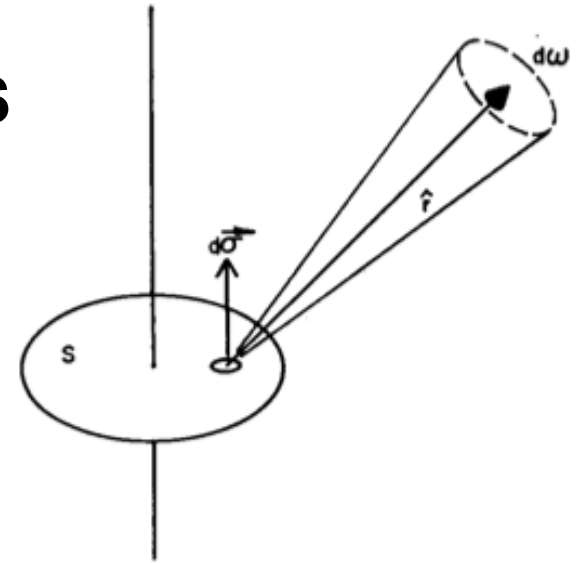
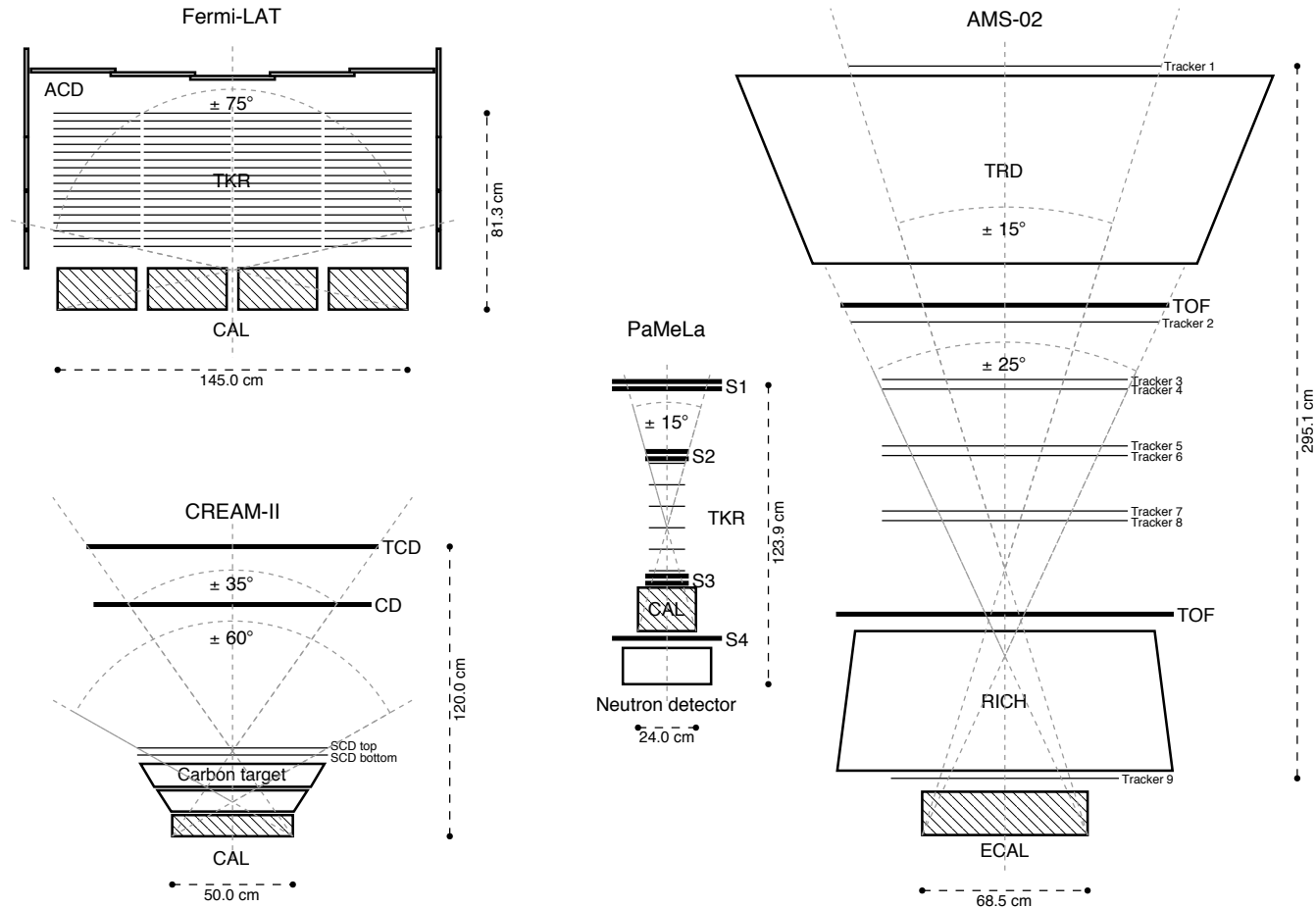


Fig. 1. A telescope with a single plane detector viewing one hemisphere.

Instrument Acceptance

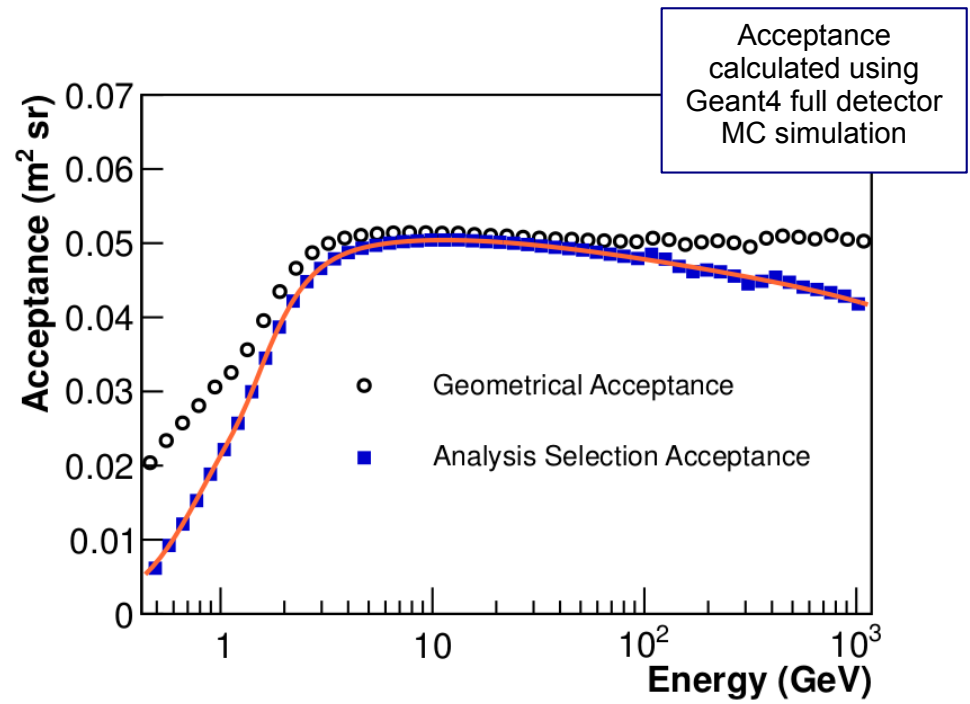
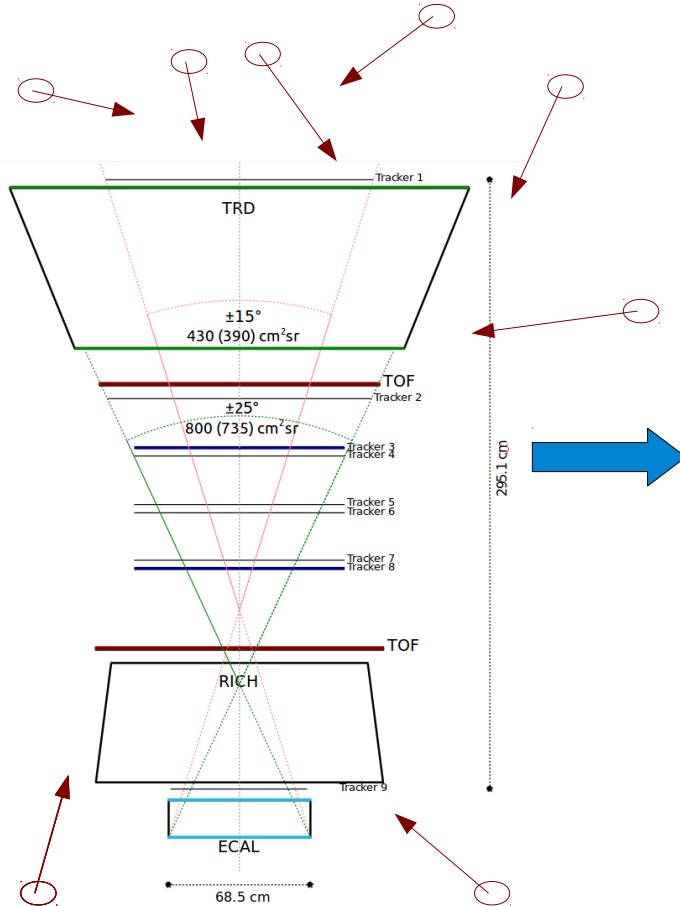
ACCEPTANCE: measurement of the collection capabilities of the detector



The more elongated is the detector, the less solid angle it can accept

Instrument Acceptance

ACCEPTANCE: measurement of the collection capabilities of the detector
Typically measured with MonteCarlo simulations including the detector geometry, materials and interactions with the detector



Effective area and acceptance

Fluxes from (gamma-ray) point sources are customarily measured in particles per unit area, time and energy, e.g. in $\text{m}^{-2} \text{s}^{-1} \text{GeV}^{-1}$. When dealing with a (at least approximately) isotropic flux of charged particles or photons, the intensity of such flux is more conveniently measured in particles per unit area, time, energy and solid angle, e.g. in $\text{m}^{-2} \text{s}^{-1} \text{GeV}^{-1} \text{sr}^{-1}$. In the first case the conversion factor between the differential source flux dF/dE and the differential count spectrum dN/dE measured by the detector (in $\text{s}^{-1} \text{GeV}^{-1}$) is the effective area A_{eff} :

$$\frac{dN}{dE} = A_{\text{eff}} \times \frac{dF}{dE}. \quad (73)$$

In the latter case the conversion factor between the differential intensity dJ/dE and the differential count spectrum dN/dE measured by the detector (again, in $\text{s}^{-1} \text{GeV}^{-1}$) is the acceptance G :

$$\frac{dN}{dE} = G \times \frac{dJ}{dE}.$$

(74) Depending on the context, this very same quantity is also referred to as geometric factor, effective geometric factor, etendue, aperture and geometrical aperture

It goes without saying that the effective area is measured in m^2 and the acceptance in $\text{m}^2 \text{sr}$.

Effective area and acceptance

Equations (73) and (74) are effectively operative definitions of the effective area and acceptance. For the reason stated above, the concept of effective area is seldom used by the cosmic-ray community; on the other hand the acceptance (call it with any of the different names mentioned in the previous paragraph) is relevant for both cosmic-ray and gamma-ray detectors.

We also note, in passing, that typically we use the equations (73) and (74) in the other direction, i.e., we divide the measured count spectrum by the effective area or acceptance to recover the actual flux or intensity.

We shall see that, when the energy redistribution due to the finite detector energy resolution is not negligible, this has profound implications.

The Flux Measurement

Precision knowledge of the detector acceptance, response and resolution, and of the data acquisition in space.

FLUX

$$\Phi(E) = \frac{N}{\Delta E \Delta T Acc \epsilon_{sel} \epsilon_{trig}}$$

Number of cosmic rays collected

Energy/Rigidity (GeV)
size of the bin

Exposure Time (s)
also called "Livetime"

Acceptance (m² sr)
usually calculated using MC sims

Particle selection efficiency
based on the statistical techniques
employed to extract N

Trigger Efficiency

Each factor uncertainty contributes equally to the final measurement.
Systematic uncertainty studies for each factor are fundamental

Effective area and acceptance

The effective area is in general defined for a give energy E and viewing direction. In the following of this section we shall indicate with θ and ϕ the polar and azimuthal angles in instrument coordinates. In broad terms (and in a somewhat arbitrary fashion), the effective area can be factored out in three different pieces:

$$A_{\text{eff}}(E, \theta, \phi) = A_{\text{geo}}(\theta, \phi) \varepsilon_{\text{det}}(E, \theta, \phi) \varepsilon_{\text{sel}}(E, \theta, \phi), \quad (75)$$

where the $A_{\text{geo}}(\theta, \phi)$ is the geometric cross-sectional area presented by the instrument toward a given direction, $\varepsilon_{\text{det}}(E, \theta, \phi)$ is the detection efficiency at a given energy and incidence direction (for gamma-ray detectors this includes the conversion efficiency) and $\varepsilon_{\text{sel}}(E, \theta, \phi)$ is the efficiency of the selection cuts (e.g., for suppressing the backgrounds).

The formal definition of the acceptance is defined as the integral of the effective area over the solid angle

$$G(E) = \int_{\Omega} A_{\text{eff}}(E, \theta, \phi) d\Omega, \quad (77)$$

Acceptance

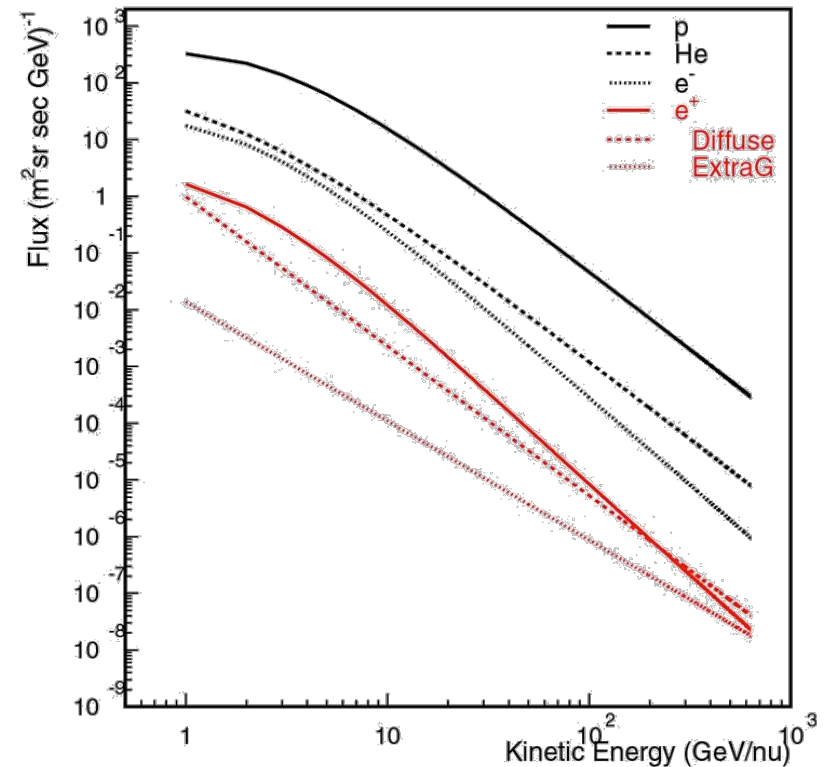
• Exposure factor: $\text{Area} \cdot \Omega \cdot T$
 Counts: $\text{Flux} \cdot \text{Area} \cdot \Omega \cdot T$



Time needed for 10% stat error (sec)
 $\text{Area} \cdot \Omega = 1 \text{ m}^2 \text{sr}$

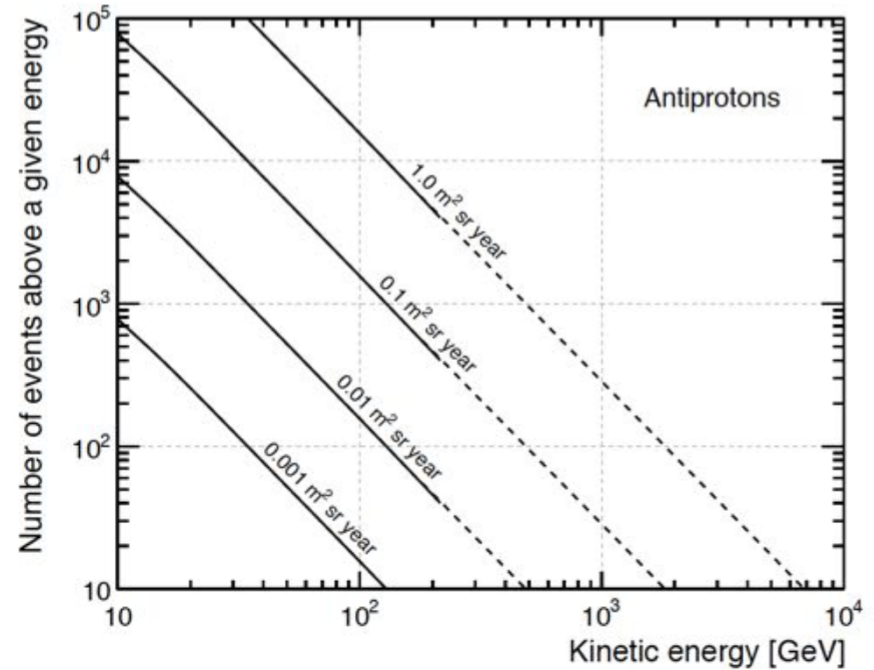
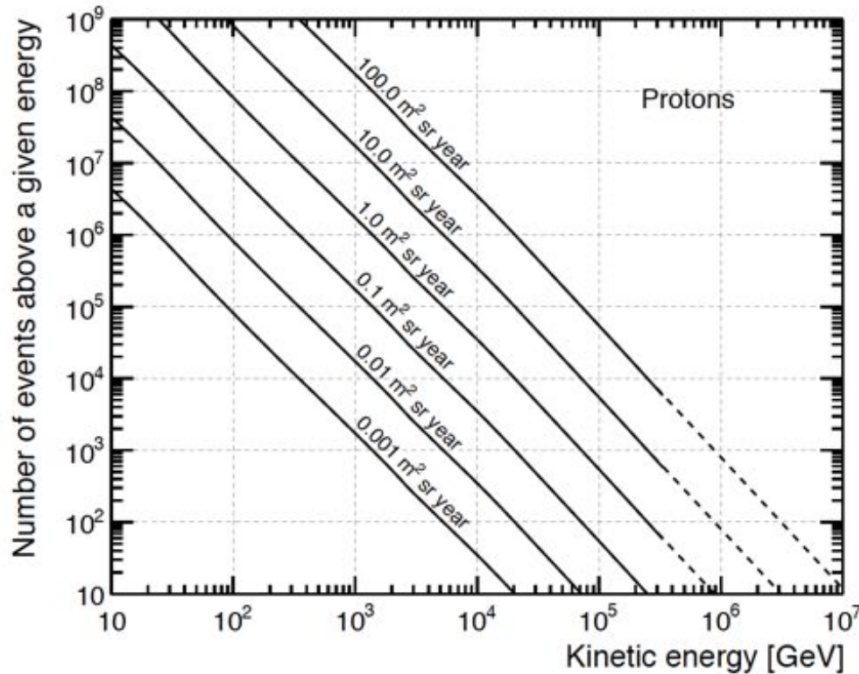
	10GeV	100 GeV	200GeV
p	4	200	700
e ⁻	500	10^5	$5 \cdot 10^5$
p/e ⁺ → factor	$10^4 - 10^5$		

Selection Efficiency assumed 1



Instrument Gathering Power

GATHERING POWER: measurement of the collection capabilities of the mission (it includes the detector lifetime)



- Statistical Error on Flux measurement $\sim 1/\sqrt{N}$
- Maximize Statistics < -- > Minimize statistical uncertainties
- Large acceptances
 - Long duration missions

Energy dispersion

- The energy dispersion $D_E(E; E_{\text{true}})$ is the probability density to measure an energy E for an event with (true) energy E_{true} .
- In general the energy dispersion depends on the incidence direction and impact point of the incoming particle. Unlike the effective area, the energy dispersion is not a scalar, but a probability density function. From an operational standpoint, the energy dispersion is essentially the distribution of the measured energy values for a monochromatic particle beam. It goes without saying that the energy dispersion is in general different for different cosmic-ray species, most notably it is typically much narrower and well-behaved for electrons, positrons and photons than for hadrons.
- The energy resolution $\sigma E / E$ is typically defined as the half width of the smallest energy window containing 68% of the energy dispersion, divided by the most probable value of the energy dispersion itself. Difficult as it might seem, this definition reduces to the ratio σ/μ in the gaussian case. At any given energy the energy resolution is a scalar and it is the figure of merit which is customarily used to summarize the information contained in the energy dispersion.

Energy dispersion

- When measuring particle spectra binned in energy, the energy dispersion originates the phenomenon of the event migration, or bin-to-bin migration—namely the fact that events that would really belong to a given energy bin are assigned to a different (hopefully neighbor) bin.
- Strictly speaking, this implies that our operational definitions of the effective area and acceptance, equations (73) and (74), no longer hold: one cannot divide the count spectrum by the effective area or the acceptance to recover the actual source flux or intensity. Whether the effect is negligible or not really depends on the measurement setup, i.e., the details of the energy dispersion and the input spectrum. The effect is sketched in figure 59.

Energy dispersion

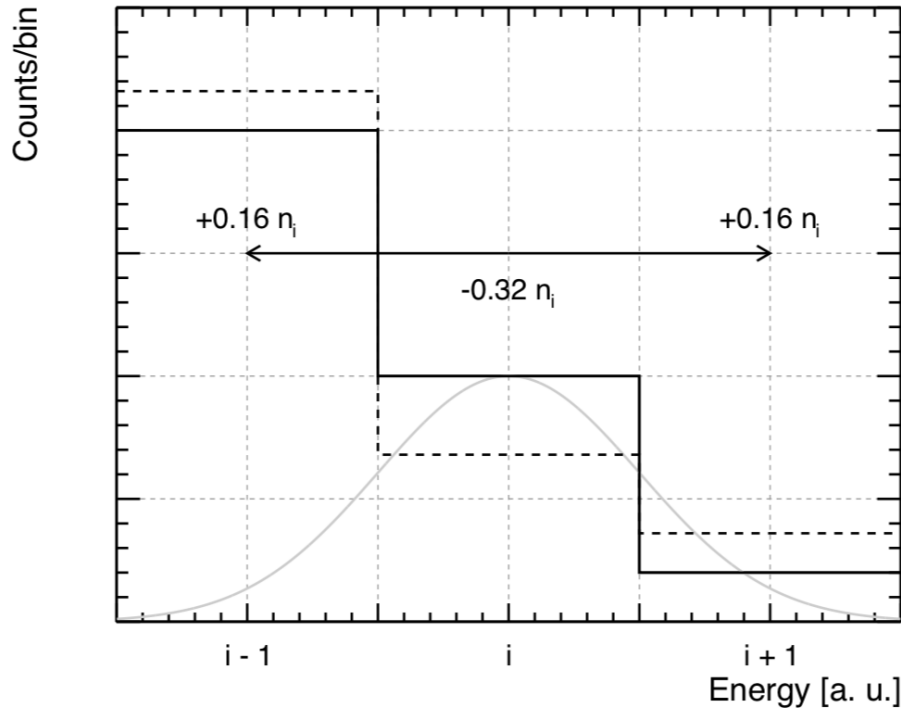


FIG. 59: Graphical illustration of the energy redistribution, or bin-to-bin migration. In this case the bin width is equal to the energy resolution and the gray gaussian illustrates the energy dispersion at the center of the i -th bin.

We note that, when measuring steeply falling spectra such as the typical cosmic-ray spectra, a prominent right tail in the energy dispersion is potentially more dangerous than a long left tail, as even a fractionally small spillover from a low-energy bin can be significant in the next energy bins, where the number of counts is much smaller.

Energy dispersion

Interestingly enough, a constant energy resolution $\sigma E/E$ (i.e., an energy dispersion whose width increases linearly with the energy), when convoluted with a power-law count spectrum with index Γ , causes an offset constant in energy, as illustrated with a toy Monte Carlo simulation in figure 60.

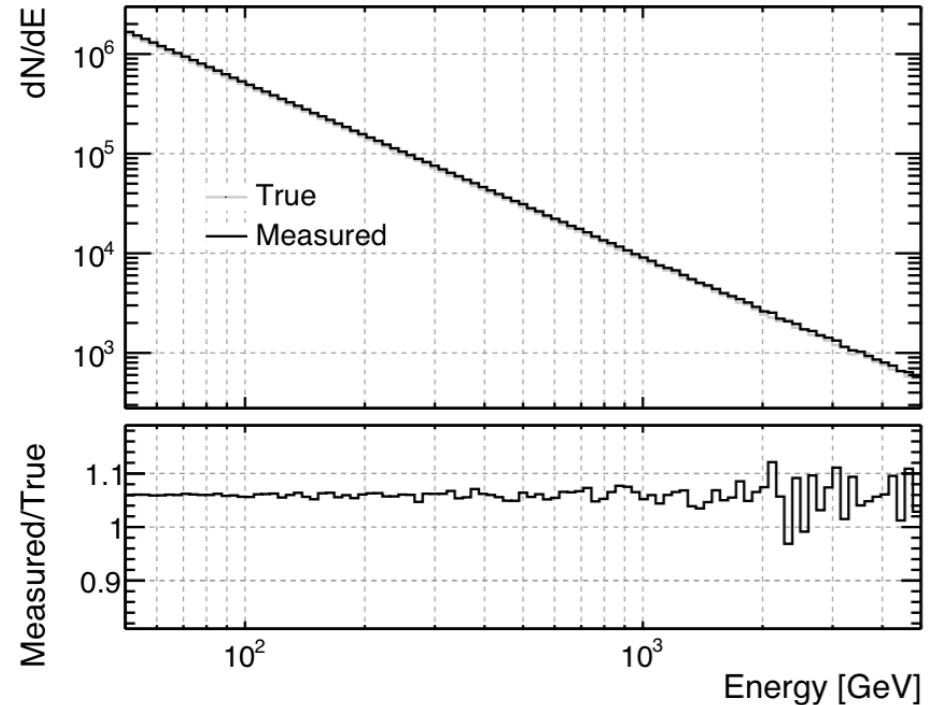


FIG. 60: Toy Monte Carlo simulation of an energy spectrum proportional to $E^{-2.75}$, measured with an energy resolution of 30% (constant in energy and with a gaussian energy dispersion). The setup is largely simplistic, but not totally unreasonable as an illustration of a typical measurement of the primary CR proton spectrum. The net effect, of the order of $\sim 6\%$, is something that must be taken into account for systematic-limited measurements.

Energy dispersion

$$\frac{dN}{dE} = \int_{-\infty}^{\infty} \frac{dN}{d\epsilon} D_E(E; \epsilon) d\epsilon = \int_{-\infty}^{\infty} N_0 \epsilon^{-\Gamma} D_E(E; \epsilon) d\epsilon$$

and, while this can be quite complicated to solve in the general case, there is a few things that can be inferred in a model-independent fashion. As the normalization factor of the energy dispersion is inversely proportional to the energy resolution (the normalization factor being, e.g., $1/\sqrt{2\pi}$ in the gaussian case), we can rewrite the convolution

$$\begin{aligned} \frac{dN}{dE} &= \int_{-\infty}^{\infty} \frac{N_0}{(\sigma_E/E)\epsilon} \epsilon^{-\Gamma} w(E; \epsilon) d\epsilon = \\ &\frac{N_0}{(\sigma_E/E)} \int_{-\infty}^{\infty} \epsilon^{-(\Gamma+1)} w(E; \epsilon) d\epsilon, \end{aligned}$$

where $w(E; \epsilon)$ is a window function which is equal to 1 for $E = \epsilon$ and effectively limits the integral to a region $\sim 2k\sigma_E$ wide around E , k being a numerical factor of the order of 1. If we let $s = k\sigma_E/E$, we can rewrite the convolution as

$$\begin{aligned} \frac{dN}{dE} &\propto \frac{N_0}{(\sigma_E/E)} \int_{E(1-s)}^{E(1+s)} \epsilon^{-(\Gamma+1)} d\epsilon = \\ &\frac{N_0 E^{-\Gamma}}{(\sigma_E/E)\Gamma} [(1-s)^{-\Gamma} - (1+s)^{-\Gamma}] \end{aligned}$$

(note that the dependence on E , as anticipated, disappeared). Now, the expression in square brackets can be expanded—and you need to go all the way up to the third order if you want to get the first non-vanishing correction—giving

$$r - 1 \approx \frac{k^2(\Gamma - 1)(\Gamma - 2)}{3} \left(\frac{\sigma_E}{E} \right)^2,$$

which contains the relevant dependencies on Γ and σ_E/E . Particularly, we note that the offset scales with the square of the energy resolution and that it is identically 0 for $\Gamma = 2$ (interestingly enough, this is a typical spectral index for gamma-ray sources). We also note that the offset is always positive for $\Gamma > 2$, which has to do with the fact that, with a steep enough spectrum, the effect of the right tail of the energy dispersion dominates over that of the left tail.

Energy dispersion

- We conclude noting that, when coupling an energy-dependent acceptance to the (energy dependent) energy dispersion, one can potentially get all kinds of spectral distortion even in the case of a plain power-law input spectrum. In general the problem must really be studied on a case-by-case basis.

Absolute energy scale

- The uncertainty in the absolute energy scale (i.e. in the most probable value of the energy dispersion) is another source of potential spectral deformation. Verifying the absolute energy scale in orbit is a non trivial task, as there isn't very many spectral features (at known position) available.
- The energy scale is typically calibrated on the ground with particle beams up to the highest available beam energies, but then extrapolating the response at (possibly much) higher energies is a challenge in many contexts.
- It is easy enough to show that, in the case of power-law count spectrum and a constant fractional error s_E on the energy scale—e.g., the measured energy is systematically higher or lower than the true energy by a factor $(1 + s_E)$ on average—the net effect is again a fractional offset constant in energy, similar to that induced by a finite energy resolution. In this case the ratio r between the count spectra dN/dE in measured and true energy is given by the combination of two effects: the numerator dN increases (or decreases, if s_E is negative) by a factor $(1 + s_E)^\Gamma$, and the denominator increases (or decreases) by a factor $(1 + s_E)$:

$$r = \frac{(1 + s_E)^\Gamma}{(1 + s_E)} = (1 + s_E)^{\Gamma-1} \approx 1 + (\Gamma - 1)s_E,$$

or

$$r - 1 \approx (\Gamma - 1)s_E. \quad (90)$$

Absolute energy scale

- For $\Gamma = 3$, for instance, an error of the absolute energy scale of 5% implies a corresponding error on the flux measurement of 10%.
- As for the case of a finite energy resolution, we conclude noting that an energy-dependent error on the absolute energy scale (or a constant error coupled to a curved input spectrum) do cause spectral deformations that need to be studied case by case.

Correcting for the energy dispersion

- if the effect of the energy dispersion cannot be ignored, equations (73) and (74) cannot be used, as they relate the source flux to the observed counts—through the effective area or the acceptance—all evaluated at the true event energy. In general, events with true energy E will contribute instead to the counts measured at a different energy E' due to the energy redistribution. If we are doing a binned analysis, the count rate in the i -th (measured) energy bin will be a sum of contributions from the source flux in several (true) energy bins:

$$n_i = C_{ij} F_j. \quad (91)$$

- C_{ij} is customarily called the detector response matrix (DRM). If n_i is measured in s^{-1} , or counts per second, and F_j in $\text{m}^{-2} \text{s}^{-1}$, the detector response matrix has the physical dimensions of an area—and it is in fact a generalization of the effective area.
- If the detector response matrix is diagonal, we are effectively back to the original discussion.

Correcting for the energy dispersion

- It goes without saying that one is typically interested in using equation (91) in the opposite direction, i.e., to recover the actual source flux from the measured counts. The reader might be tempted to say that the problem is trivially invertible by doing

$$F_i = (C_{ij})^{-1} n_j. \quad (92)$$

An effective way to understand that this is actually a terrible idea is a simple and amusing argument by Barlow. Assume that we have two energy bins and the detector response matrix reads, in some units:

$$C = \begin{pmatrix} 0.6 & 0.4 \\ 0.4 & 0.6 \end{pmatrix}.$$

The reader can verify directly that the inverse matrix reads

$$C^{-1} = \begin{pmatrix} 3 & -2 \\ -2 & 3 \end{pmatrix}.$$

Correcting for the energy dispersion

- If we measure $n = (10, 10)$, equation (92) gives a flux estimate of $F = (10, 10)$ —fair enough. But if we do measure $(13, 7)$, which is within a mild statistical fluctuation from the previous pair, we get $(25, -5)$, i.e. a nonsense. In some sense the answer is right: $(25, -5)$, folded with our DRM, gives indeed $(13, 7)$. But it's an answer with little or no physical meaning.
- As it turns out, unfolding is a thoughtfully studied problem and algorithms exist that can do a decent job under many different conditions.

Detector response function

- La risposta in energia dice qual'è la probabilità che una particella con energia “vera” E sia misurata con energia E_{mis} , $R(E_{\text{mis}}, E)$
- Entra nella determinazione del rate
$$\frac{dN(E_{\text{mis}})}{dt dE_{\text{mis}}} = \int dE' G(E', t) \varepsilon_{\text{eve}}(E', t) \varepsilon_{\text{sel}}(E', t) R(E_{\text{mis}}, E') J_0(E', t)$$
occorre invertire l'equazione per ottenere $J_0(E, t)$
 G, ε, R sono in genere ottenute dai dati e da simulazioni MC

The role of the event selection

In the context of pretty much any scientific analysis one has to deal with the problem of separating the signal (e.g., the particular CR species under study) from the background (e.g., all the other species, possibly much more abundant, that might mimic, in a way or another, the signal we are interested in). We shall refer to the entire process of isolating the signal from the background as the event selection.

In general the instrument response functions are not intrinsic characteristics of the detector: they always subtend a specific event selection and a detector may very well have different response functions in the context of different analyses.

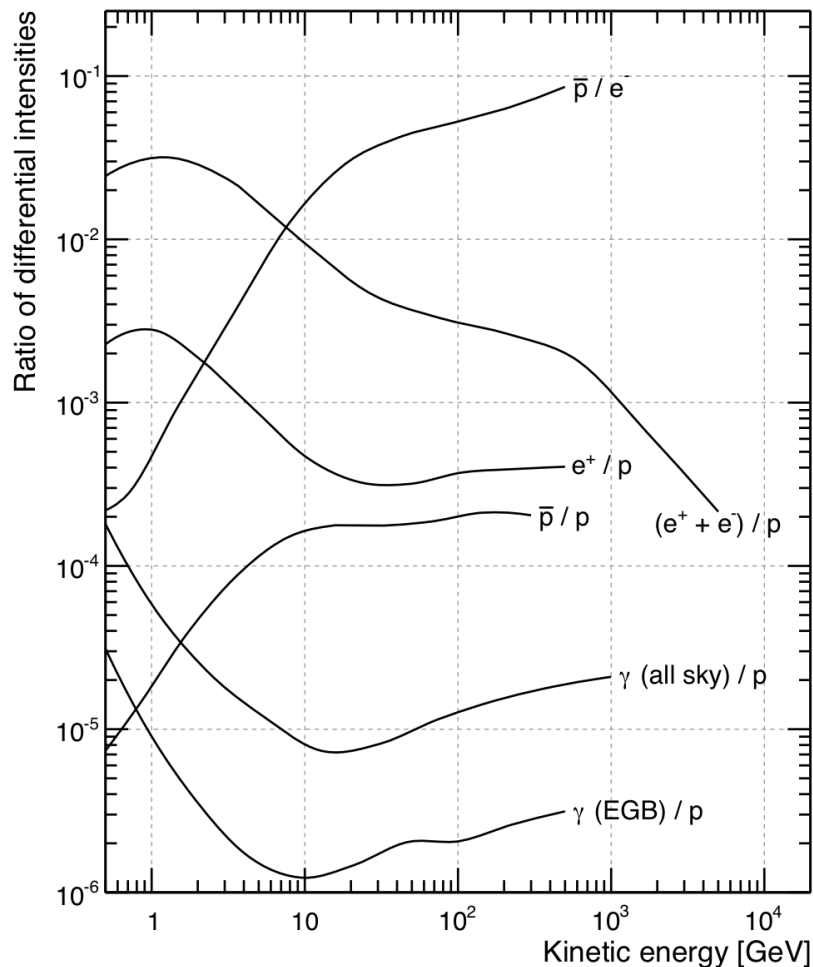


FIG. 50: Ratio of the differential fluxes, as a function of the energy, for some specific pairs of cosmic-ray species.

If one is interested in measuring, say, the all-electron ($e^+ + e^-$) spectrum by means of a calorimetric experiment, the main challenge from the standpoint of the background rejection, is the much larger ($10^2 - 10^4$) proton flux. The all-electron spectrum being significantly steeper ($\Gamma_e \sim 3.1$) than the proton spectrum ($\Gamma_p \sim 2.75$), the electron-to-proton ratio decreases with energy—and, due to the cutoff measured by H.E.S.S., steepens significantly past ~ 1 TeV. This implies that the detector must feature a proton rejection power of at least 10^5 in order to have a relatively small background that can be safely subtracted in the data analysis phase. Different how the event topologies for electrons and protons are, this is really saying that we are only allowed to mis-tag one proton in 100.000 (while keeping a reasonable electron efficiency), which is obviously a non trivial task.

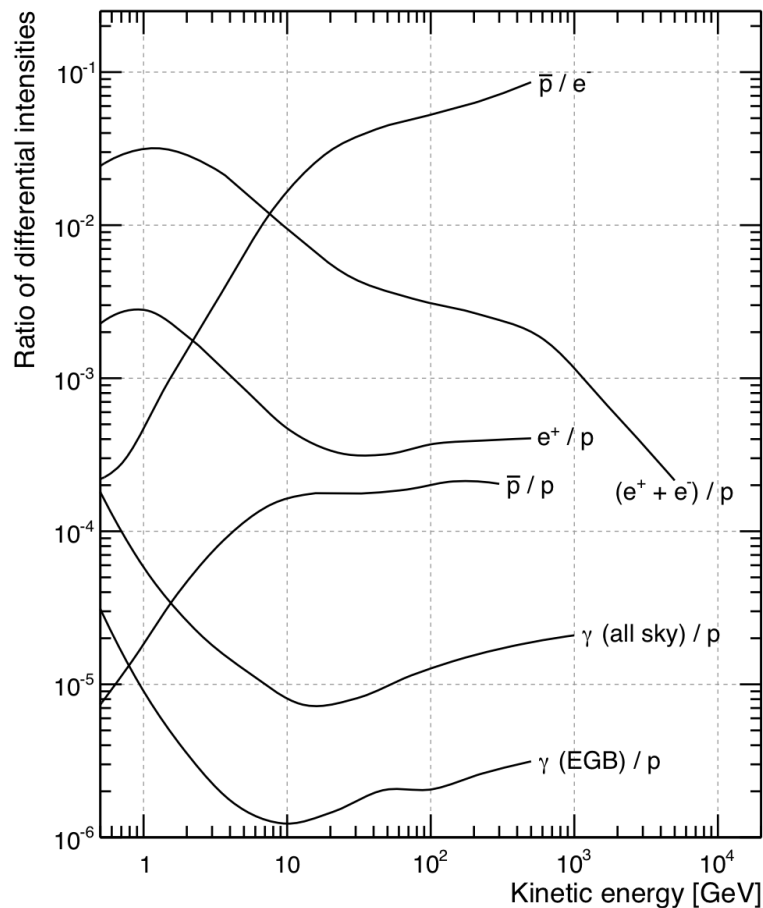


FIG. 50: Ratio of the differential fluxes, as a function of the energy, for some specific pairs of cosmic-ray species.

Life is even harder for gamma rays, as they are substantially less abundant than any of the four singly-charged CR species. Figure 50 shows that for any celestial gamma ray there are 10^4 – 10^5 protons of the same energy. Photons pointing back to their sources, this does not necessarily implies that any gamma-ray analysis is intrinsically more difficult than, say, the measurement of the positron fraction—when studying a gamma-ray source, restricting the sample to a small region of interest around the source itself can allow to reduce the back-ground by orders of magnitude. Nonetheless, the measurement of the faint isotropic extra-galactic gamma-ray background is a good example where a proton rejection factor of the order of 10^6 is really required (and, to this respect, it is fortunate that plastic scintillators can be used to assemble efficient anti-coincidence shields to isolate neutral particles).

We should also emphasize that, while much less abundant than protons, high-energy electrons and positrons generally look more similar to photons in calorimetric experiments (they all produce electromagnetic showers), and can therefore constitute an important source of background for gamma rays.

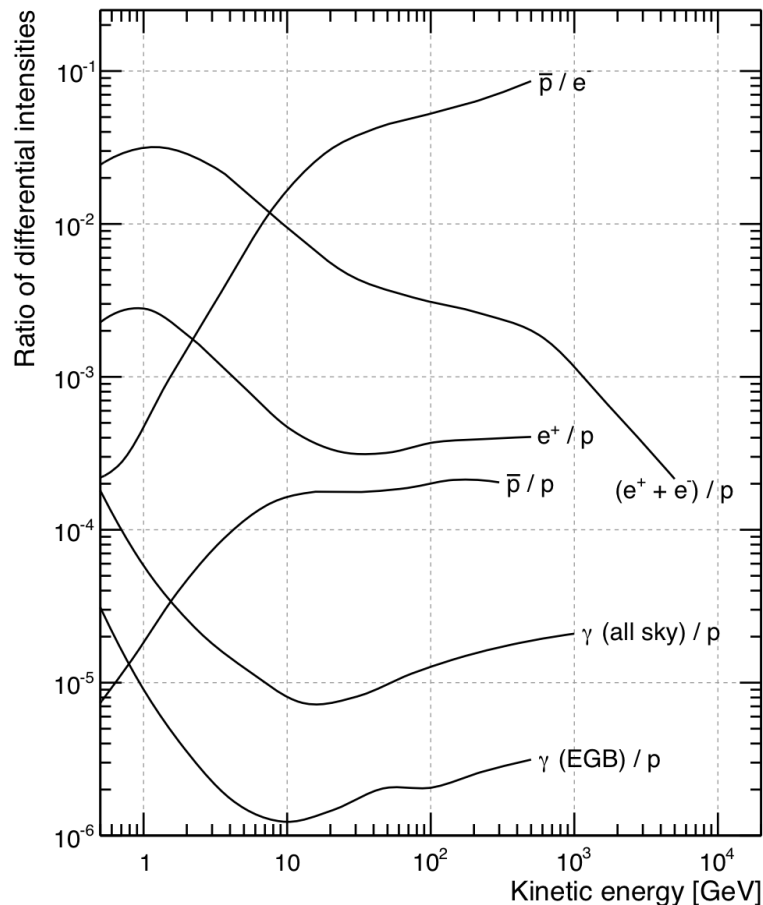


FIG. 50: Ratio of the differential fluxes, as a function of the energy, for some specific pairs of cosmic-ray species.

For magnetic spectrometers most of the curves in figure 50 are actually important. At low energy, where charge confusion is negligible, the relevant figures are the \bar{p}/e -ratio for the measurement of the antiproton fraction and e^+/p ratio for that of the positron fraction.

At high energy, on the other hand, where charge confusion is the main limiting factor, the important figures are the e^+/e^- and \bar{p}/p ratios—and in this regime antiprotons are relatively harder to separate.

At this point it should be clear, however, that different science analyses, in general, require different levels of rejection power—and hence different event selections and different response functions.

Discriminating variables and rejection power

The binary problem of separating signal and back- ground in a given event sample is very common in high- energy physics. This is generally achieved by exploiting one or more discriminating variables, i.e. topological properties of the event that are different, on average, for signal and background.

The transverse size of the shower in an electromagnetic calorimeter is a prototypical example of a discriminating variables that is useful for separating hadrons from electrons or gamma rays. Other examples include: the signal in a transition radiation detector or in a Cherenkov counter, the average dE/dx in the layers of a tracking detectors, the pulse height in a scintillator and many others. When a high level of purity is required, it is customary to use many different variables, possibly combining them by means of multivariate classification techniques such as Fisher discriminants, classification trees, boosted decision trees and others.

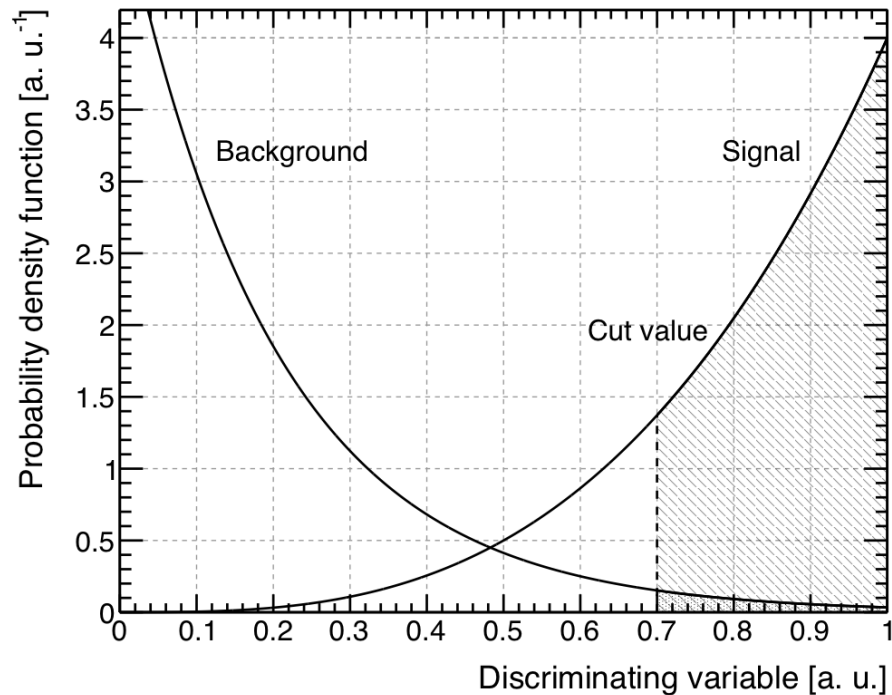


FIG. 51: Illustrative probability density functions, for signal and background, of a generic discriminating variable (note that the shape of the curves, though not necessarily unrealistic, is purely fictional).

Figure 51 shows an example of the probability density functions, for signal and background, of a fictional discriminating variable x in the interval $[0, 1]$ that we shall use for illustrative purposes. A cut on the discriminating variable (e.g., the act of selecting events for which, say, $x > x_0$) defines the values of the efficiency for signal and background:

$$\begin{aligned}\varepsilon_{\text{sig}} &= \int_{x_0}^1 p_{\text{sig}}(x) dx \\ \varepsilon_{\text{bkg}} &= \int_{x_0}^1 p_{\text{bkg}}(x) dx.\end{aligned}\tag{70}$$

(At this point you want to be sure that $\varepsilon_{\text{sig}} > \varepsilon_{\text{bkg}}$, and possibly $\varepsilon_{\text{sig}} \gg \varepsilon_{\text{bkg}}$; otherwise you should probably look for a better discriminating variable.)

Given a selection cut (or a set of selection cuts), the rejection power R is formally defined as

$$\mathcal{R} = \frac{\varepsilon_{\text{sig}}}{\varepsilon_{\text{bkg}}}.$$

The rejection power is a useful concept as it relates the number of signal and background events before and after the cut

$$\left. \frac{n_{\text{sig}}}{n_{\text{bkg}}} \right|_{\text{after}} = \mathcal{R} \left. \frac{n_{\text{sig}}}{n_{\text{bkg}}} \right|_{\text{before}}.$$

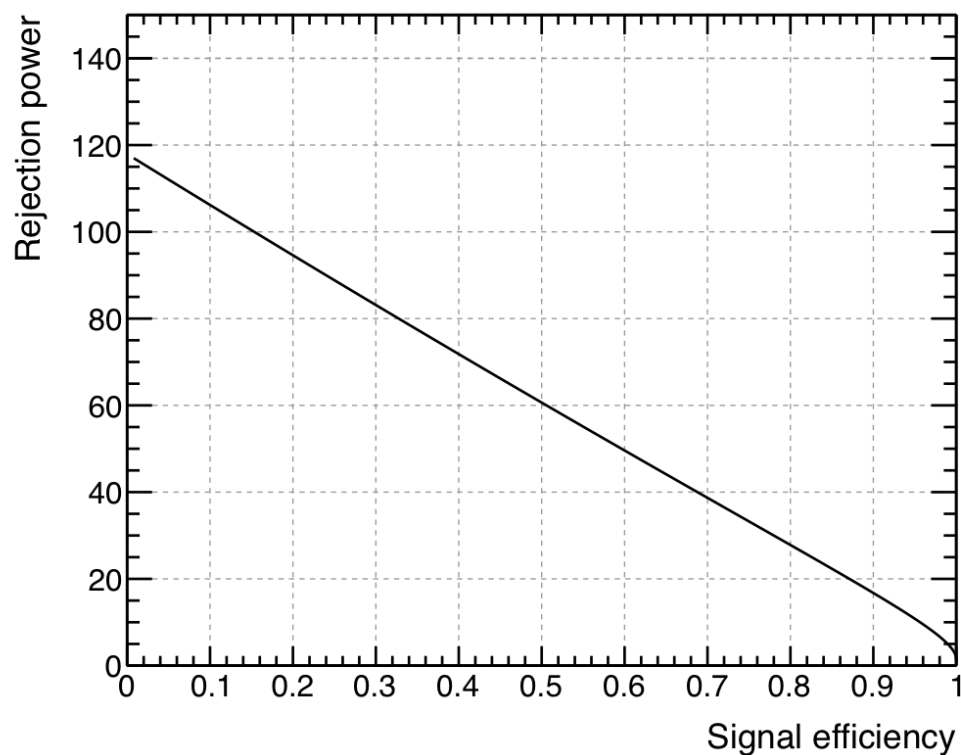


FIG. 52: Illustrative trade-off between the signal efficiency and the rejection power. The plot refer to the probability density functions shown in figure 51.

In order to be able to do a meaningful background subtraction, one typically wants the number of signal events to be much larger than the number of background events in the final sample, which sets the necessary rejection power necessary for a given analysis, once the initial ratio is known (again, see figure 50). It is worth stressing that whether it is practically possible to achieve the necessary rejection power is hostage of the shape of the probability density functions of the discriminating variables. In real life the optimal cut value is determined by a trade off between the signal efficiency and the rejection power, as illustrated in figure 52.

Trigger efficiency

- A trigger is an electronic signal indicating the occurrence of a desired correlation spatial and temporal in the detector signals.
- The desired correlation is determined by examining the physical processes of interest in order to find a characteristic signature that distinguishes it from other processes that will occur simultaneously.
- Needed to select interesting events from background and reduce the data to be saved on disk for offline analysis

Experimental Constraints

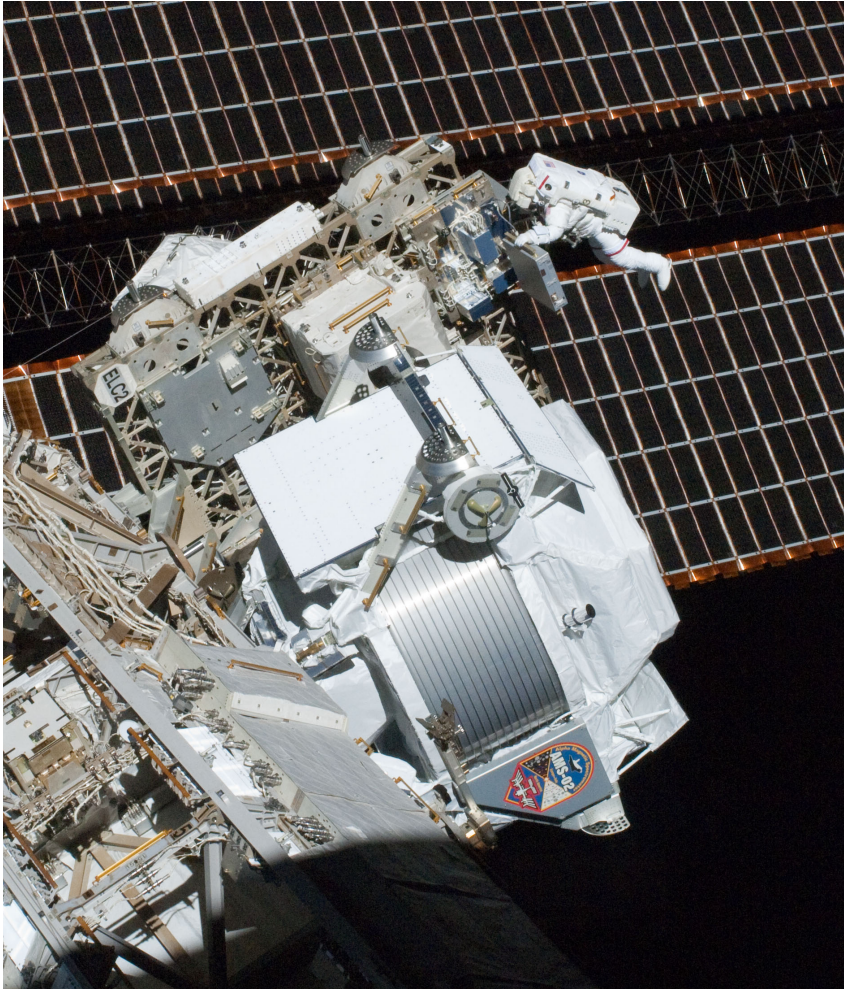
Different experiments have very different trigger requirements due to operating environments

- Timing structure of beam
- Rate of producing physics signals of interest
- Rate of producing backgrounds
- **Cosmic Ray Expts** – no periodic timing structure, background/calibration source for many other experiments.
- Fixed Target Expts – close spacing between bunches in train which comes at low rep rate (\sim Hz)
 - Backgrounds from un-desirable spray from target
 - Cosmics are particularly a background for neutrino beams
- **e+e- collider** – very close bunch spacing (few nsec), beam gas and beam wall collisions
- **ep collider** – short bunch spacing (96ns), beam gas backgrounds
- **pp/ppbar collider** – modest bunch spacing (25-400ns), low produced soft QCD

Example

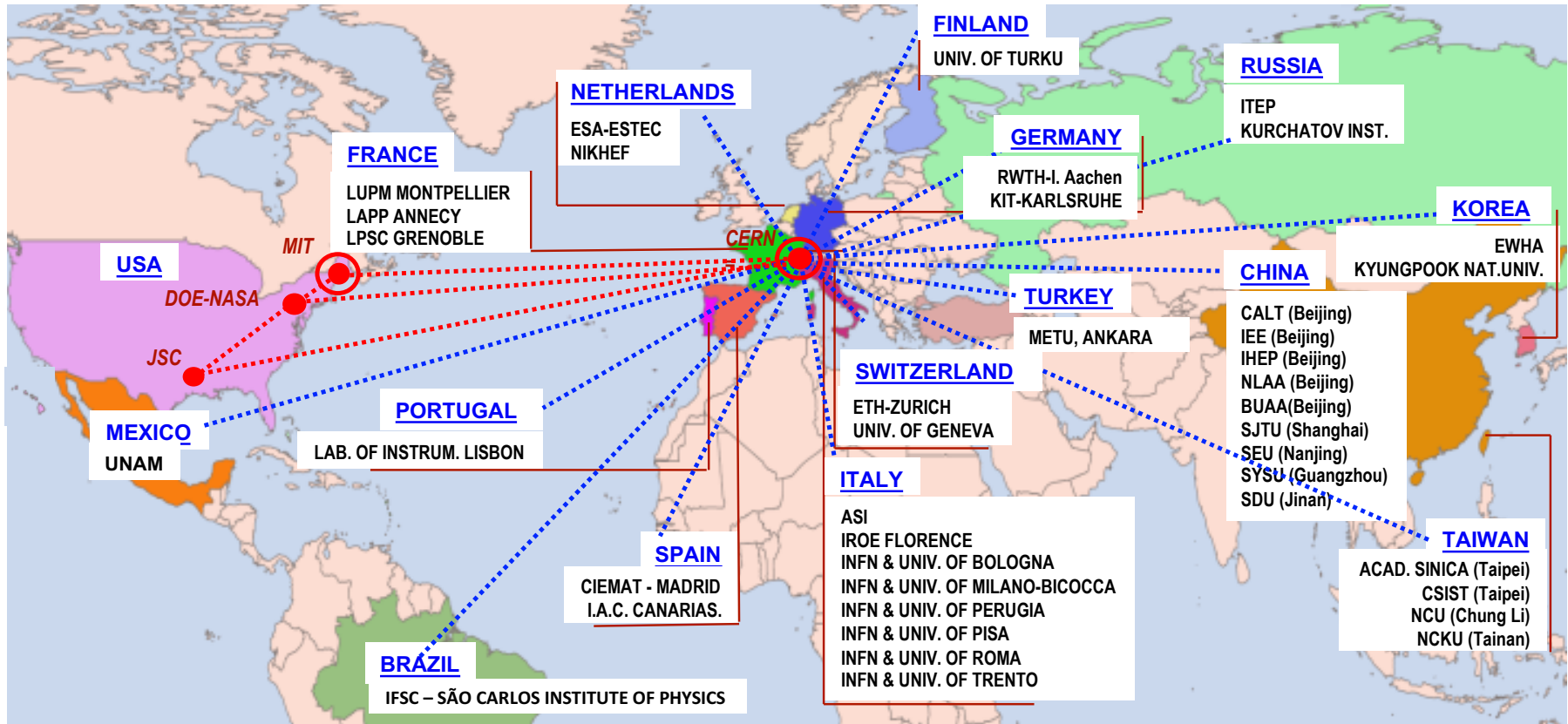
- The main purpose of the trigger logic is to take a fast and efficient decision whether a particle crossing the detector has the potential to be well measured by the various sub-detectors or not.
- If a particle is missed by the trigger is lost for ever
- The decision is tuned to the particle properties, such as its type (photon, lepton, hadron), its charge, potentially its energy and, to some extent, its trajectory through the detector (for example, if the particle is in the acceptance of a specific tracker configuration or not) → Different types of trigger (“Levels”)
- As an example, the AMS trigger uses the combined information coming from the ToF, ACC and ECAL sub-detectors, which are analyzed inside a dedicated electronics board, the JLV1 .
- The processing of all the different signals takes about 1 μ s which represents a significant contribution to the dead time of the experiment. This is the time while the detector is in a busy state and cannot detect new particles. In order to minimize this dead time, a complex decision tree architecture is adopted with three different stages : the Fast, Level1 and Level3 trigger logics.
- Only if the conditions of the previous stage are met can the next level be considered. At present, only the Fast and Level 1 Trigger are used for the data acquisition.

The AMS-02 detector

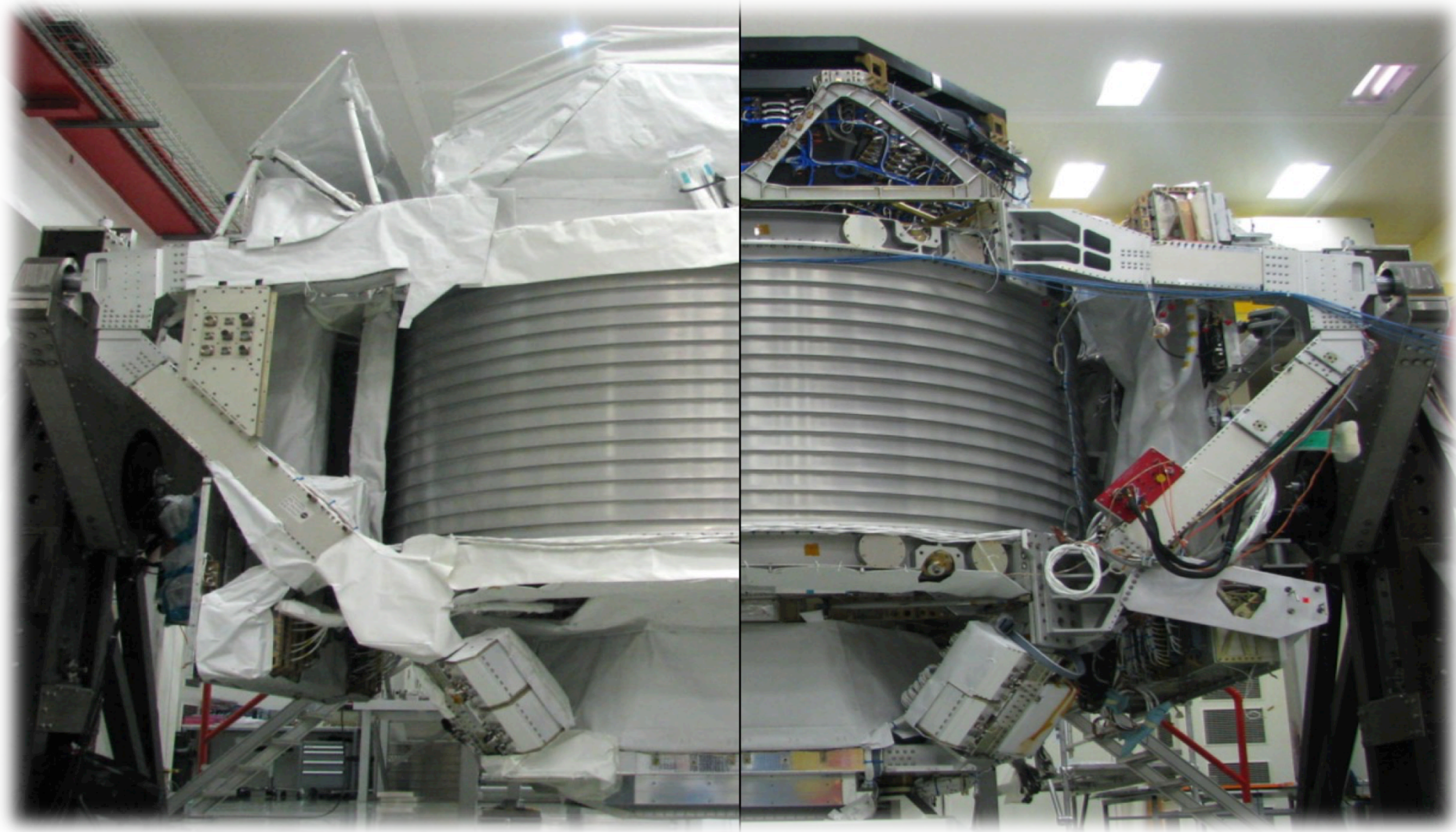


- **Size** 5 x 4 x 4 m, 7500 kg
 - **Power** 2500 W
- **Data Readout** 300,000 channels
- **<Data Downlink>** ~ 12 Mbps
- **Magnetic Field** 0.14 T
- **Mission duration** until the end of the ISS operations (currently 2024)

The AMS-02 Collaboration



The AMS-02 detector



The AMS-02 detector

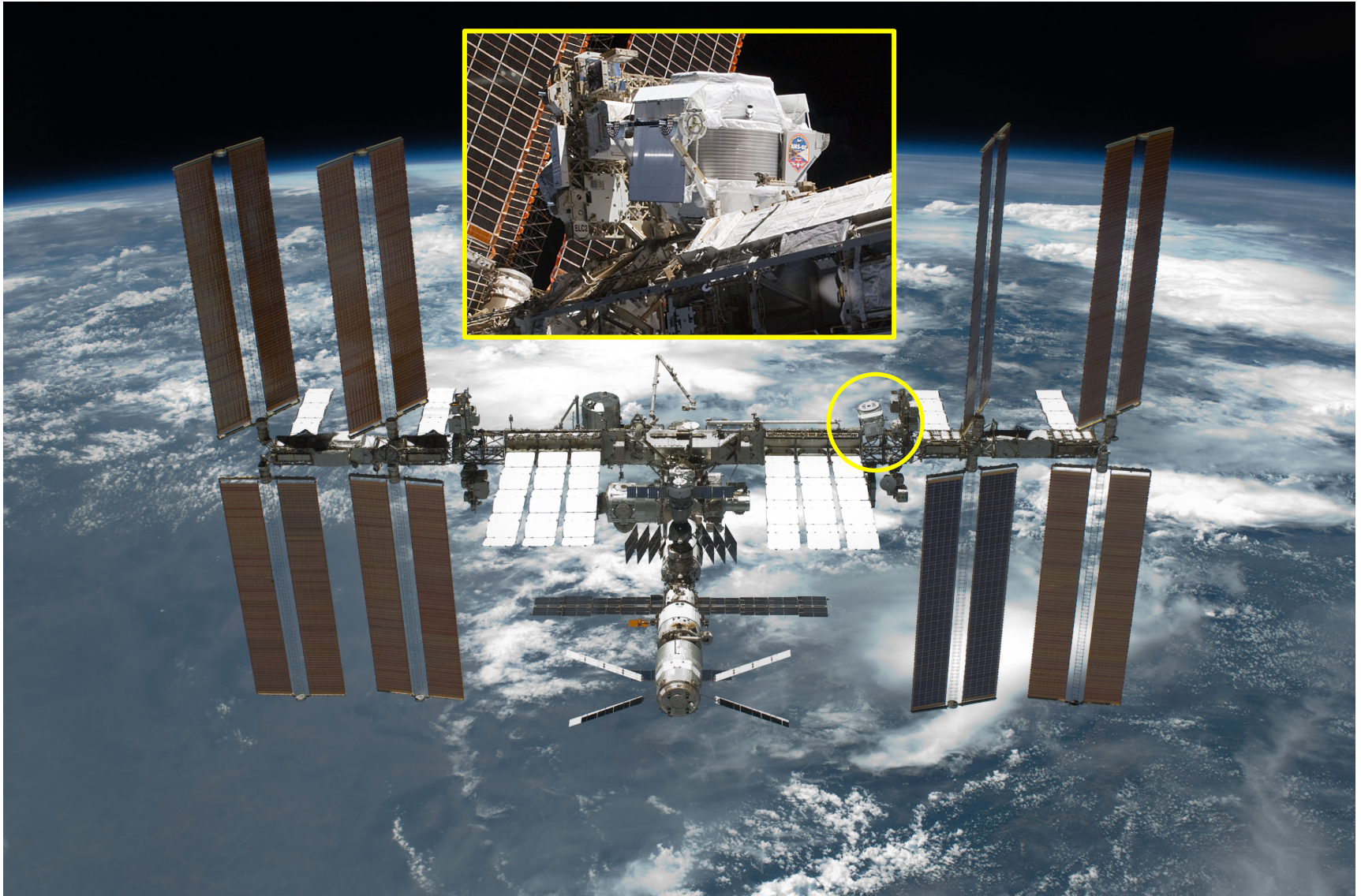


© Michele Famiglietti / AMS Collaboration

The AMS-02 detector



AMS-02 on the ISS



AMS-02 Physics

FUNDAMENTAL PHYSICS

- Indirect search for Dark Matter (e^+ , anti-p,....)
- Search for primordial antimatter (anti-He)

COSMIC RAY COMPOSITION AND ENERGETICS

- Precise measurement of the energy spectra of H, He, Li, B, C to provide information on CR interactions and propagation in the galactic environment

TO ACHIEVE THIS.....

Particle identification and Energy measurement up to TeVs

- Matter/antimatter separation using magnetic field
- e/p separation using independent subdetectors

Maximize the data sample

- Detector size (acceptance)
- Exposure time: ISS in space

AMS: TeV precision spectrometer

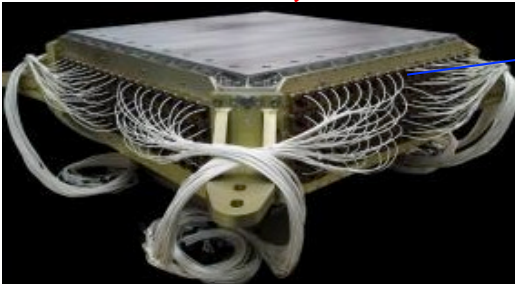
TRD
Identifies e^+ , e^-



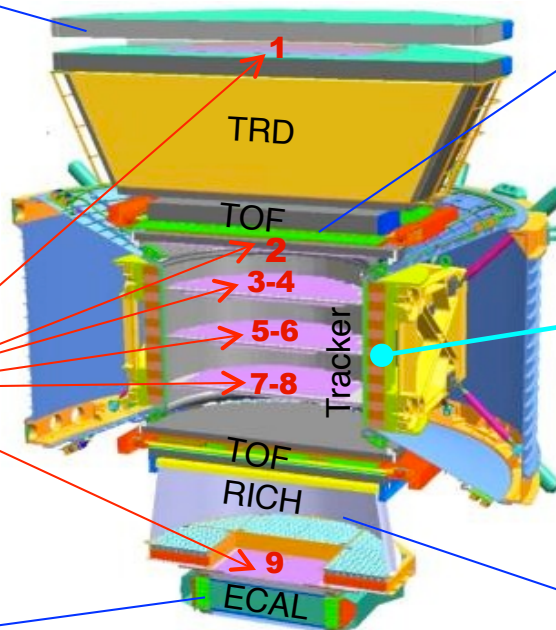
Silicon Tracker
 Z, P



ECAL
 E of e^+ , e^-



Particles and nuclei are defined
by their charge (Z)
and energy ($E \sim P$)



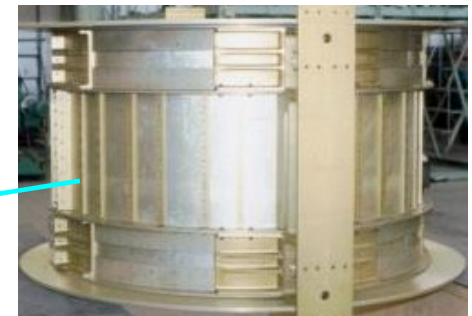
Z and $P \sim E$

are measured independently by the
Tracker, RICH, TOF and ECAL

TOF
 Z, E



Magnet
 $\pm Z$

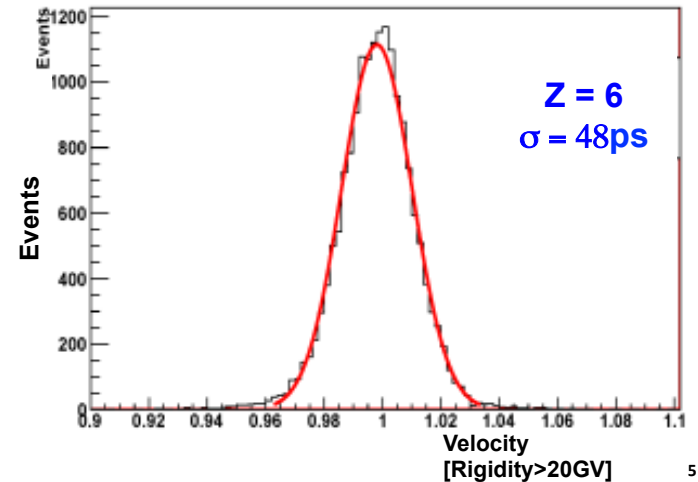
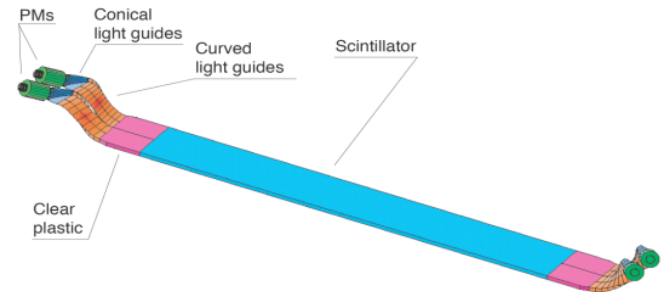
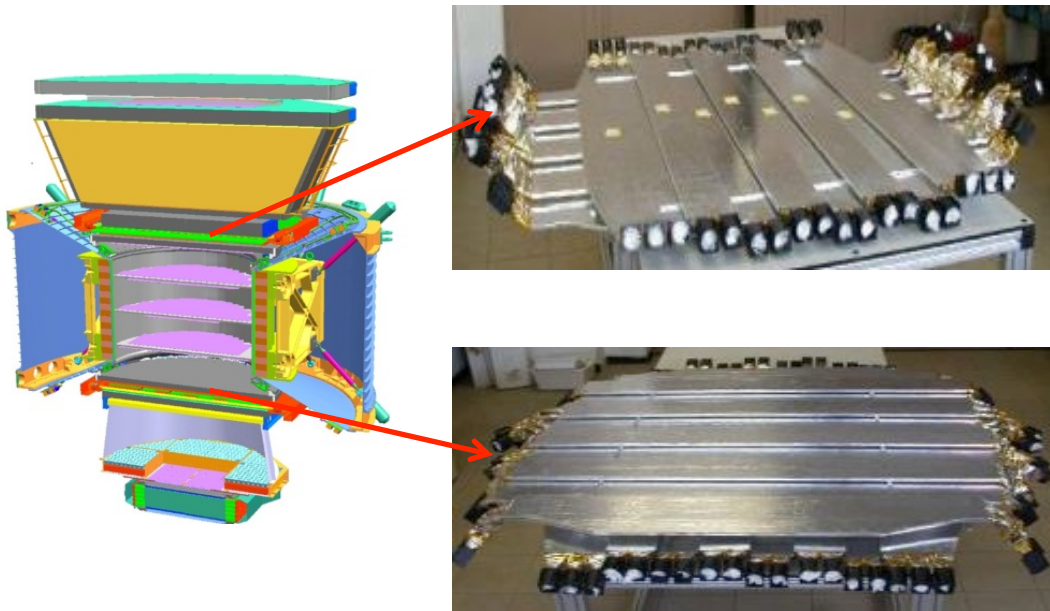


RICH
 Z, E



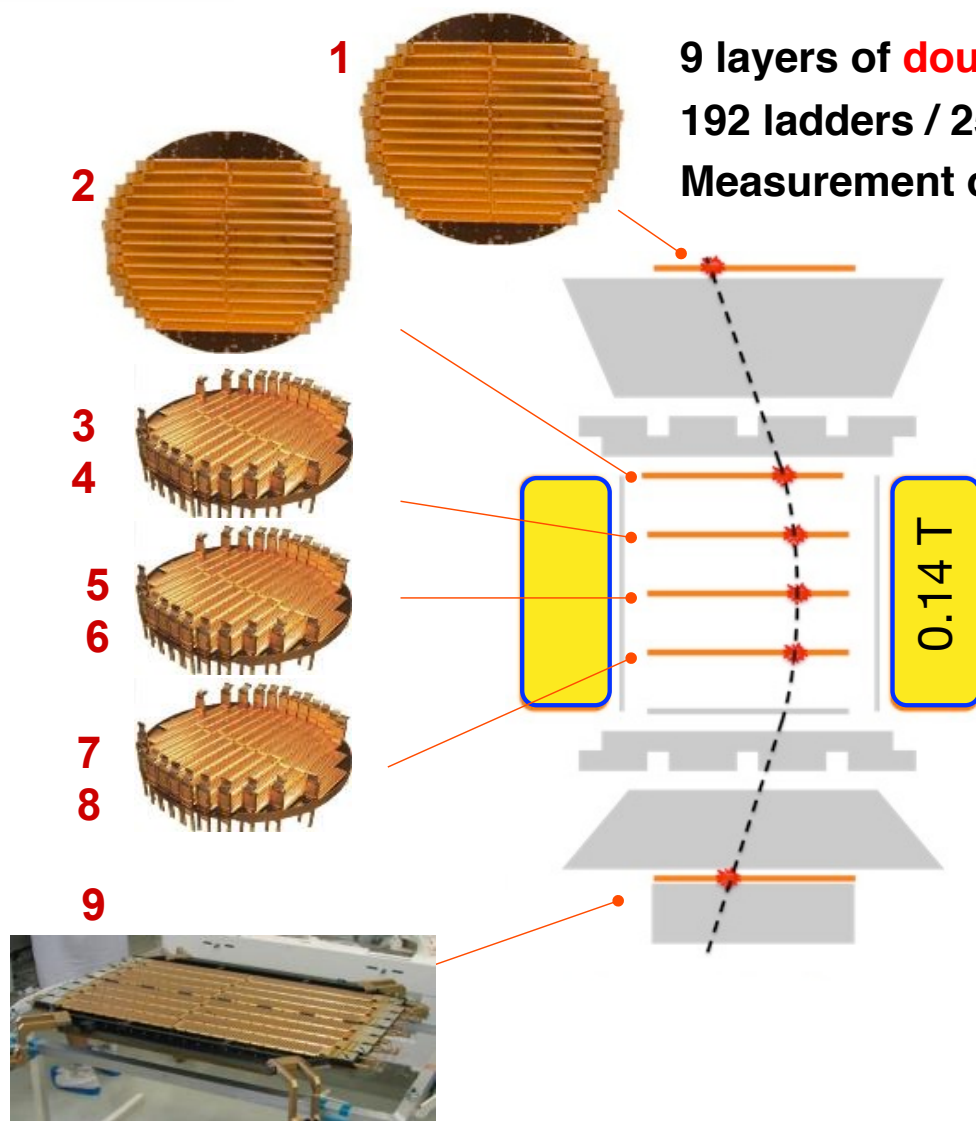
Time of Flight TOF

Fast scintillator planes coupled with PMTs for fast light readout
Time of flight resolutions ~ 160 ps $\rightarrow d\beta/\beta^2 \sim 4\%$ for $Z=1$ particles, better for higher charges

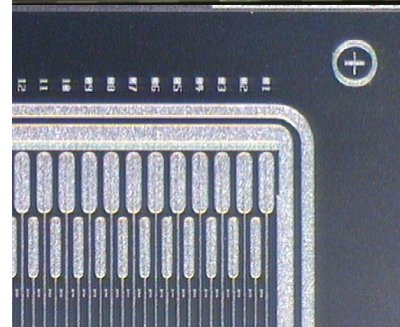


Fast signal used to provide the experiment trigger to charged particles

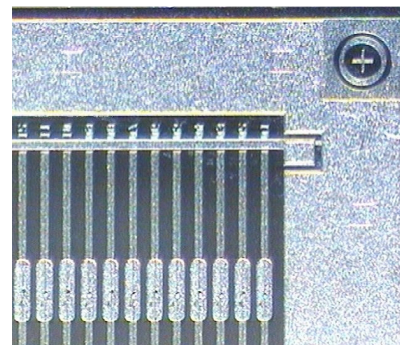
Magnetic Spectrometer



$10\mu\text{m}$ coordinate resolution



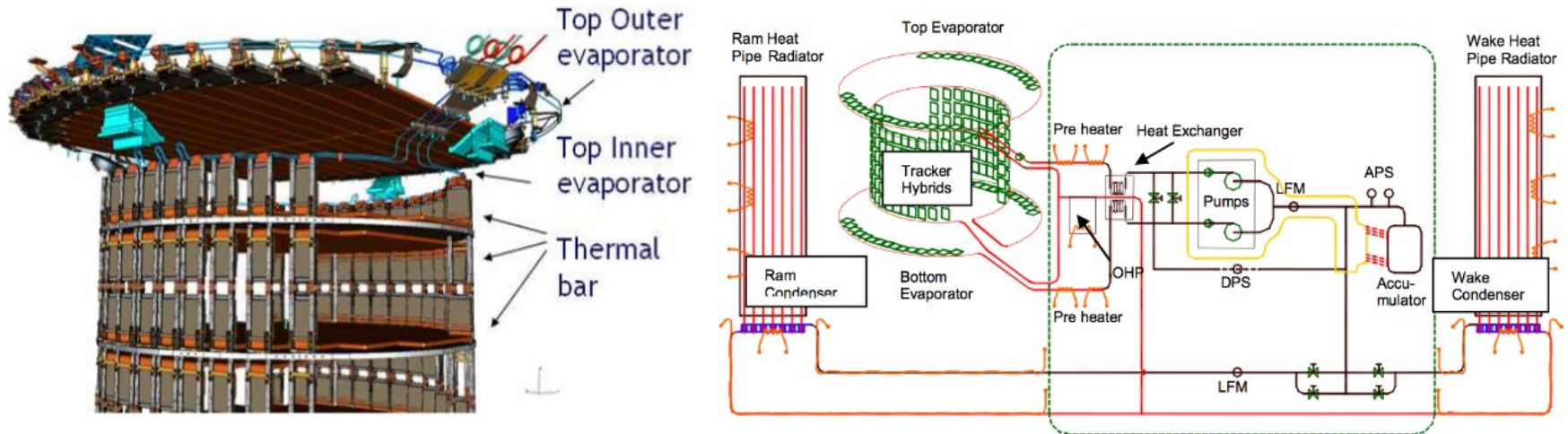
P-side (bending dir)
 $27.5\mu\text{m}$ pitch
 $104\mu\text{m}$ readout



N-side
 $104\mu\text{m}$ pitch
 $208\mu\text{m}$ readout

Tracker Thermal Control System

150 W to be dissipated from Inner Tracker



2-phases CO₂ cooling system (4x redundant)

CO₂ pumped through an evaporator and boils due to the heat produced by electronics.

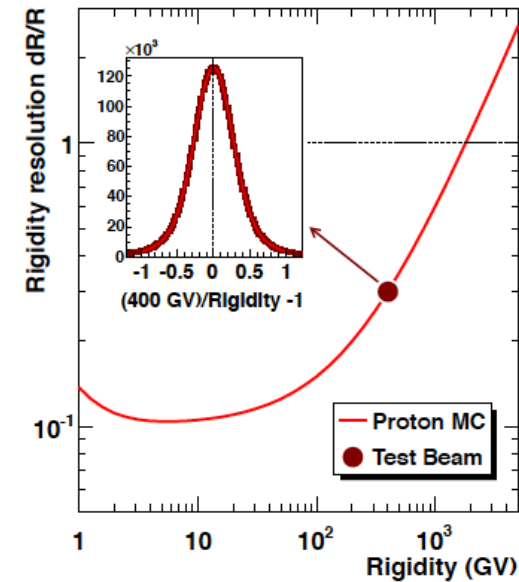
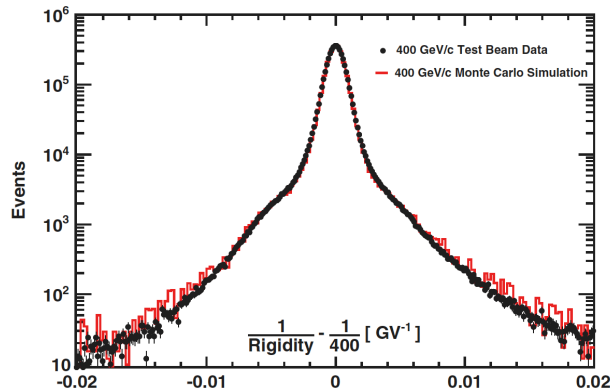
Exiting/Entering CO₂ thermally connected (CO₂ is entering at the boiling point).

CO₂ dissipates heat through dedicated radiators (condenser)

The new cooling system has been just installed with the most complex operation since the Hubble telescope repair

Magnetic Spectrometer

The spectrometer resolution is studied using test beam particles and MC simulations



Magnetic Spectrometer

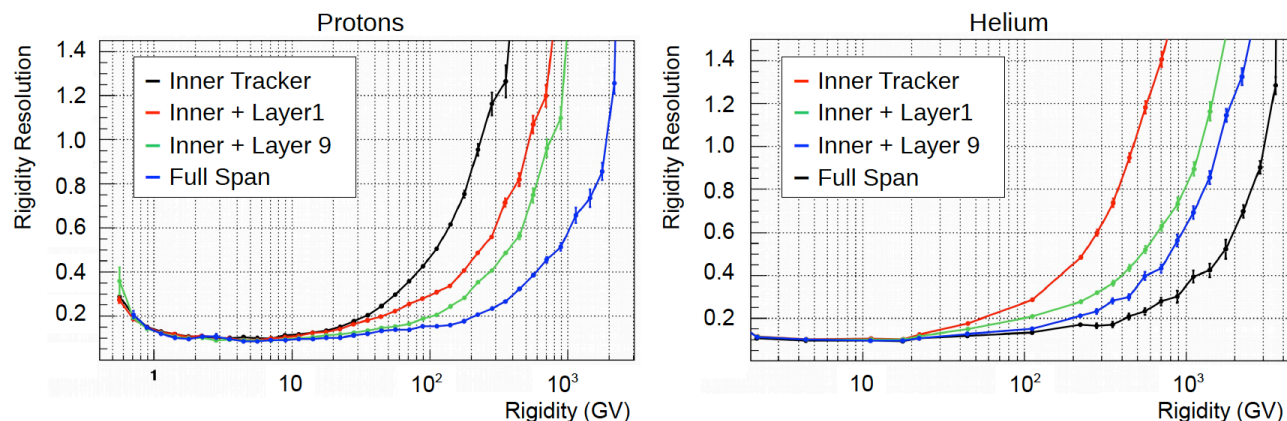
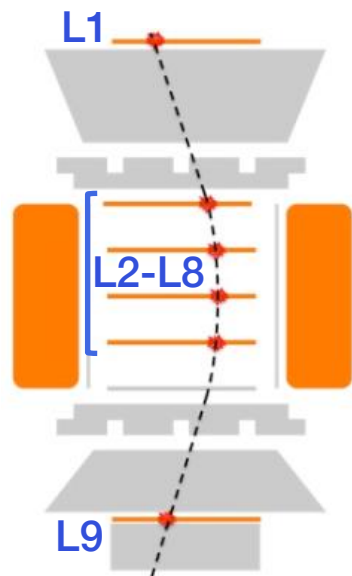


Figure 2.12: Rigidity measurement resolution for protons (**Left**) and Helium (**Right**) estimated from MC. Different colors identify different Tracker spans. The presence of the external layers used to increase the trajectory lever of arm allows to measure the rigidity of particles crossing the Tracker layers up to the TeV range

At low energies, the rigidity measurement resolution is dominated by the multiple scattering in the tracker material ($dR/R \sim \text{cost}$).

At high energies, the resolution is defined by the curvature measurement ($dR/R \sim R$).

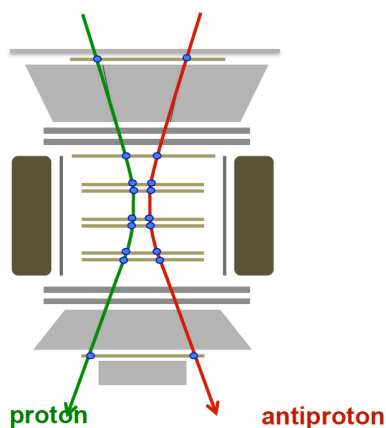
The maximum detectable rigidity is defined as the rigidity when the resolution is 100% (Cannot distinguish between negative and positive curvatures)

Magnetic Spectrometer

Charge Confusion (or Flip)

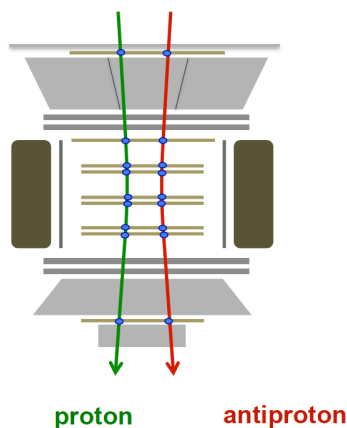
Tracker Resolution (statistical)

Trajectories at low energy



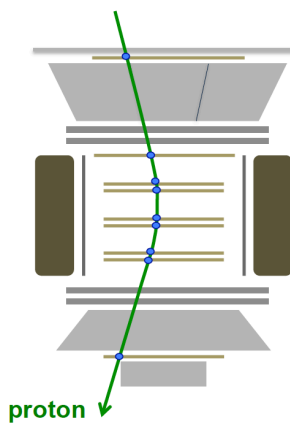
Larger is the energy, straighter is the particle's trajectory
(straighter is the trajectory, higher is the confusion...)

high energy



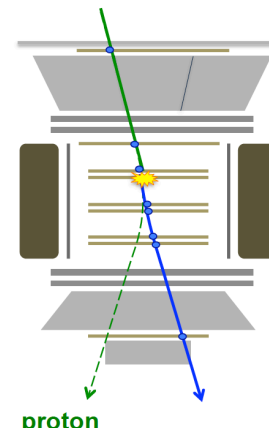
Interactions with the material

Clean proton trajectory

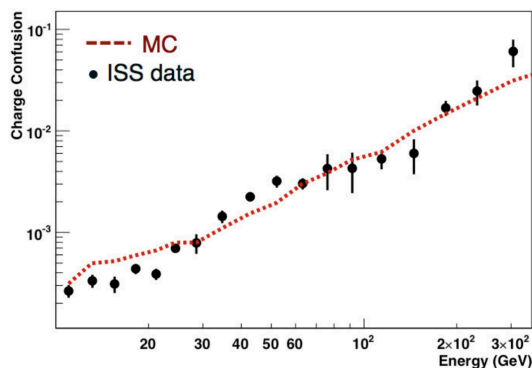


→ well-reconstructed proton

Occurrence of nuclear scattering

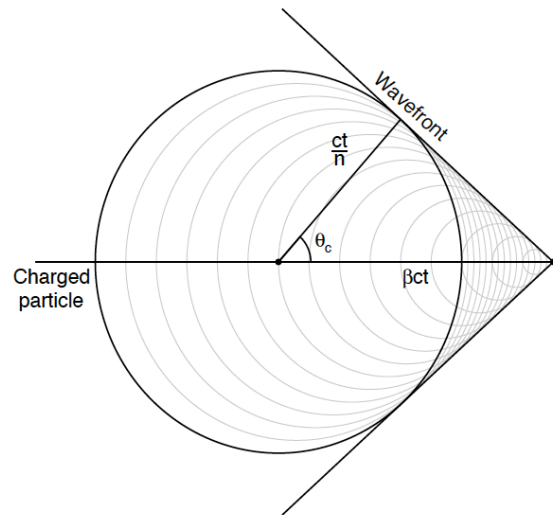


→ distorted trajectory
→ fake antiproton



The amount of charge confusion increases with energy, limiting the capabilities to correctly measure the fraction of antimatter in cosmic rays

Ring Imaging Cherenkov RICH



Cherenkov radiation is emitted when a charged particle moves in a medium at a speed greater than the speed of light *in that medium*

$$\beta > \frac{1}{n}. \quad (52)$$

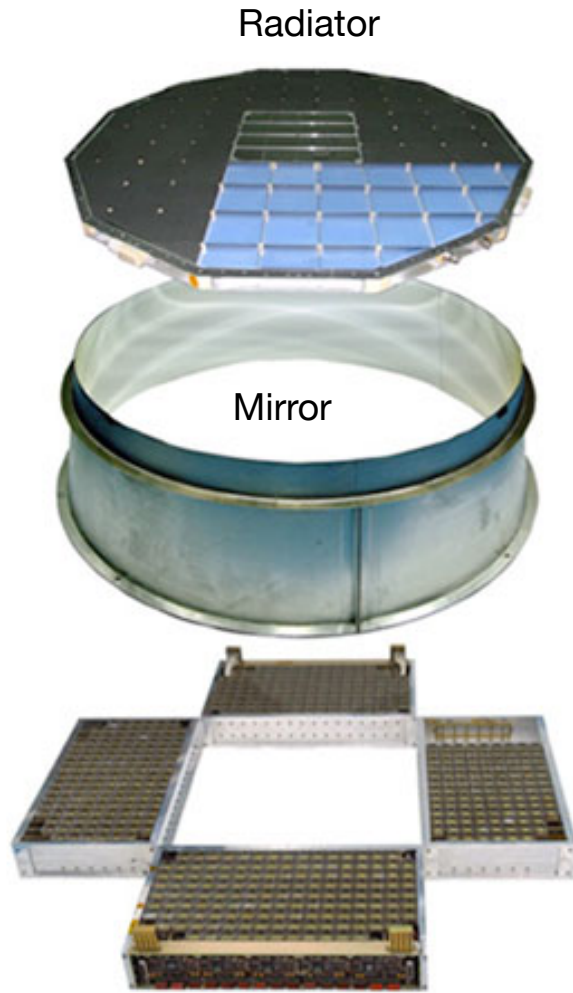
$$\cos \theta_c = \frac{1}{n\beta}$$

Geometry: Cherenkov ring aperture used to measure the particle velocity

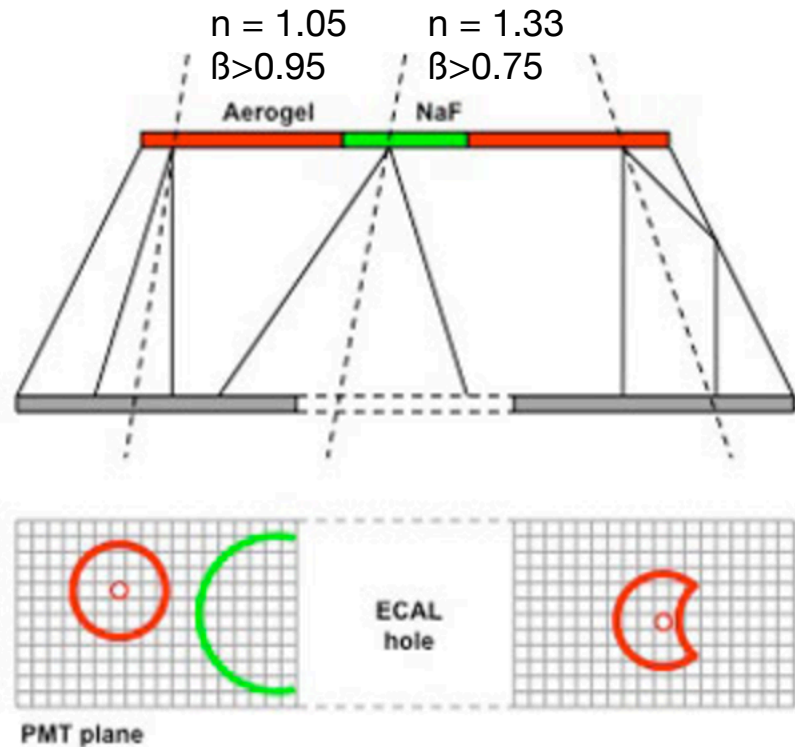
$$\frac{d^2 N}{dx d\lambda} = \frac{2\pi\alpha z^2}{\lambda^2} \left(1 - \frac{1}{\beta^2 n^2(\lambda)} \right)$$

Intensity: number of UV photons proportional to particle charge

Ring Imaging Cherenkov RICH

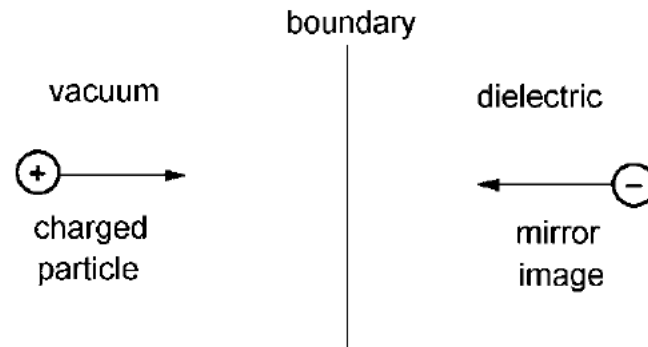


10,880 photosensor plane



Measurement of velocity with $d\beta/\beta \sim 0.1\%$

Transition Radiation



Radiation emitted when charged particles cross boundaries between media.

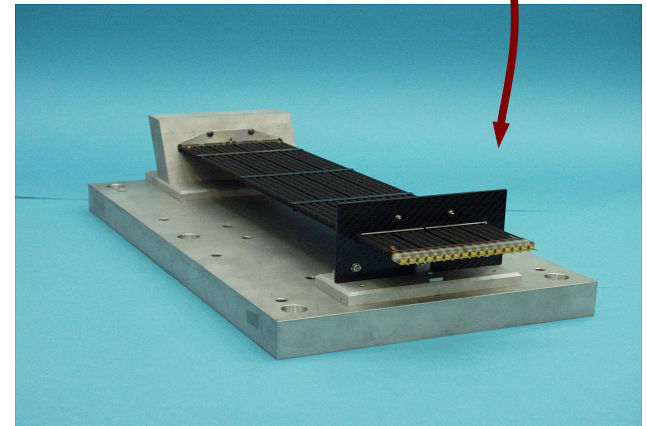
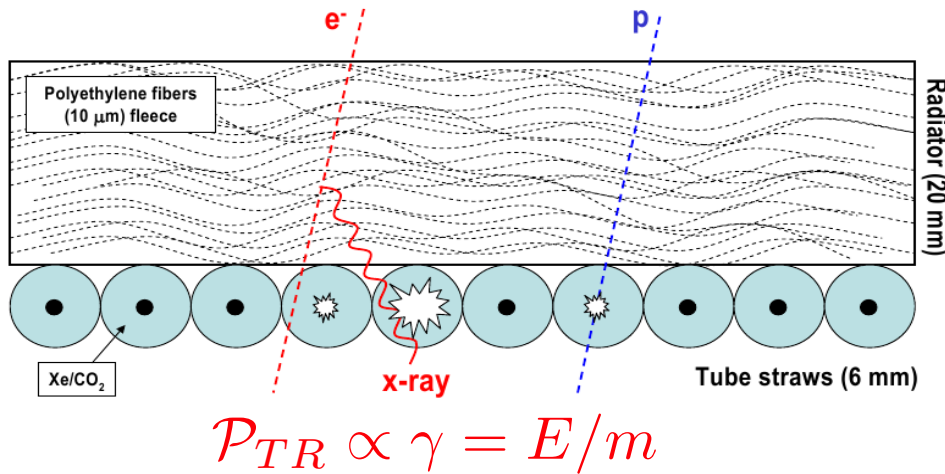
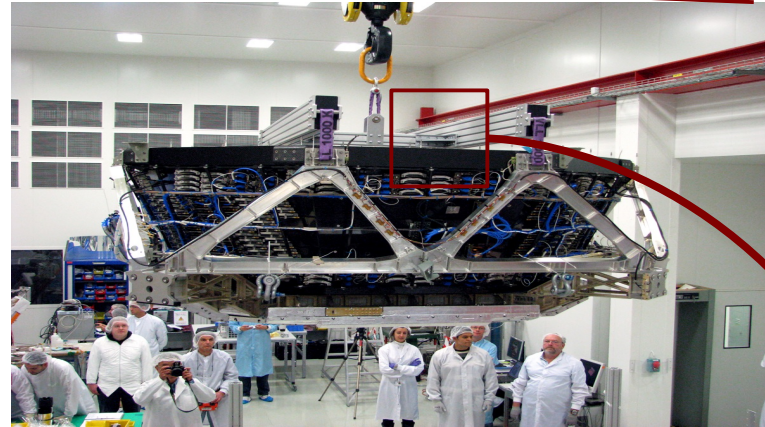
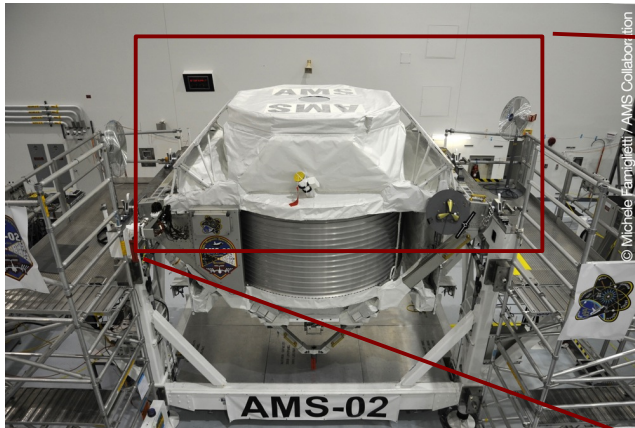
For each crossing, the probability of emission is very small (prop. to α) \rightarrow T.R. gives a small contribution to the total energy losses.

BUT it has a very peculiar dependence on the particle energy. $\mathcal{P}_{TR} \propto \gamma = E/m$

Since it depends on γ (and not on β) it is fundamental to identify high energy particles.

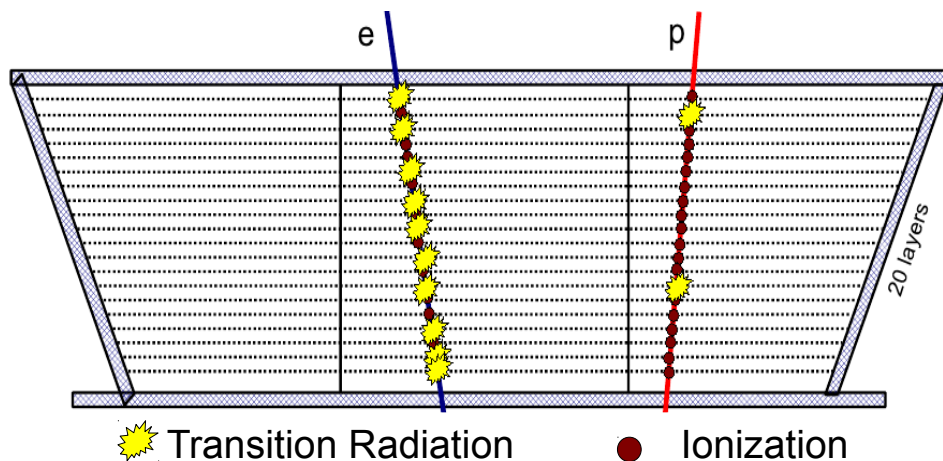
The T.R. emission is dominated by X-rays, that can be detected by gaseous detectors

Transition Radiation Detector TRD



20 Layers of radiator (fleece) to induce X ray radiation
 Straw tubes for $\sim\text{KeV}$ xray detection (Xe/C02 gas)

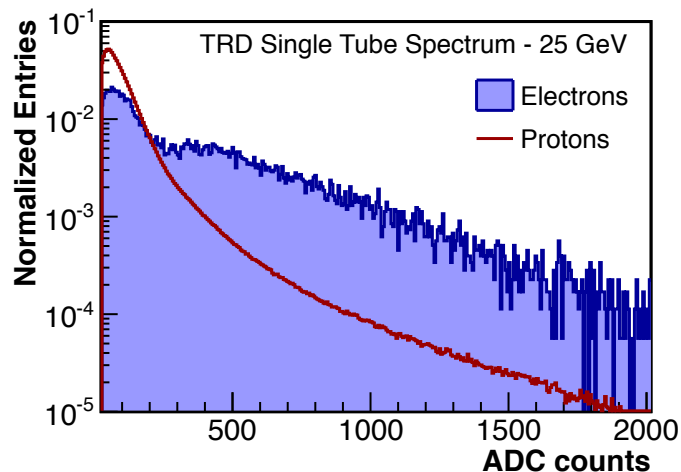
Transition Radiation Detector TRD



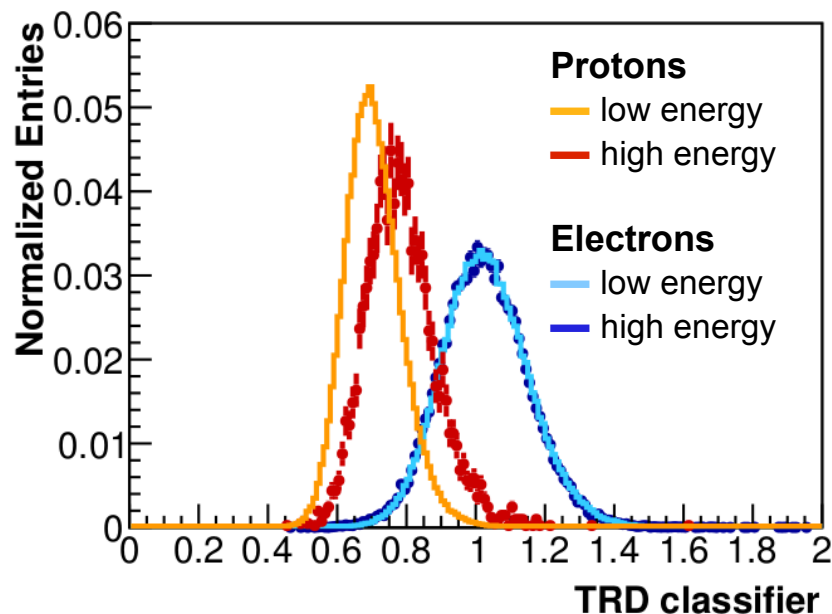
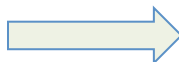
$$\mathcal{P}_{TR} \propto \gamma = E/m$$

For same Rigidity or Energy particles

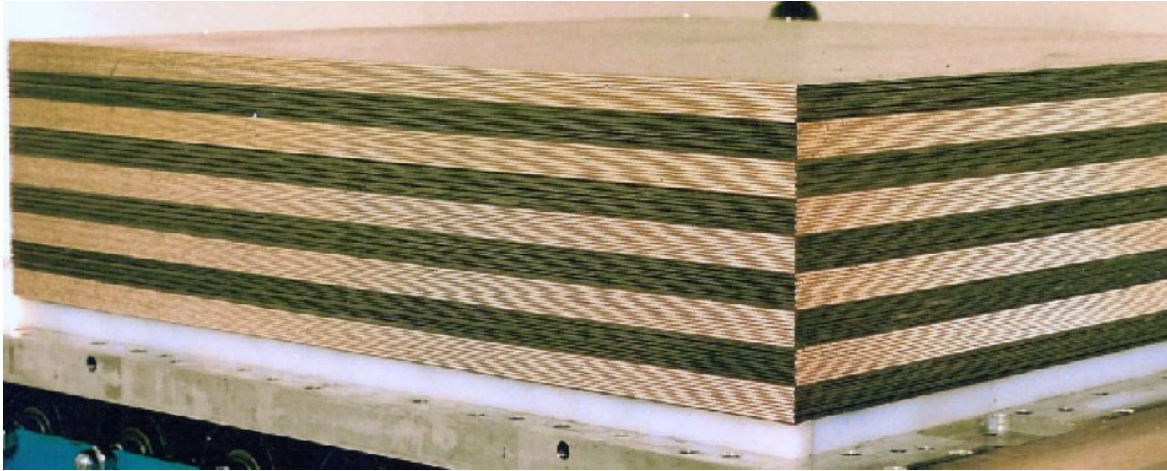
$$\mathcal{P}_{TR}(e^{\pm}) \gg \mathcal{P}_{TR}(p)$$



$$P_e = \eta \sqrt{\prod_i^n P_e^{(i)}(A)}$$



Electromagnetic Calorimeter ECAL



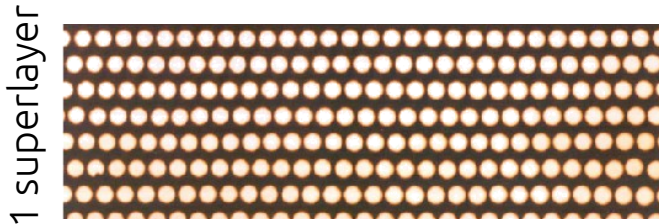
SAMPLING CALORIMETER

Lead + Scintillating fibers

66 x 66 x 17 cm³

1296 readout cells

17 X₀, 0.6 λ_{nucl}

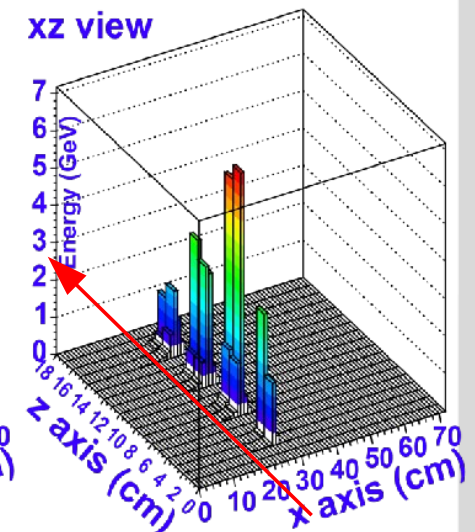
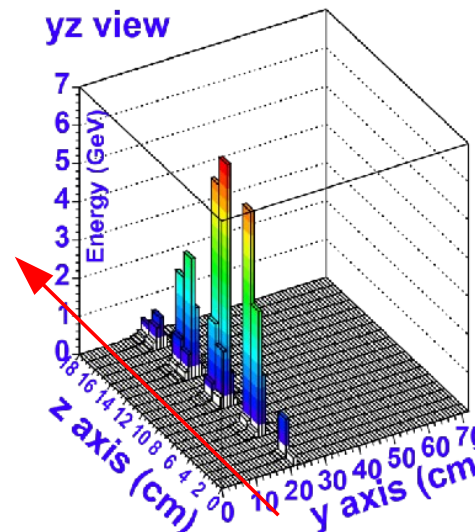


1 superlayer

50,000 fibers, $\Phi=1\text{mm}$

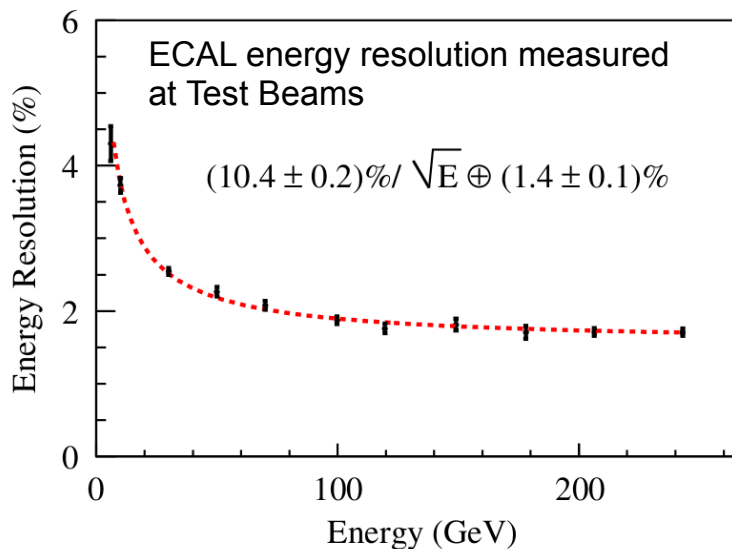
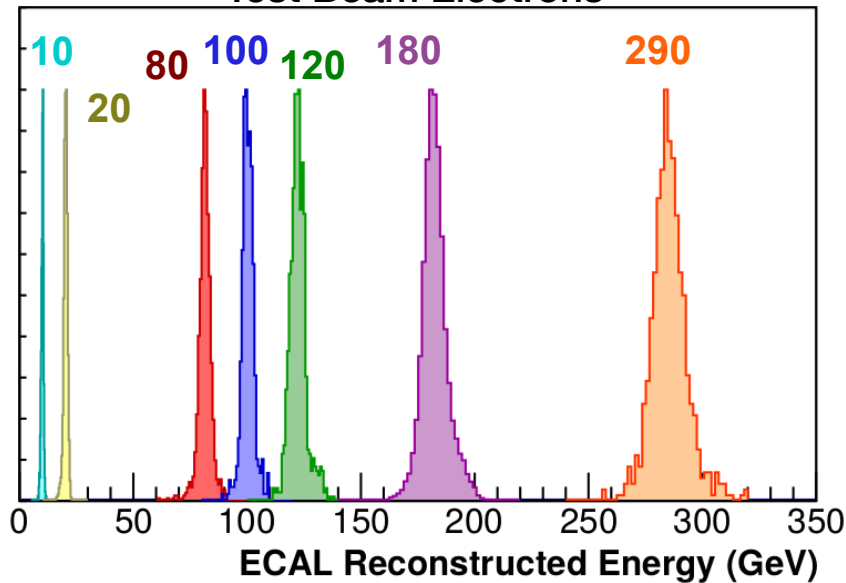
Uniformly distributed in 600 kg of lead

Energy and **arrival direction**
measurement of electrons and photons up
to 1 TeV

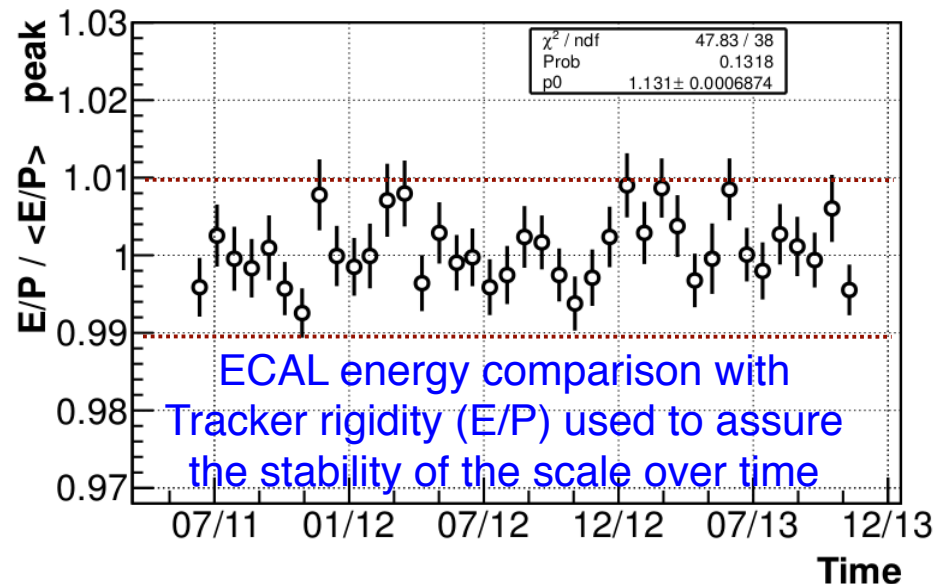


Energy Measurement

Test Beam Electrons

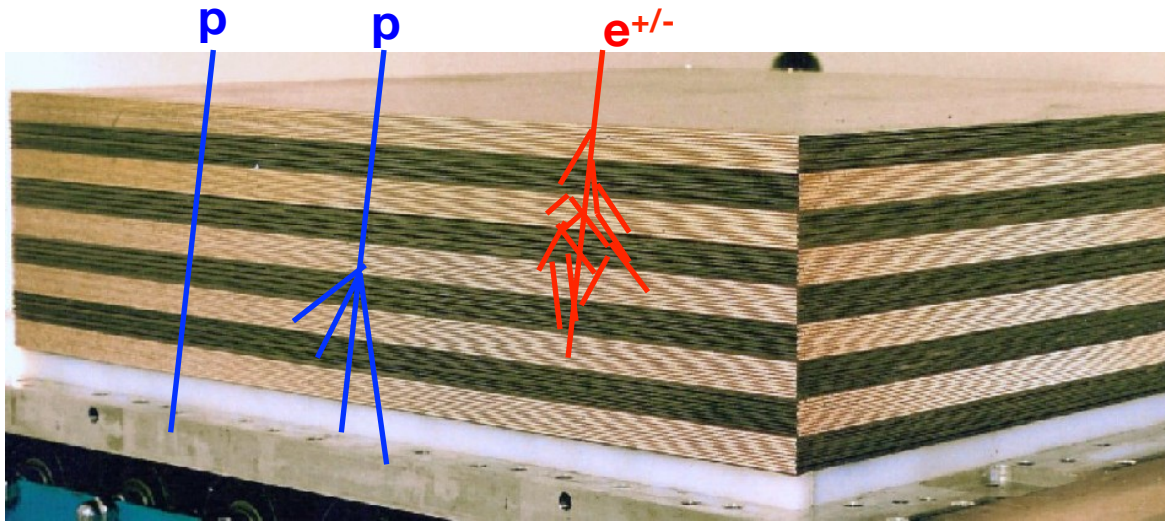


- ECAL energy resolution $\sim 2\%$
- ECAL energy absolute scale tested during test beams on ground
- We have no line in space (as in collider exp.) to calibrate the energy scale in orbit!
 - MIP ionization used to cross-calibrate the energy scale in orbit



Calorimeter resolution improves at high energy (compare with spectrometer)

Electromagnetic Calorimeter ECAL

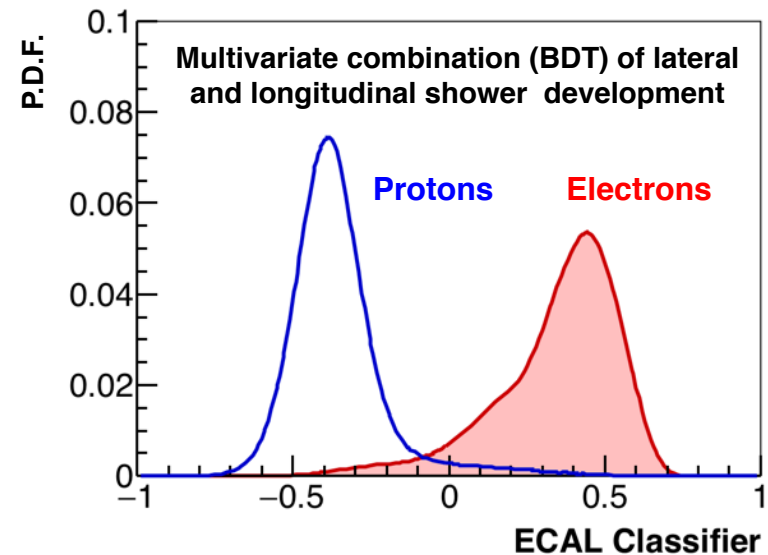
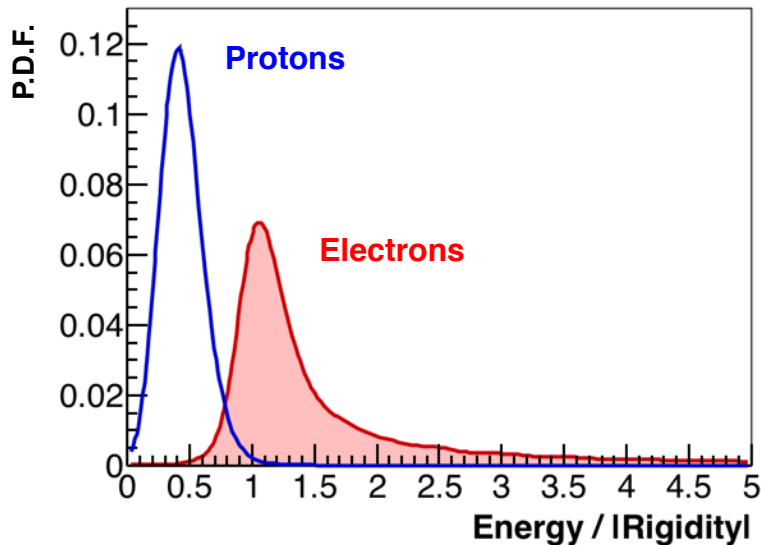


Electrons

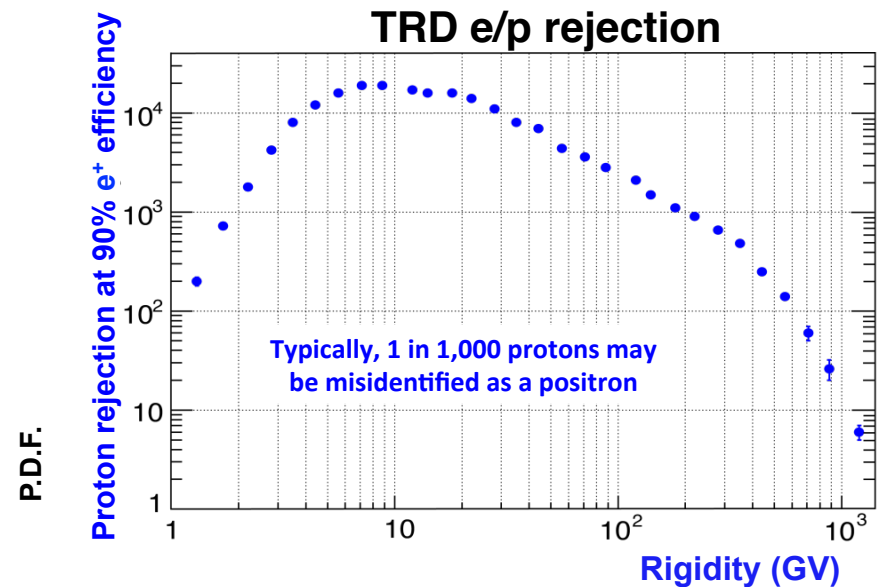
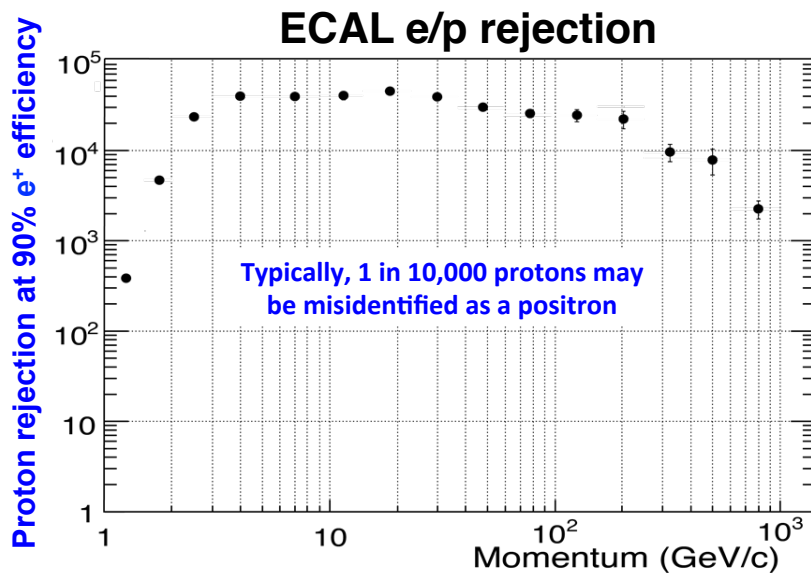
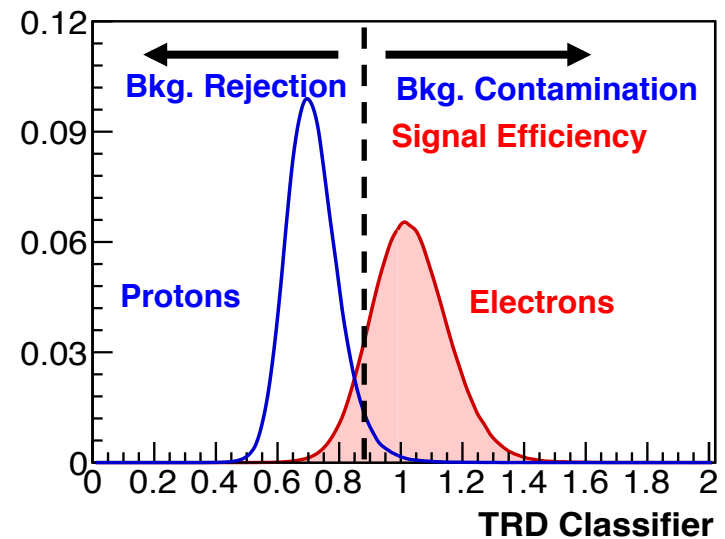
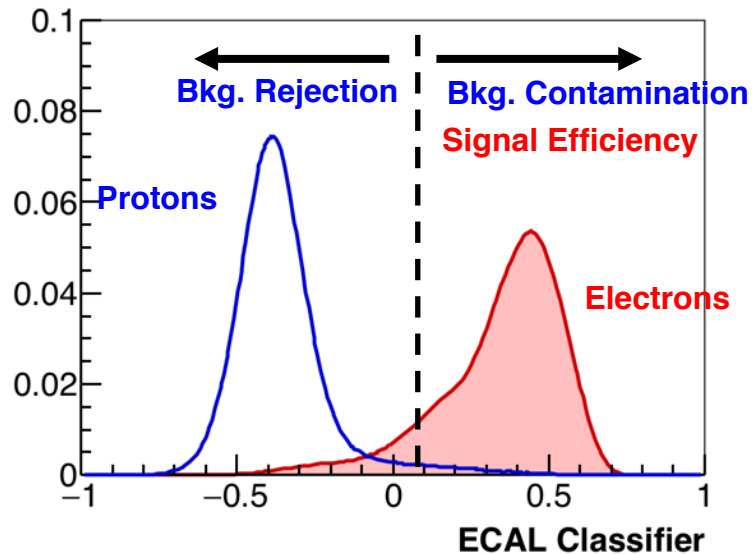
Electromagnetic Shower
Energy contained
 $E_{\text{ECAL}} \sim P_{\text{TRACKER}}$

Protons

MIP or Hadronic Shower
Irregular shower
 $E_{\text{ECAL}} \ll P_{\text{TRACKER}}$

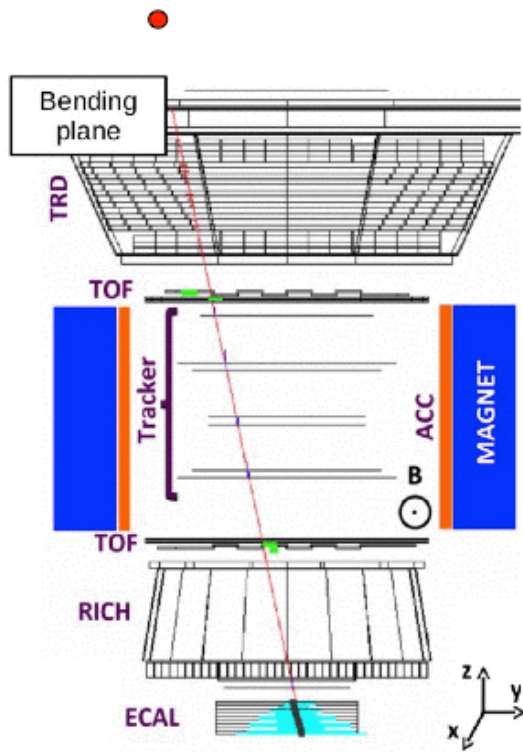


ECAL and TRD e/p separation



AMS: TeV precision spectrometer

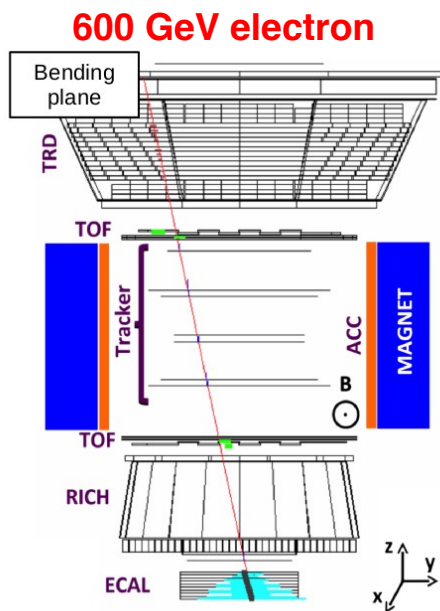
Full coverage of **anti-matter** and **CR physics**



	e^-	p	He
TRD 20 layers			
TOF 4 layers			
TRK 9 layers			
RICH			
ECAL 20 layers			

AMS: TeV precision spectrometer

Full coverage of **anti-matter** and **CR** physics



	e^+	e^-	p	\bar{p}	He	$\bar{\text{He}}$
TRD 20 layers						
TOF 4 layers						
TRK 9 layers						
RICH						
ECAL 18 layers						

e/p separation
charge ($|Z|$)

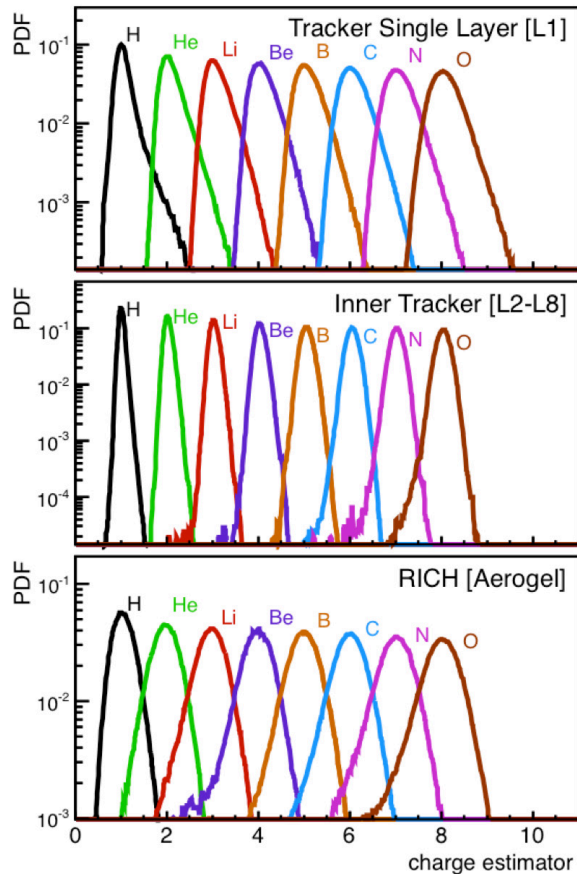
trigger
velocity (β)
charge ($|Z|$)

momentum (p)
sign ($\pm Q$)
charge ($|Z|$)

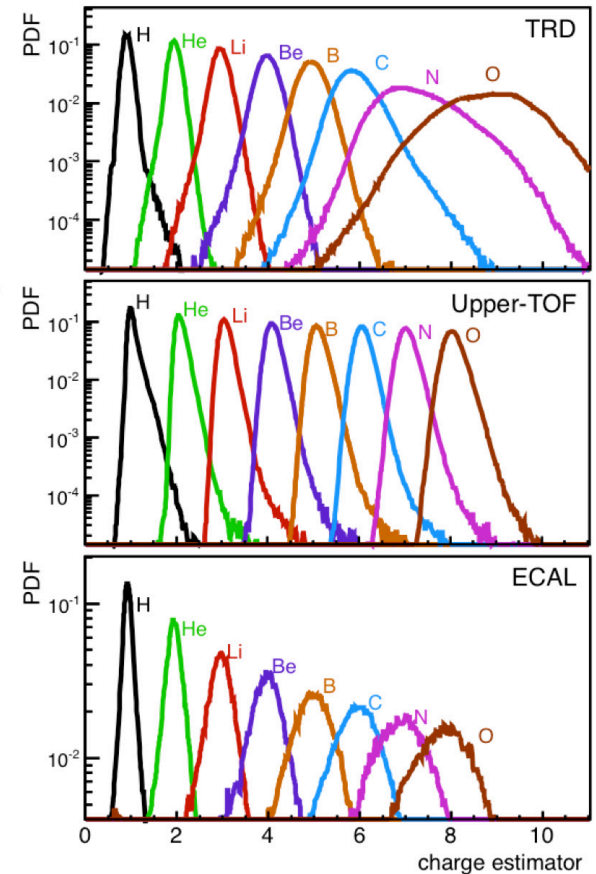
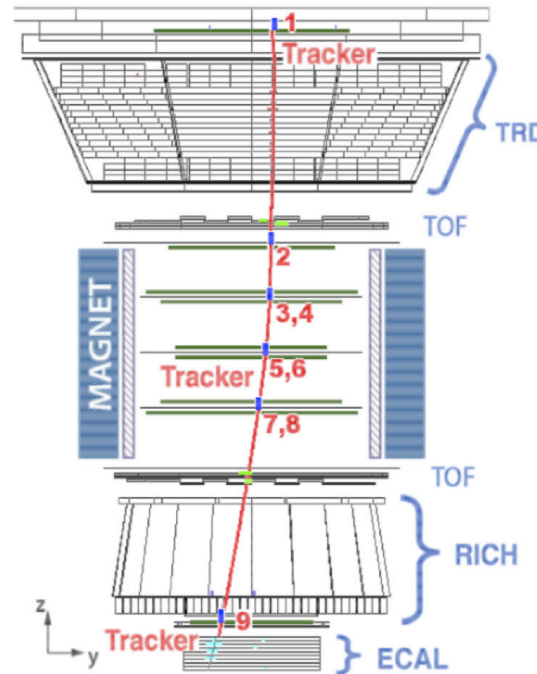
velocity (β)
charge ($|Z|$)

e^+ energy
e/h separation
 γ trigger

AMS-02 Charge Measurement



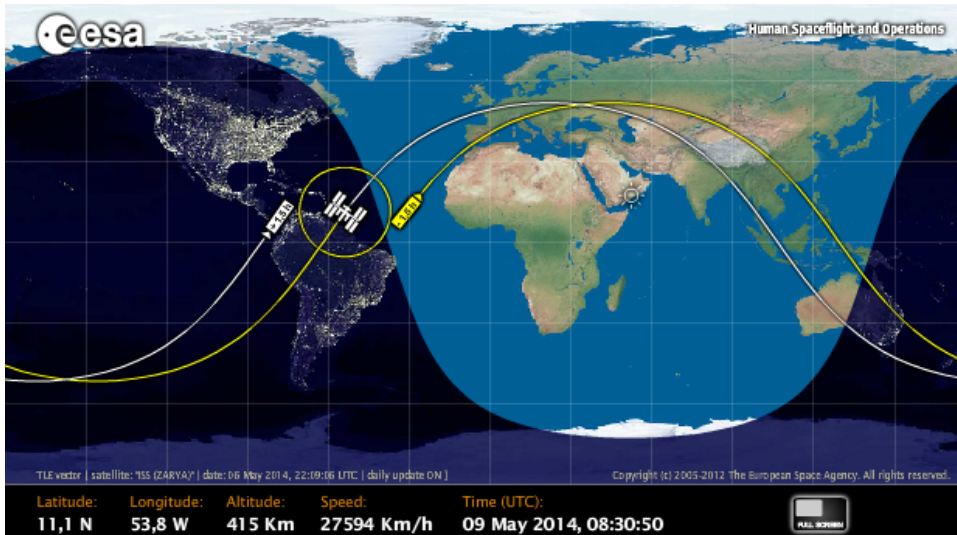
Charge Measurements of Light CR Nuclei



Redundant measurements of the nuclear charge at different depths of the detector.

Precise understanding of nuclear fragmentation in the materials.

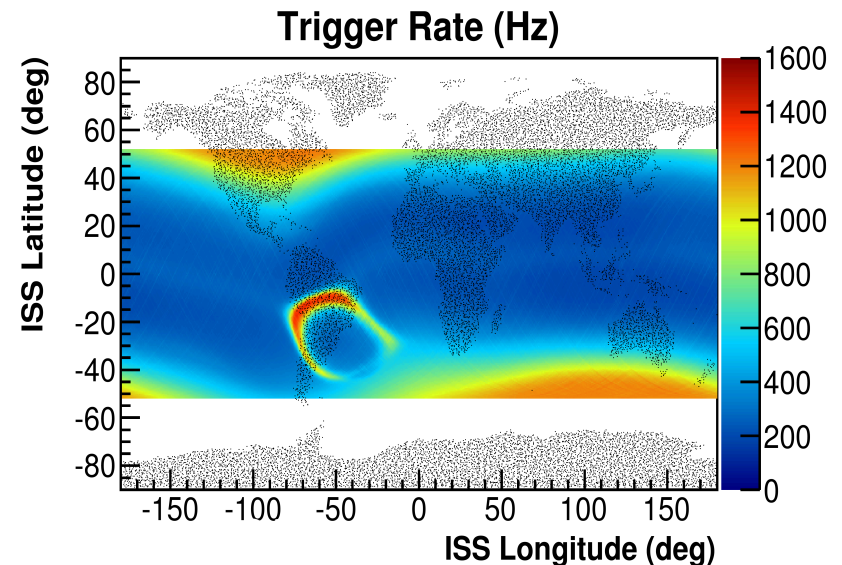
AMS orbit



ISS orbit period ~ 90 min
+/- 50 deg latitude covered

DAQ operations depend on orbit position

Increase of trigger rate in polar region (low magnetic field and trapped particles) and in the South Atlantic Anomaly



Detector operated continuously around the clock since May 2011 with no major interruptions

Trigger

Each time a detector decides to save the information of a particle crossing, the electronics freezes the analog information on all the sensors ($\sim 300,000$ for AMS), digitizes them and package them to send to ground. This procedure lasts $O(100 \mu\text{s} - 1 \text{ ms})$.

The flux of cosmic rays through the detector volumes is typically higher than the digitization capabilities. Only a fraction of the total cosmic rays crossing the detector volumes has to be recorded (typically, particles crossing the interesting detector fiducial volume and above a certain energy threshold)

The **trigger** is a system that decides whether the instrument should freeze the analog information and save the **event**. It is based using information from fast detectors and combining it in a simple AND-OR logic.

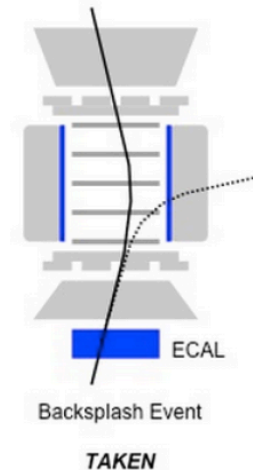
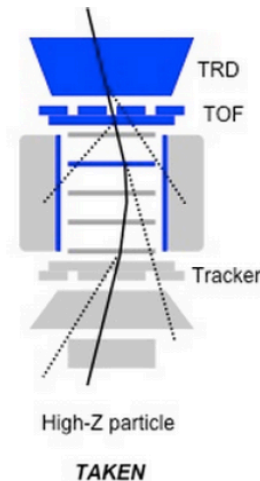
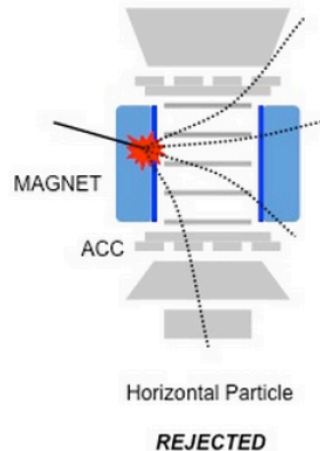
The trigger represent a very delicate system. If an interesting event is not triggered, it will be lost forever. Typically, the trigger selection it is a compromise between the maximum number of events stored with respect to the capabilities of data storage and transfer and event pileup.

Trigger

AMS uses the fast information of the **TOF** the trigger charged particles, the external **anticoincidence** to veto cosmic rays outside the acceptance, and the fast **ECAL** information to trigger photons (that do not leave energy in the TOF)

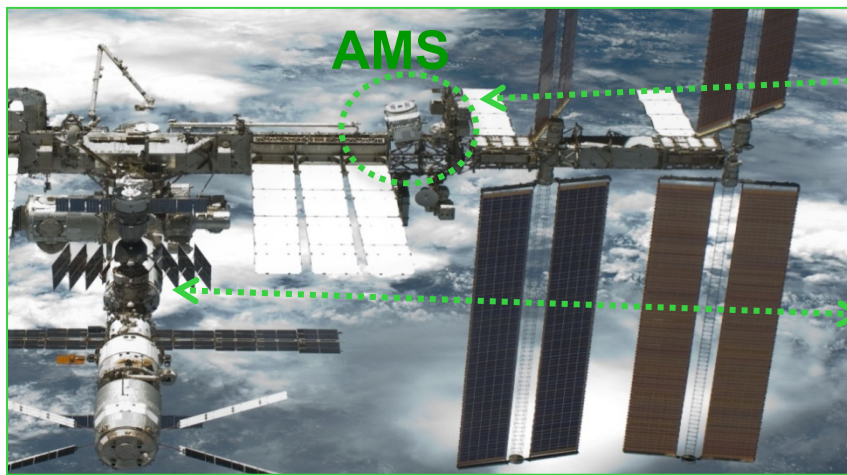
AMS-02 Triggers:

- Unbiased 3/4
- Charged $Z=1$
- Charged Ions
- “Slow” ions
- Electrons
- Photons
- Unbiased em



If any of these conditions is satisfied, the event is triggered

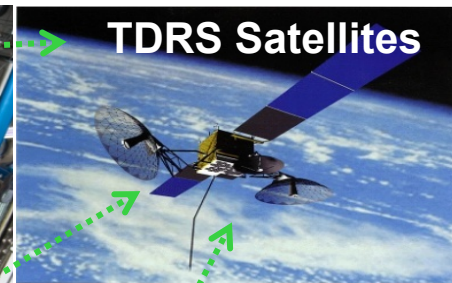
Data transfer



AMS



Astronaut at ISS AMS Laptop



TDRS Satellites

Ku-Band

High Rate (down):
Events <10Mbit/s>
≈30 billion triggers
70 TB of raw data

Flight Operations

Ground Operations

S-Band

Low Rate (up & down):
Commanding: 1 Kbit/s
Monitoring: 30 Kbit/s



AMS Payload Operations Control and Science Operations Centers (POCC, SOC) at CERN



AMS Computers at MSFC, AL



White Sands Ground Terminal, NM

AMS physics results

LEPTONS / ANTIMATTER

- Positrons fraction $e^+/(e^++e^-)$
- Electron and Positron fluxes (e^+ , e^-)
- Electron plus Positron flux (e^++e^-)
- Antiprotons/protons

Sensitive to
Dark Matter signal

HADRONS

- Proton and Helium (p, He)
- Lithium, Beryllium, Boron (Li, Be, B)
- Carbon, Nitrogen, Oxygen (C, N, O)

Probes to improve
the astrophysical background
knowledge

AMS-02 is providing precise data to **search for new physics** in the Cosmic Ray channels while **improving the understanding of the astrophysical background** with a coherent set of data

AMS physics results

LEPTONS / ANTIMATTER

- Positrons fraction $e^+/(e^++e^-)$
- Electron and Positron fluxes (e^+ , e^-)
- Electron plus Positron flux (e^++e^-)
- Antiprotons/protons

Sensitive to
Dark Matter signal

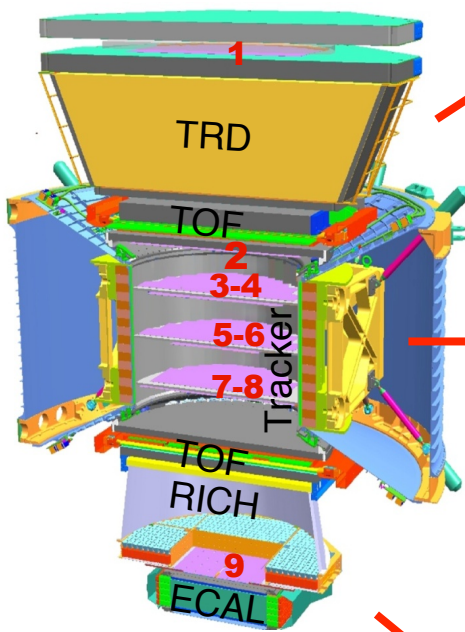
HADRONS

- Proton and Helium (p, He)
- Lithium, Beryllium, Boron (Li, Be, B)
- Carbon, Nitrogen, Oxygen (C, N, O)

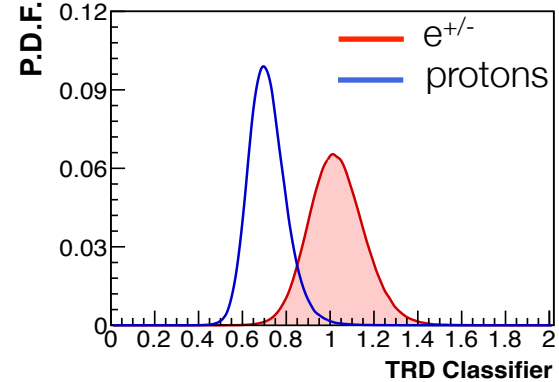
Probes to improve
the astrophysical background
knowledge

AMS-02 is providing precise data to **search for new physics** in the Cosmic Ray channels while **improving the understanding of the astrophysical background** with a coherent set of data

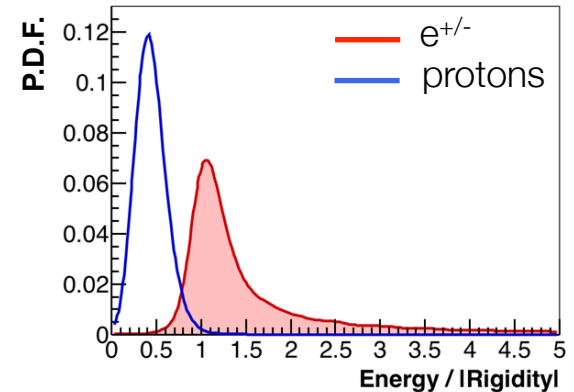
Identification of $e^{+/-}$



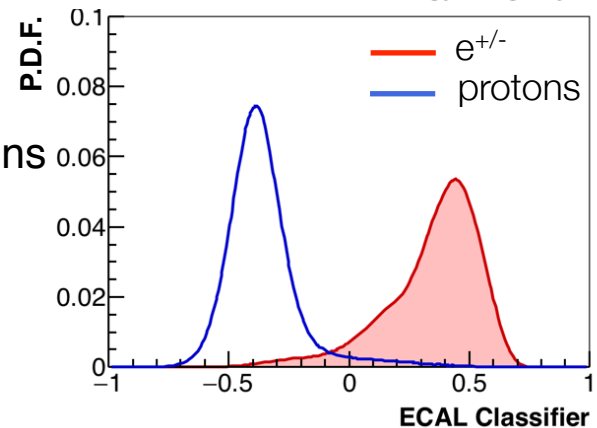
TRD
Transition Radiation
to identify $e^{+/-}$



TRACKER
Momentum P
 $e^{+/-}$: $P_{\text{TRK}} = E_{\text{ECAL}}$
Protons: $P_{\text{TRK}} \gg E_{\text{ECAL}}$

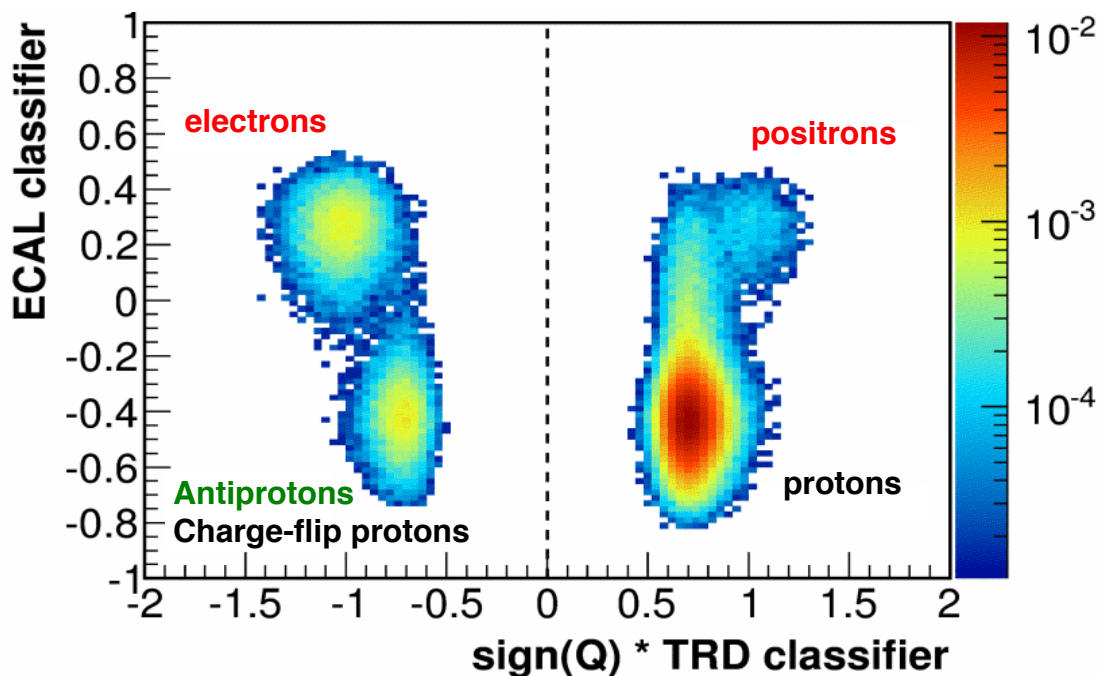


ECAL
Shower Topology
to separate $e^{+/-}$ from protons



Identification of $e^{+/-}$

The whole ECAL and TRD subdetector information is gathered in the so called “**classifier**” 1-D variables, trained to reject protons.

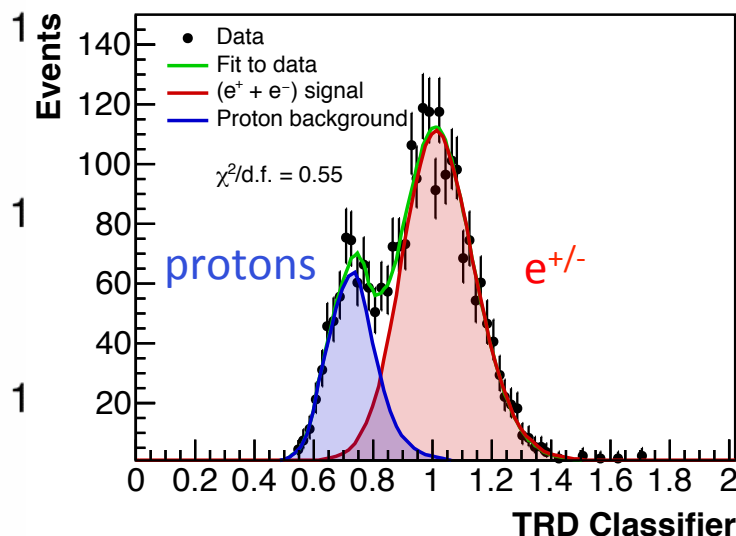
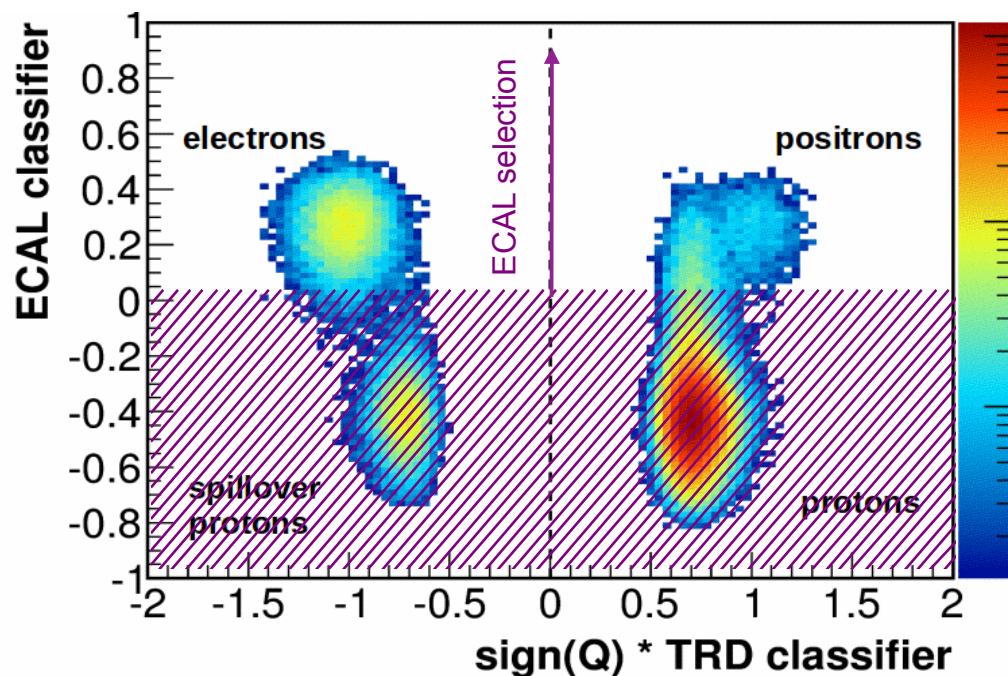


ECAL and TRD, separated by the magnet, efficiently and independently discriminate the signal ($e^{+/-}$) from the background (protons)

Identification of (e^+e^-)

TRD Classifier template fit

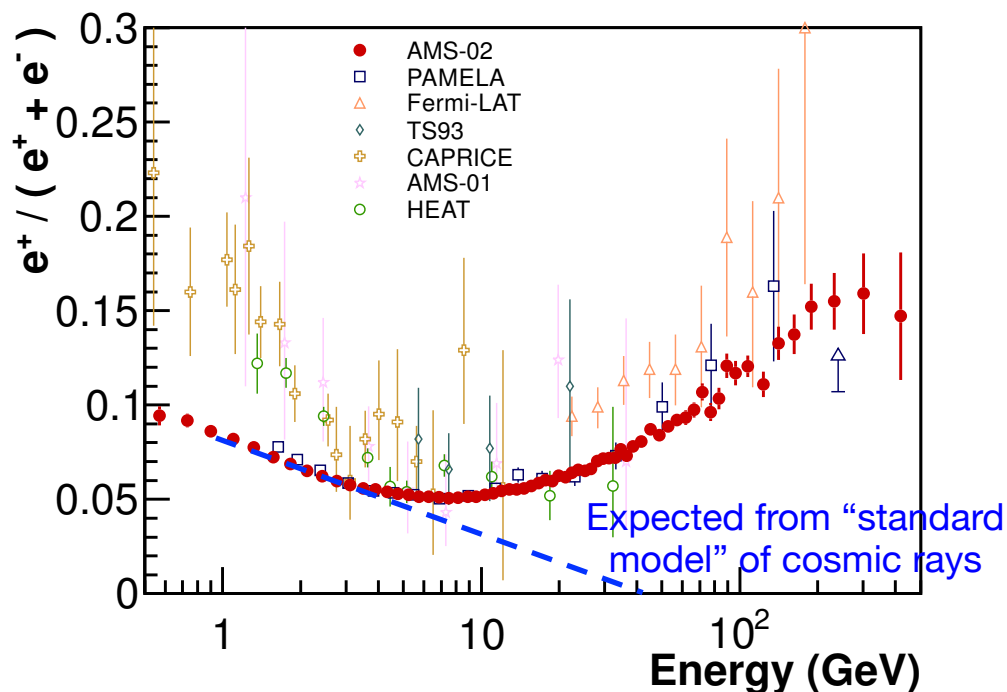
Reference spectra for the signal and the background are fitted to data as a function of the TRD classifier for different cuts on the ECAL BDT estimator



1. **ECAL** efficiently removes the majority of background protons
2. **TRD** independently evaluates the tiny remaining protons in the selected $e^{+/-}$ sample

Positron Fraction

Rise in the fraction of positrons (antimatter) over electrons (matter) not expected by the current Standard Model of CR origin and propagation

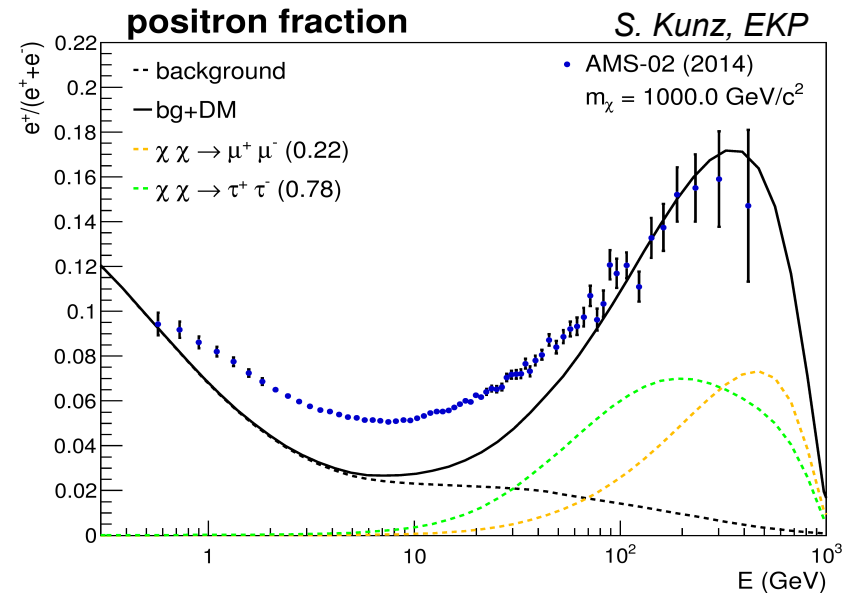
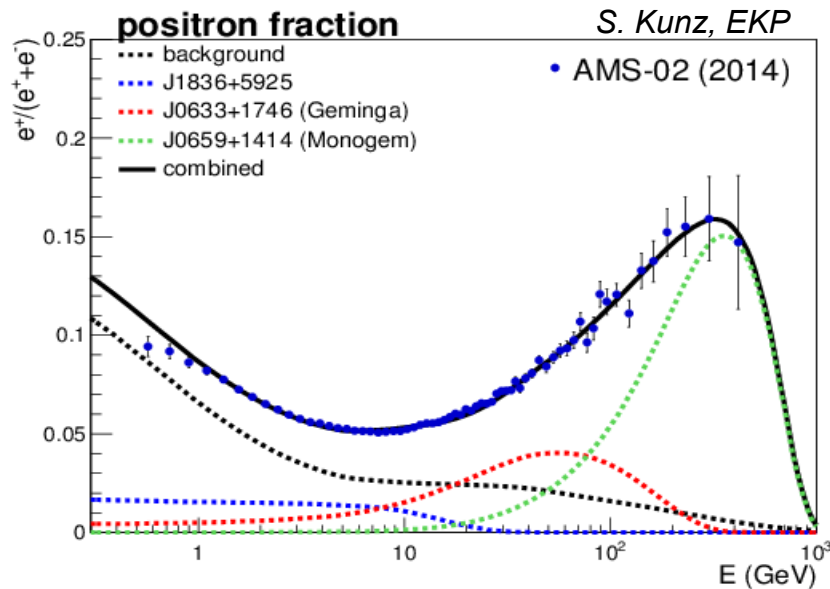
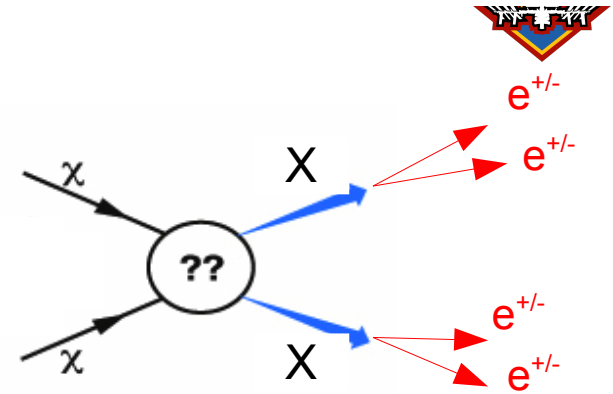
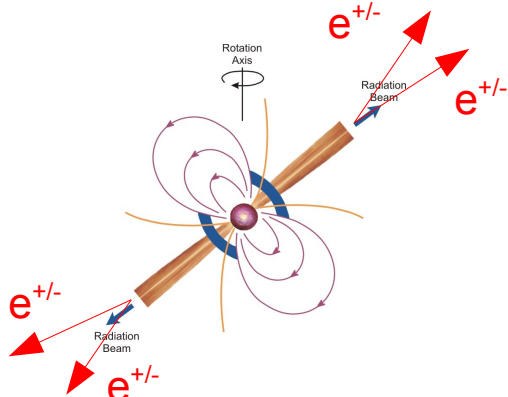


Unprecedented accuracy and energy range allowed a detailed study of the positron fraction behavior with energy

Positron Fraction

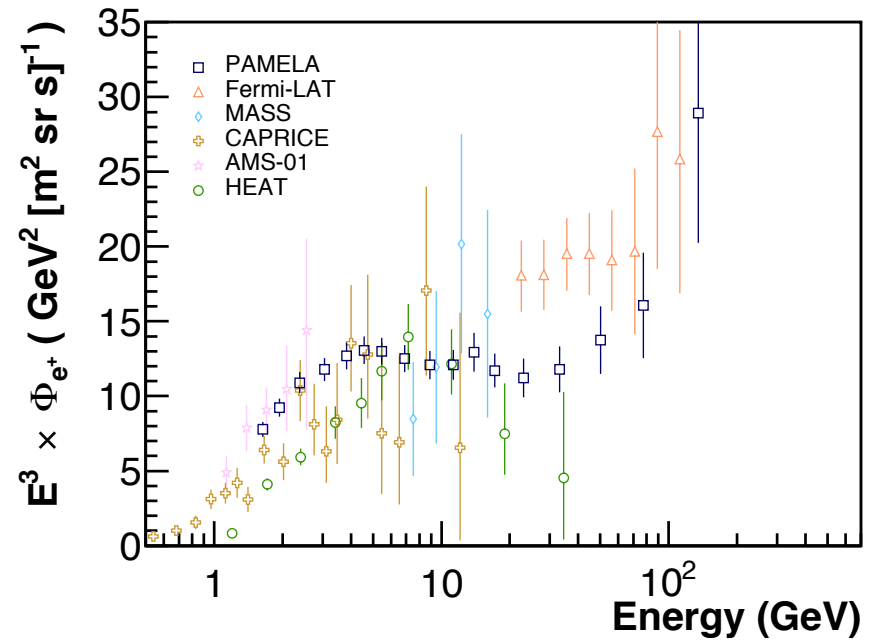
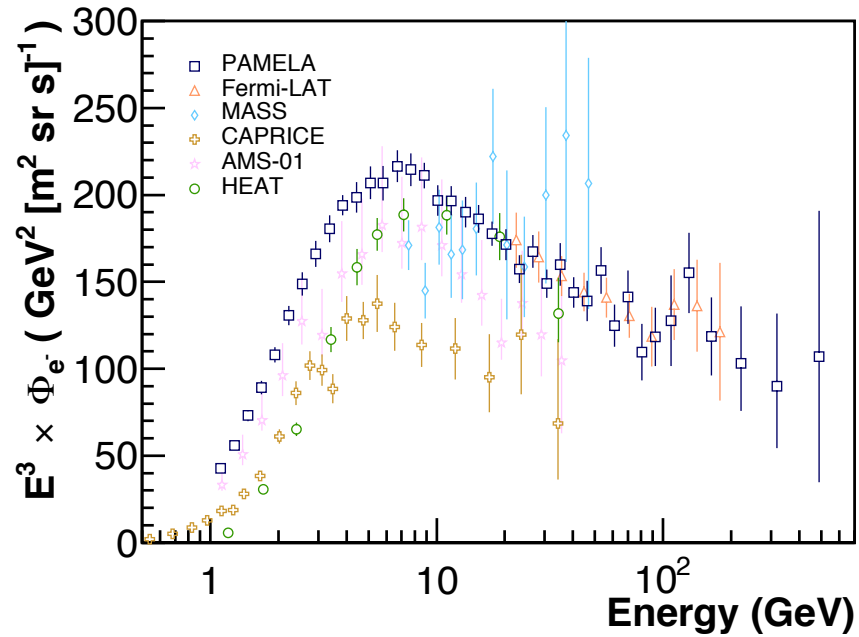
■ PULSARS

■ Dark Matter annihilation



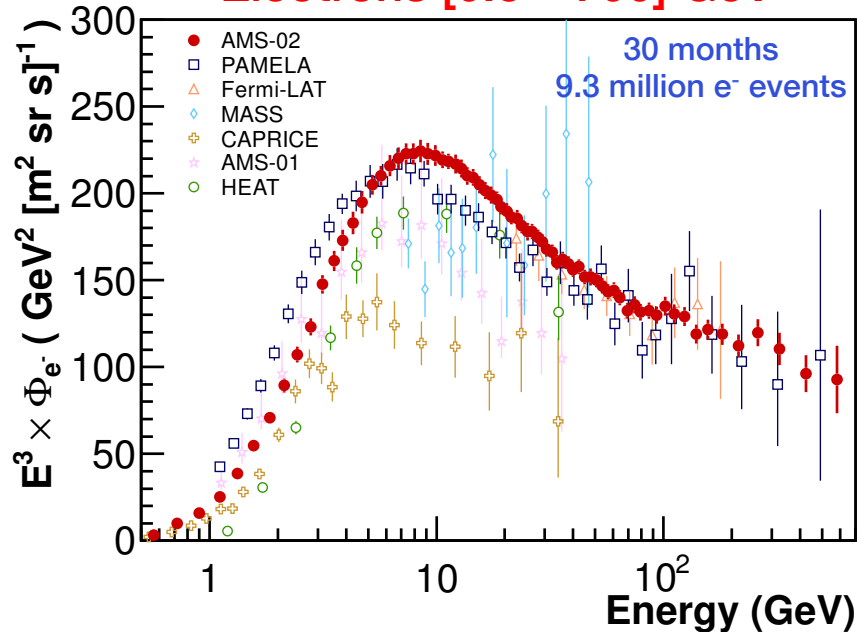
- Both mechanisms can be tuned to explain the data.
- The measurement of the spectral shape alone cannot disentangle between the two sources.....

e^+ and e^- Fluxes

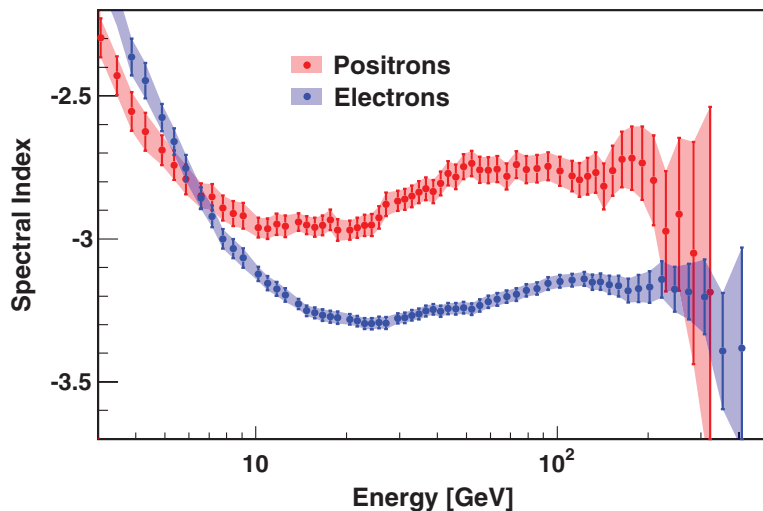
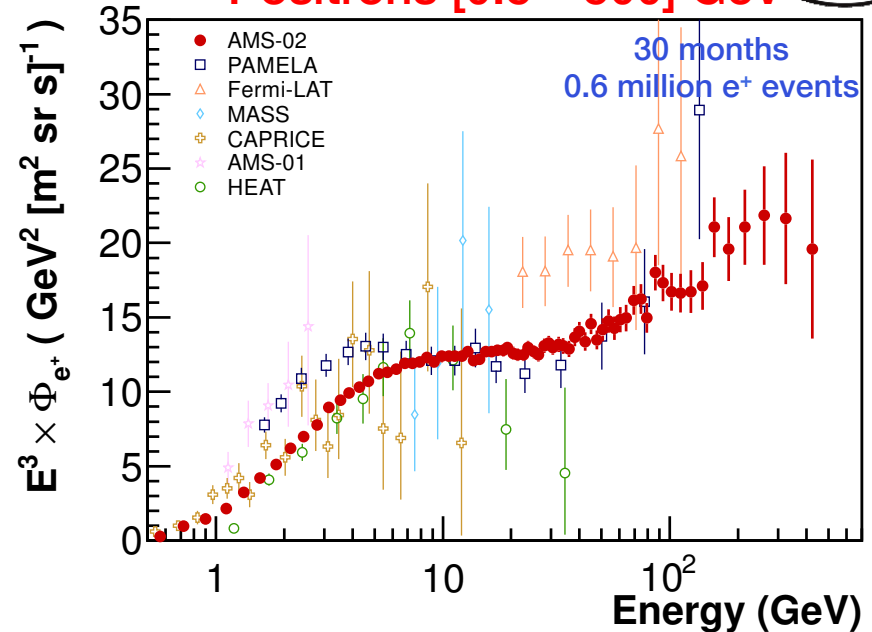


e^+ and e^- Fluxes

Electrons [0.5 – 700] GeV



Positrons [0.5 – 500] GeV



e^+ and e^- flux are significantly different in their magnitude and energy dependence

The positron fraction rise is due to an **excess of positrons**, not due to a unpredicted decrease of electrons.

What is AMS observing?

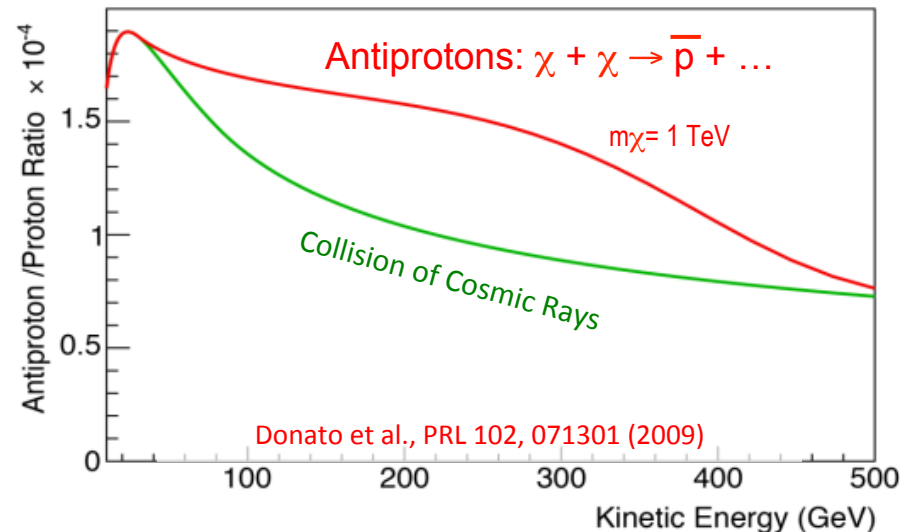
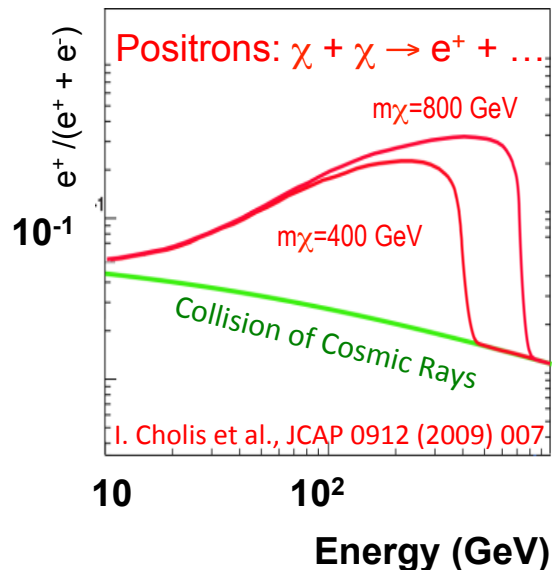
Something “different” with respect to conventional models of e^+ production by collisions of CR hadrons with the interstellar medium (ISM)

Astrophysical Sources?

- Local sources as pulsars ($e^{+/-}$ only source, anisotropy..)
- Additional acceleration mechanisms (reacceleration of CR hadrons in old SNRs)

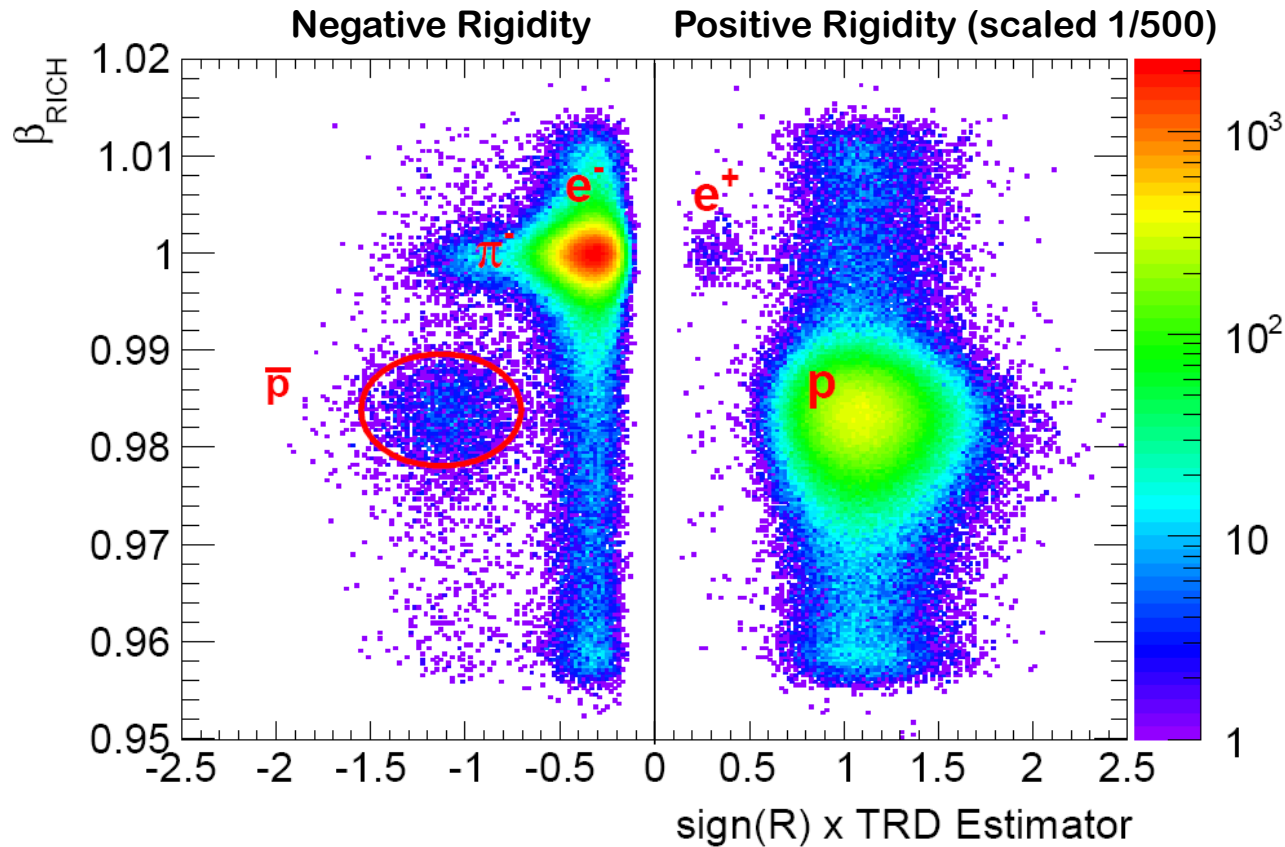
Dark matter?

- Isotropic distribution arrival for $e^{+/-}$
- Signatures in other channels (like antiprotons)



Antiprotons

The low energies: measurement of velocity β is still possible



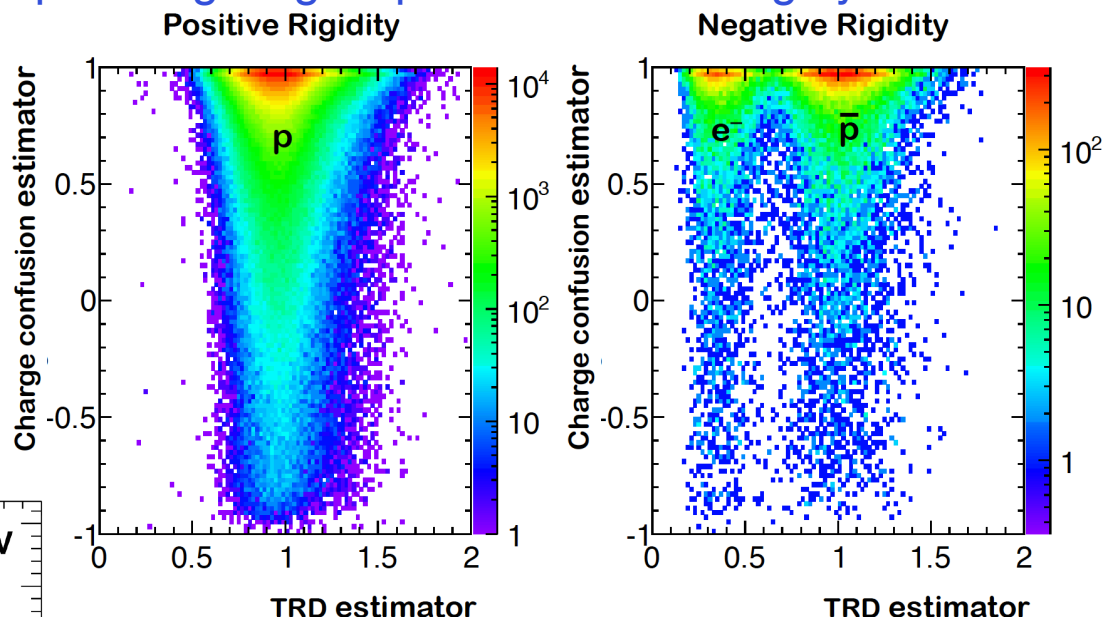
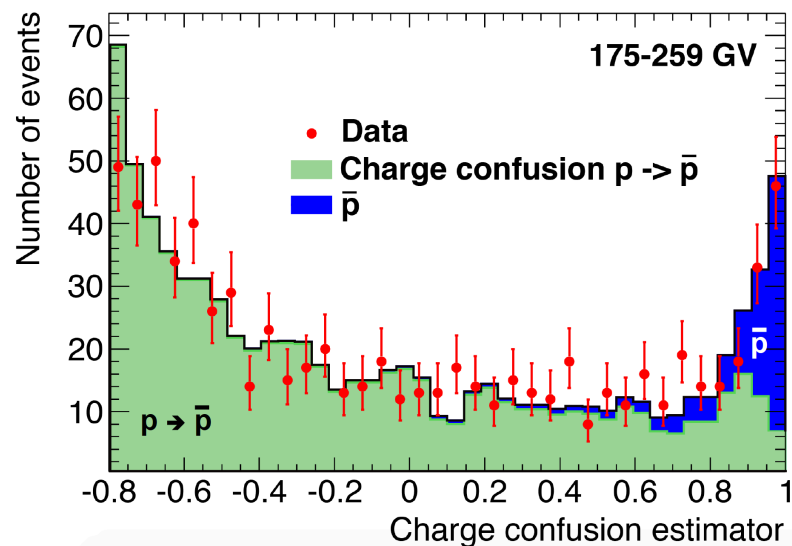
Below 10 GV, the RICH and TRD efficiently separate antiprotons from $e^{+/-}$ and local pions produced by interactions of CRs with the detector material

Antiprotons

The high energies: cannot measure β , analysis based on TRD and tracker

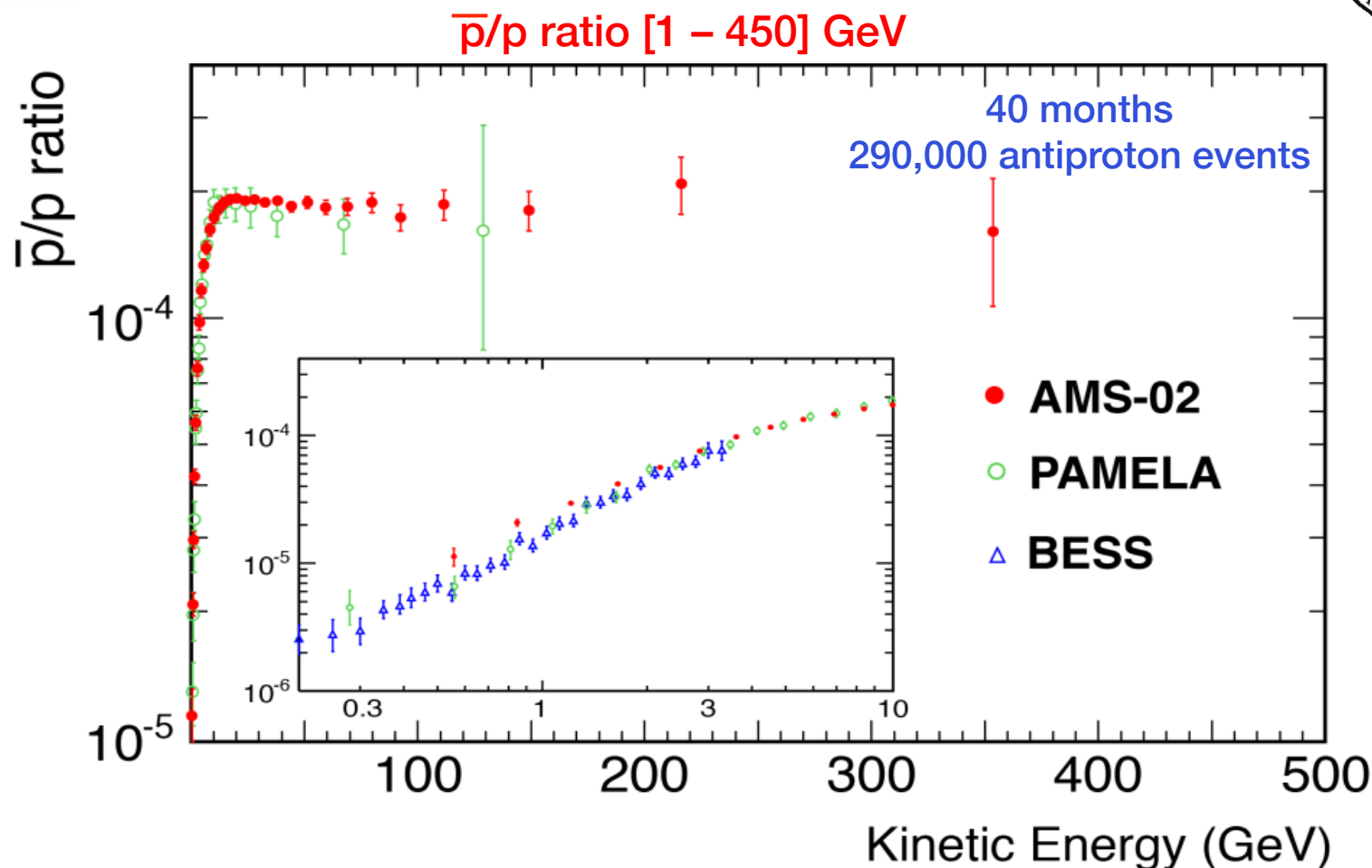
Anti-p are 10^4 less abundant than p. Charge sign flip is the dominating systematic

- TRD discriminates e^- / anti-p
- The negative “anti-p” sample is dominated by charge-flip protons



Reference spectra of charge-flip protons and genuine anti-p have been fit to data to estimate the background in the selected “negative-charge” sample

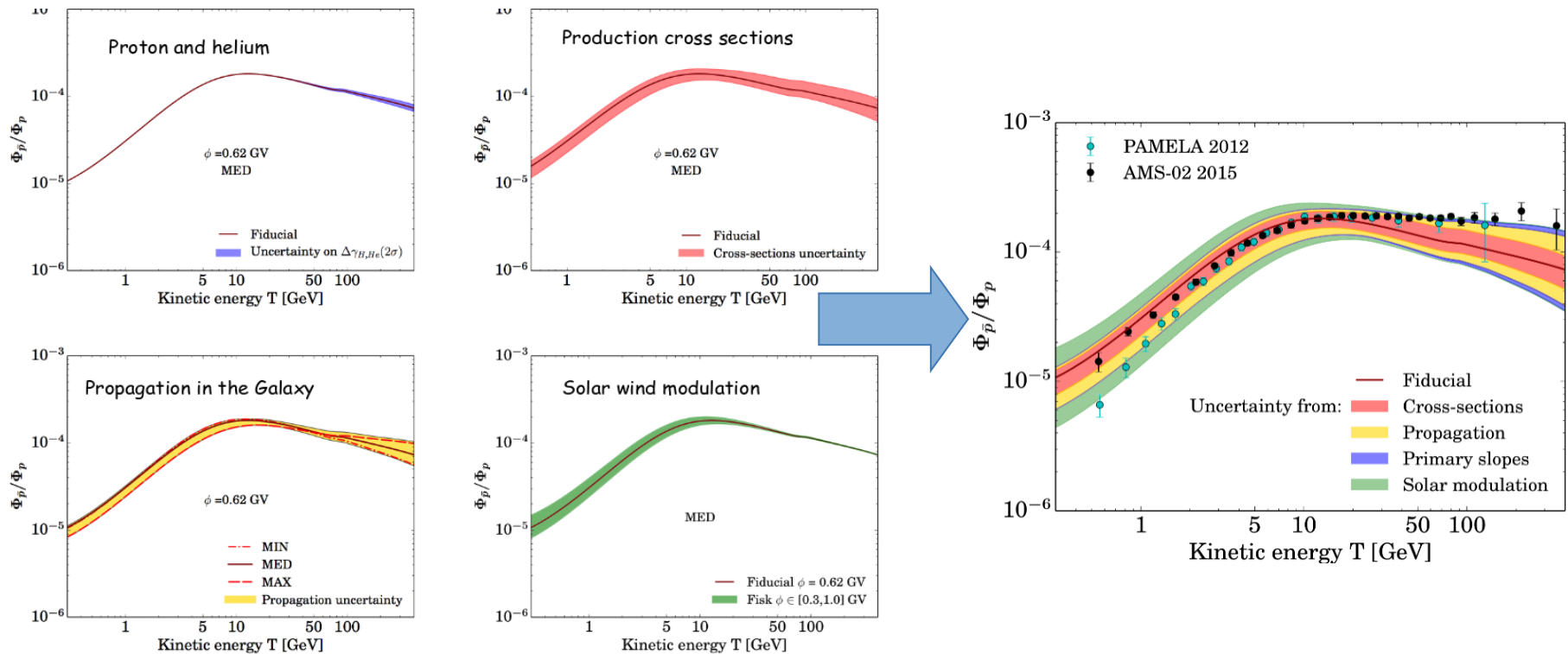
Antiprotons



The antiproton ratio does not decrease at high energies. Could this be a hint of Dark Matter annihilation?

Antiprotons

The accuracy of the AMS measurement challenges the current knowledge of cosmic background



uncertainties from secondary anti-p production cross sections and propagation models are much larger than AMS02 errors in the anti-p ratio measurement

AMS physics results

LEPTONS / ANTIMATTER

- Positrons fraction $e^+/(e^++e^-)$
- Electron and Positron fluxes (e^+ , e^-)
- Electron plus Positron flux (e^++e^-)
- Antiprotons/protons

Sensitive to
Dark Matter signal

HADRONS

- Proton and Helium (p, He)
- Lithium, Beryllium, Boron (Li, Be, B)
- Carbon, Nitrogen, Oxygen (C, N, O)

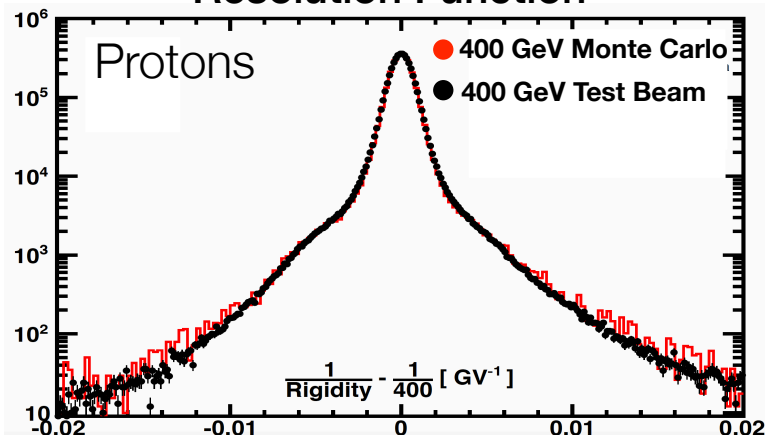
Probes to improve
the astrophysical background
knowledge

AMS-02 is providing precise data to **search for new physics** in the Cosmic Ray channels while **improving the understanding of the astrophysical background** with a coherent set of data

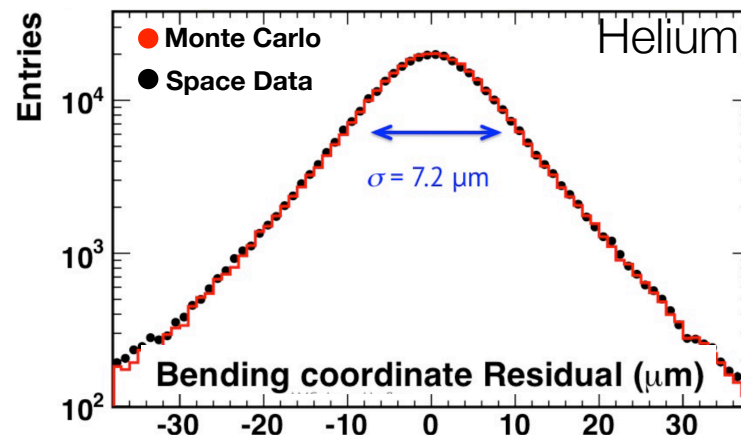
Proton and Helium Fluxes

The AMS-02 Tracker Rigidity resolution has been checked comparing Test Beam data and Monte Carlo Simulations to Space data.

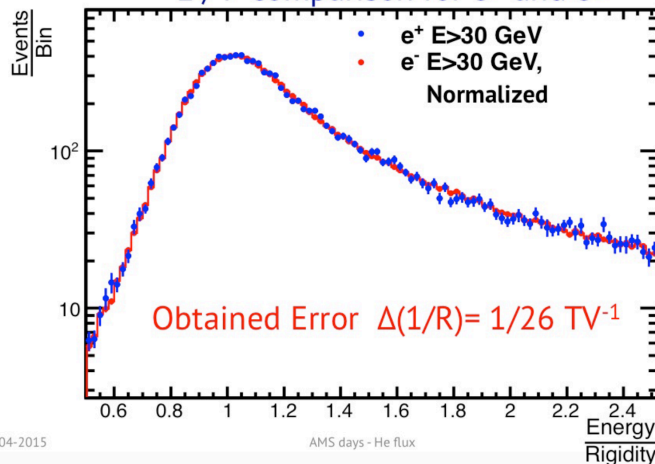
Resolution Function



Coordinate resolution



E / P comparison for e^+ and e^-



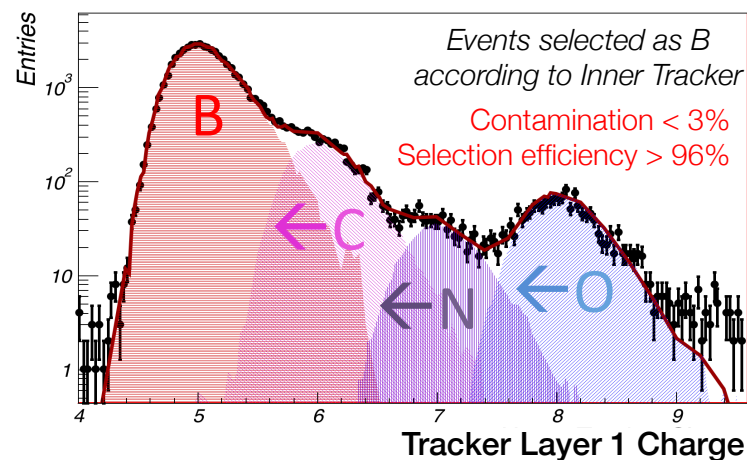
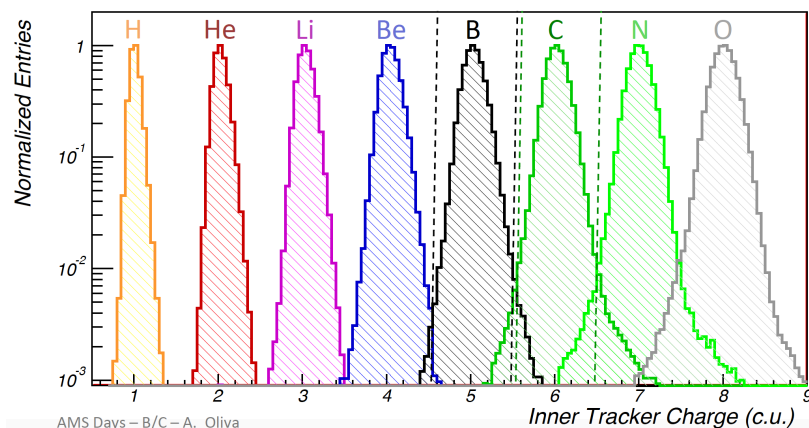
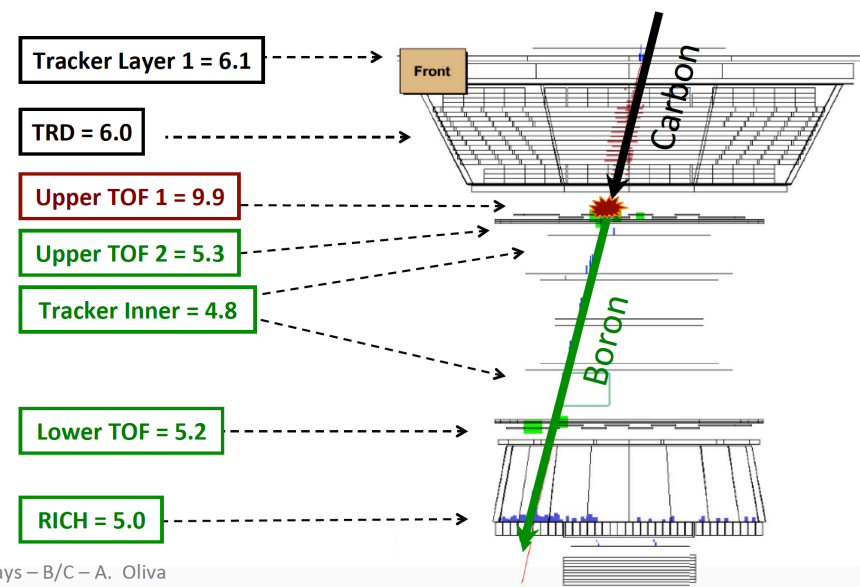
The **redundant measurement** of the e^{\pm} energy with the ECAL is used to further control the Tracker rigidity scale

Identification of nuclei

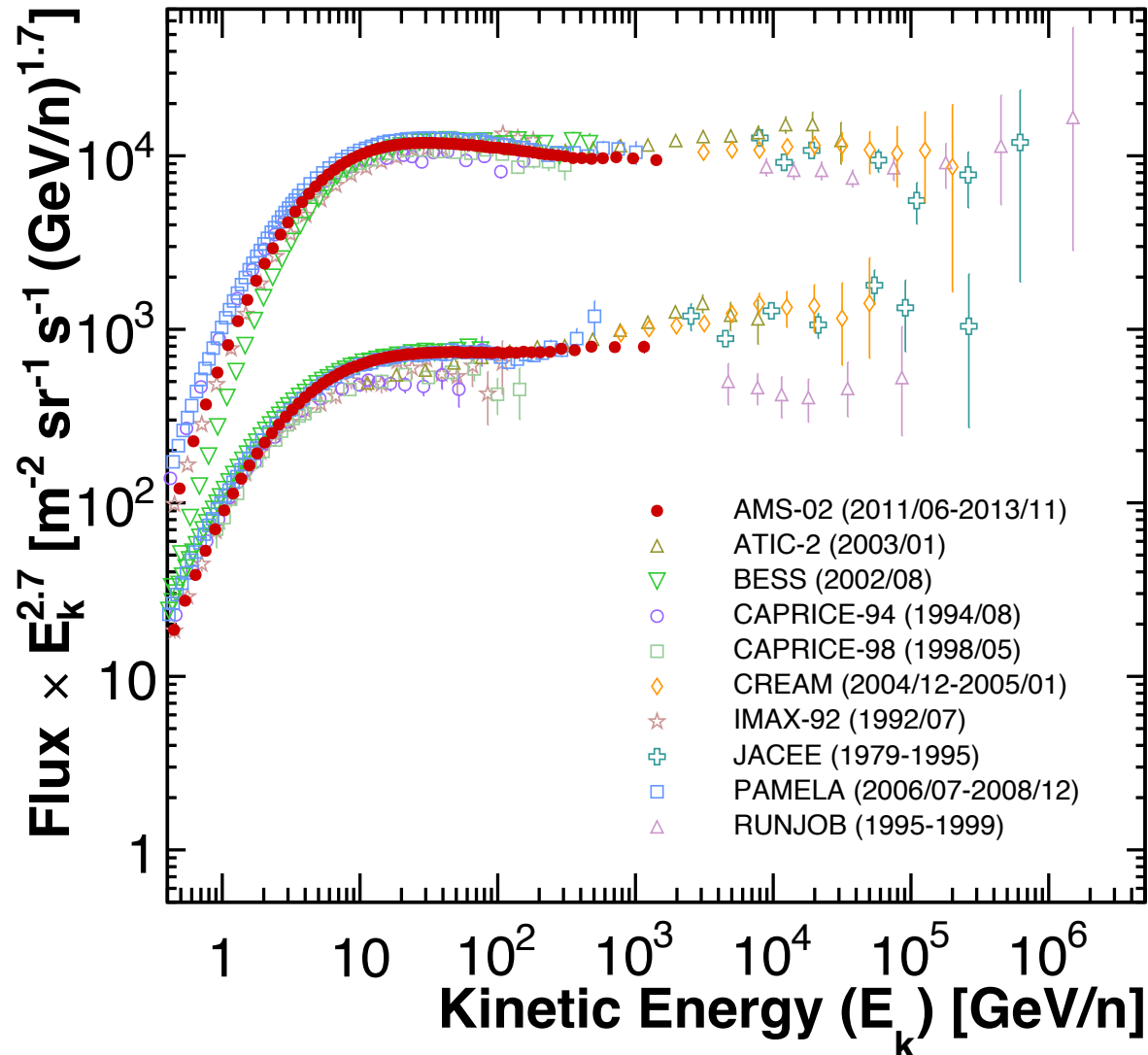
Heavy nuclei can interact with the detector materials and can be mis-identified in the detector

Nuclei identification

1. Inner Tracker Charge selection
2. Tracker Layer 1 Charge used to estimate fragmentation

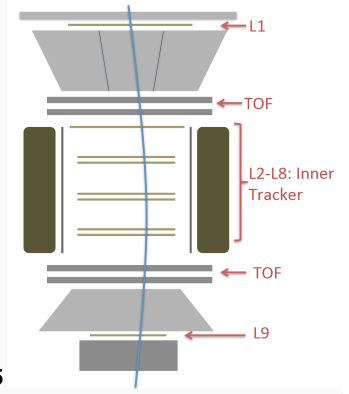
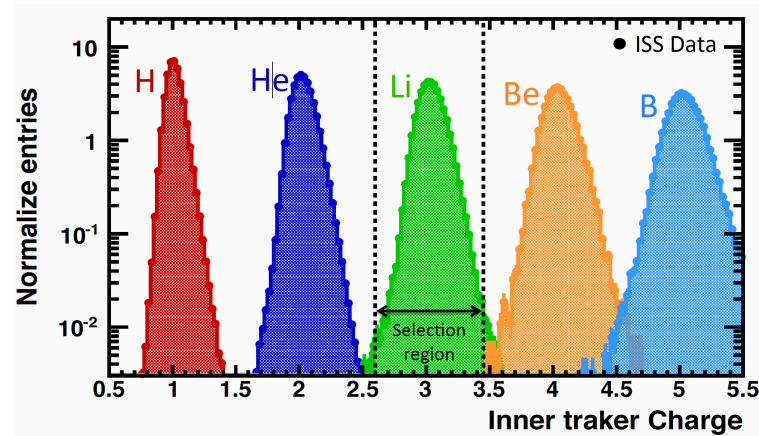
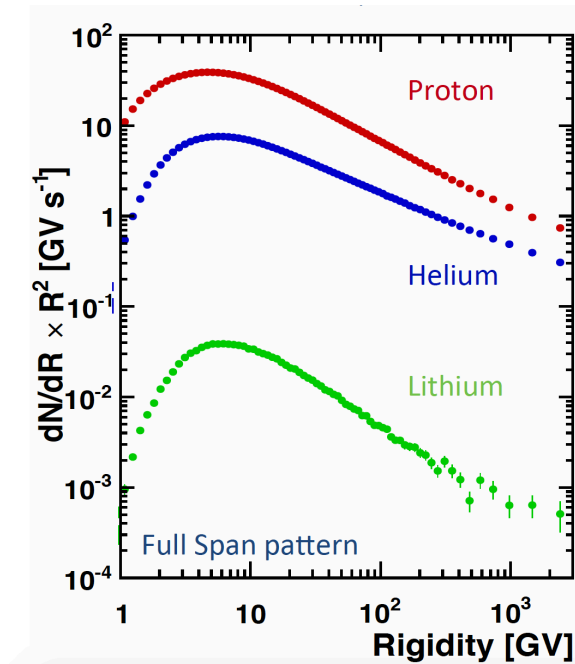


Proton and Helium Fluxes

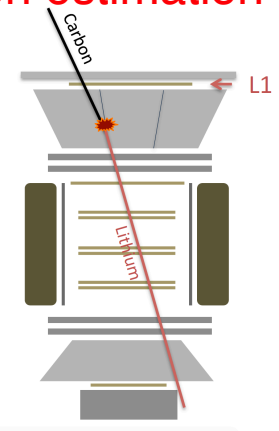
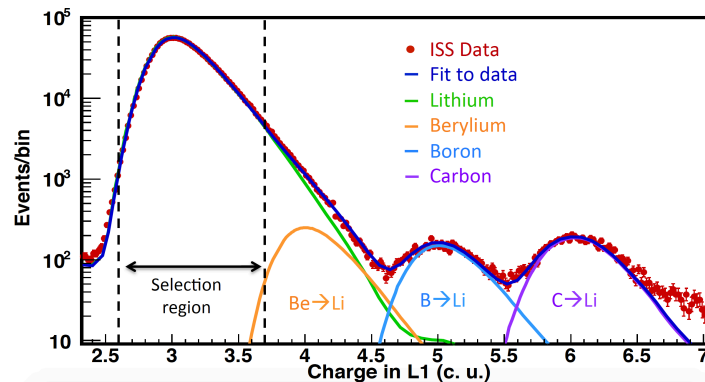


Lithium

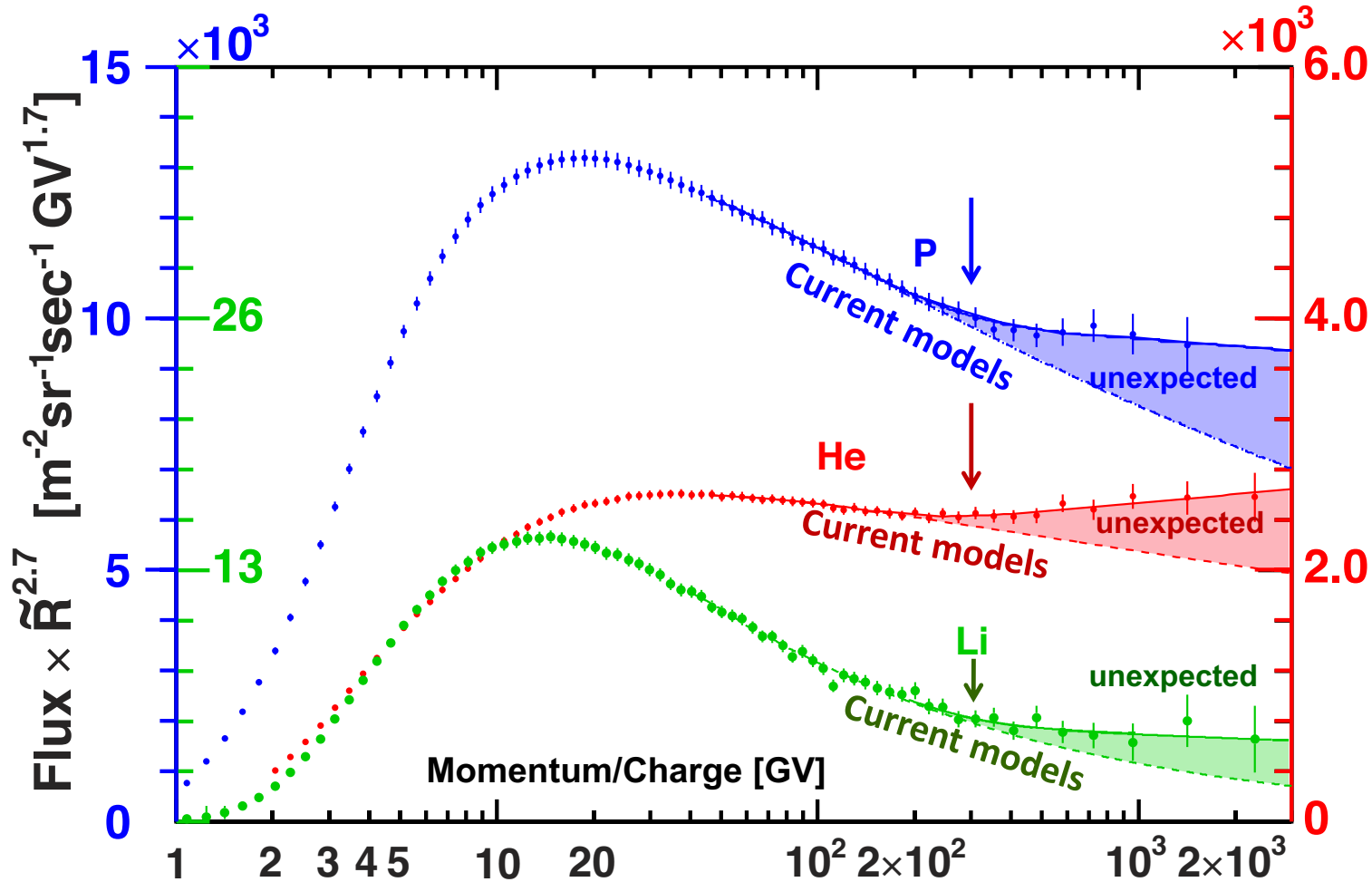
Inner Tracker |Z| selection



Tracker L1 fragmentation estimation



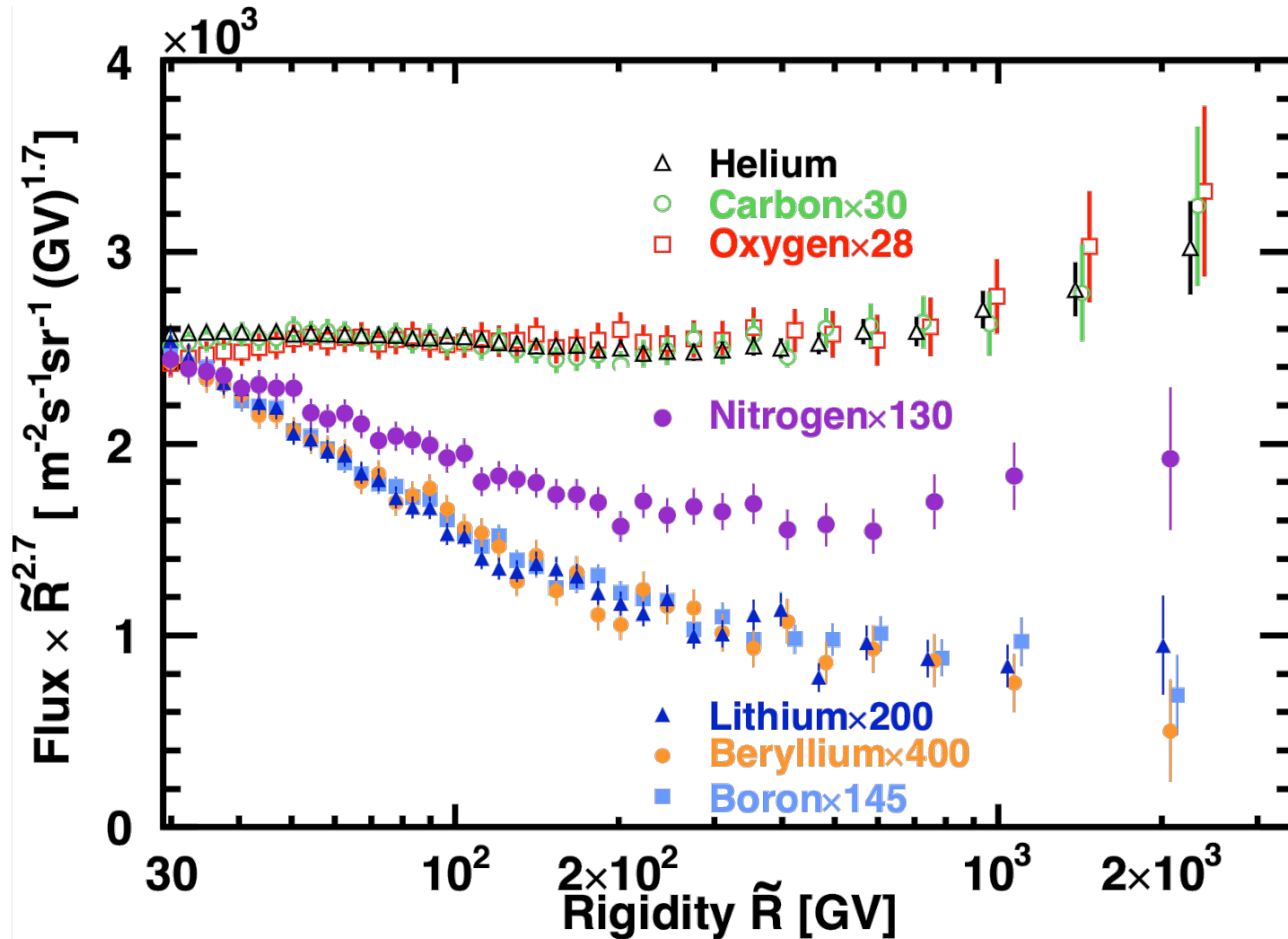
Light Nuclei



Nuclei spectra harden with increasing rigidity

Both fluxes cannot be described by single power laws (traditional assumption).
A break in the power law at $R \sim 300$ GV is required to describe the data.

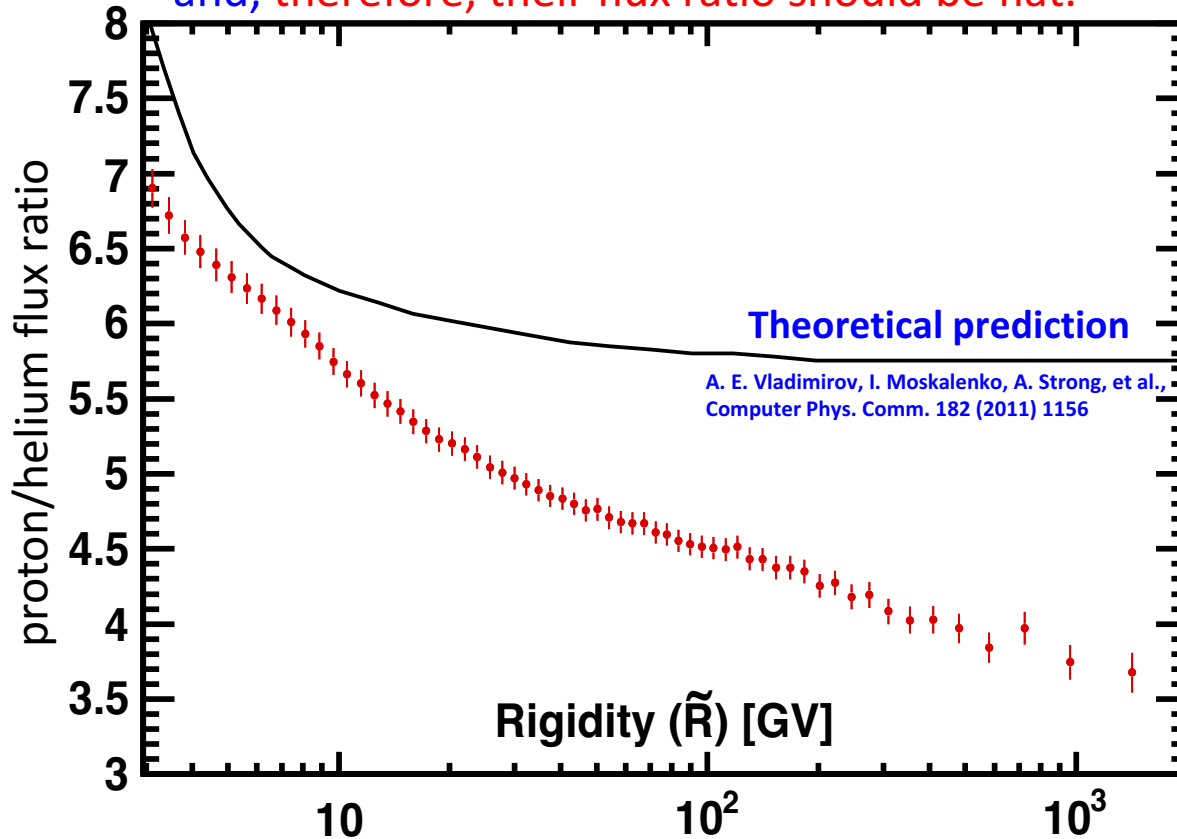
Proton and Helium Fluxes



Primary and secondary cosmic rays have characteristically different rigidity dependencies

Proton and Helium Fluxes

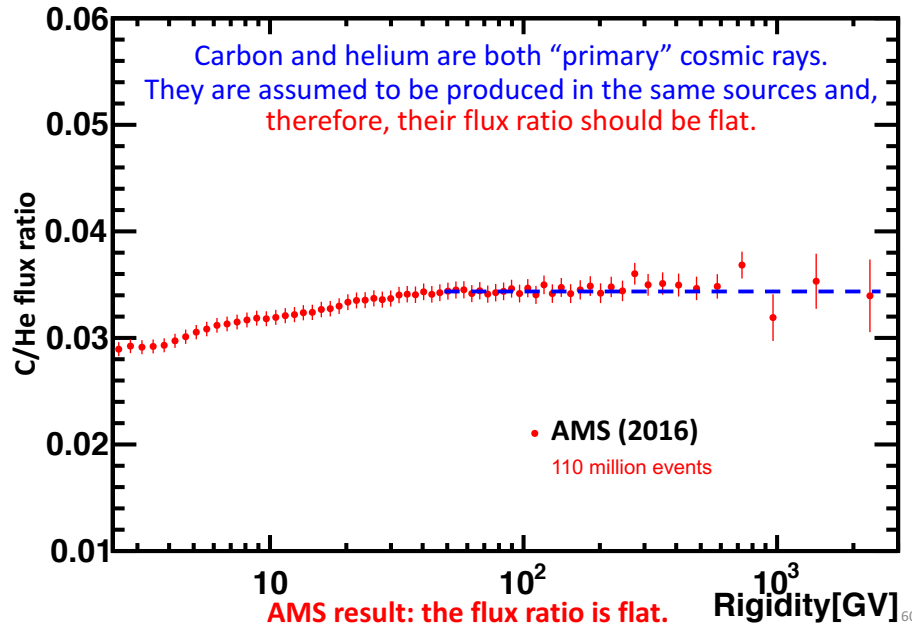
Protons and helium are both “primary” cosmic rays. Traditionally, they are assumed to be produced in the same sources and, therefore, their flux ratio should be flat.



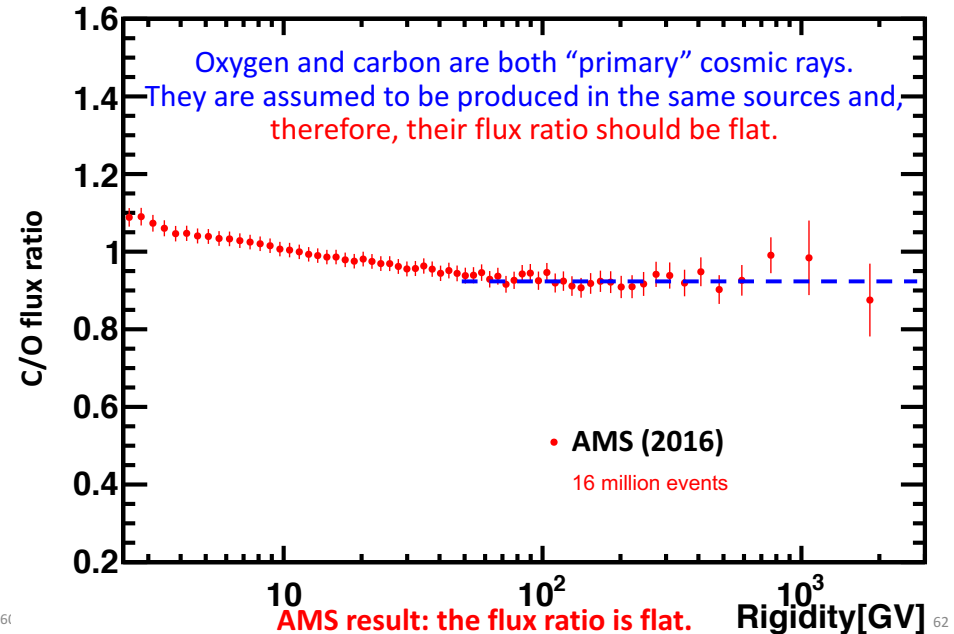
The H/He spectrum shows an unexpected energy dependence. This may hint to unpredicted phenomena in the primary CR propagation or acceleration

Heavier Nuclei

Carbon / Helium

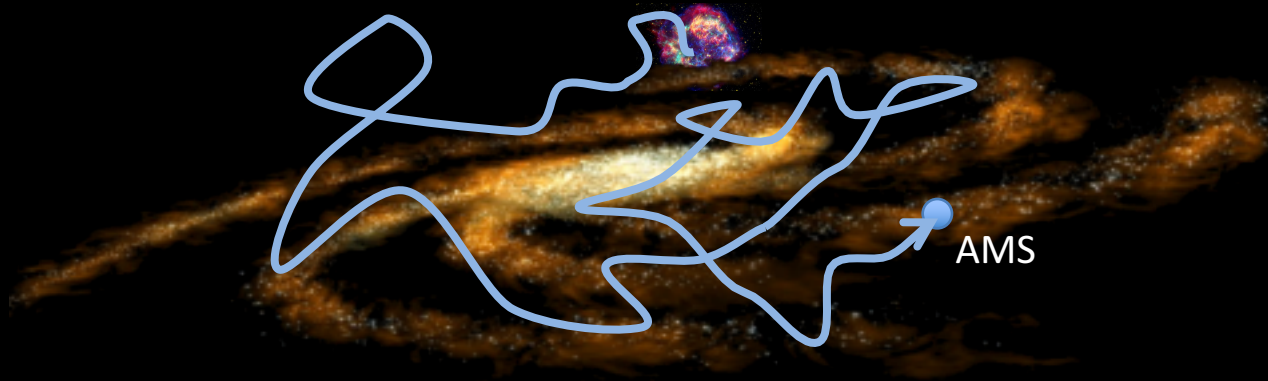


Carbon / Oxygen



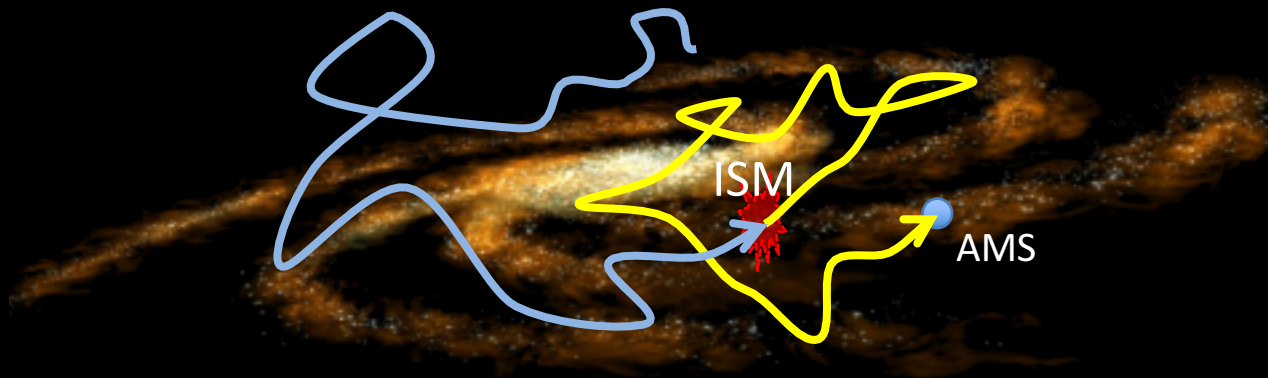
Current acceleration and propagation model well explain the relative rigidity spectra of primary cosmic rays for CNO elements and for He, but not for protons

Primary Cosmic Rays (p, He, C, O, ...)



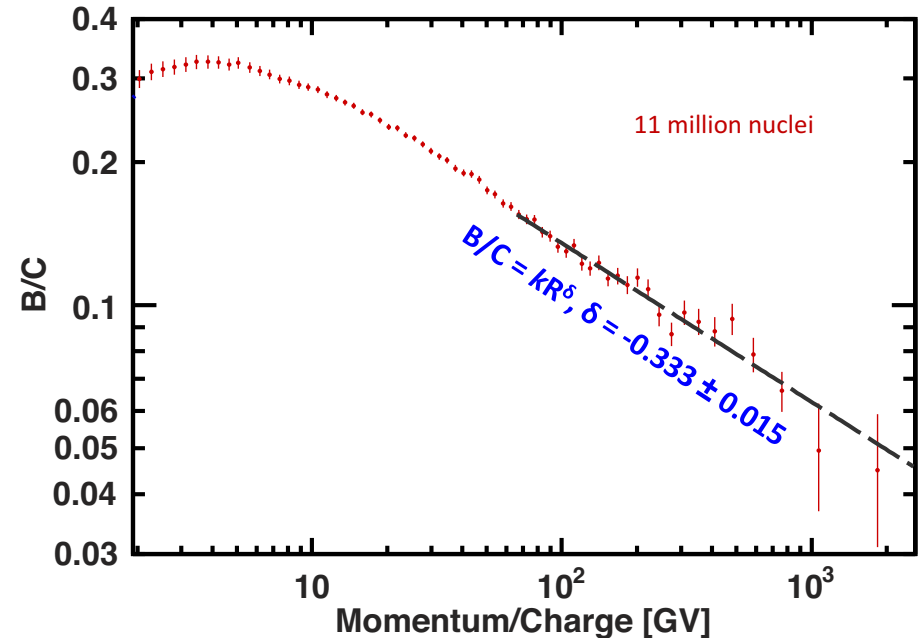
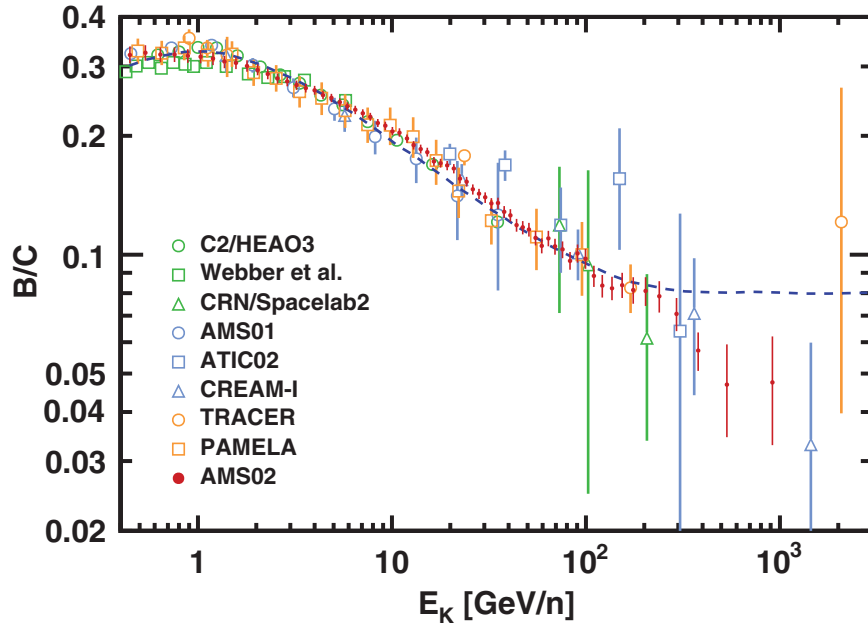
Primary cosmic rays carry information about their original spectra and propagation.

Secondary Cosmic Rays (Li, Be, B, ...)



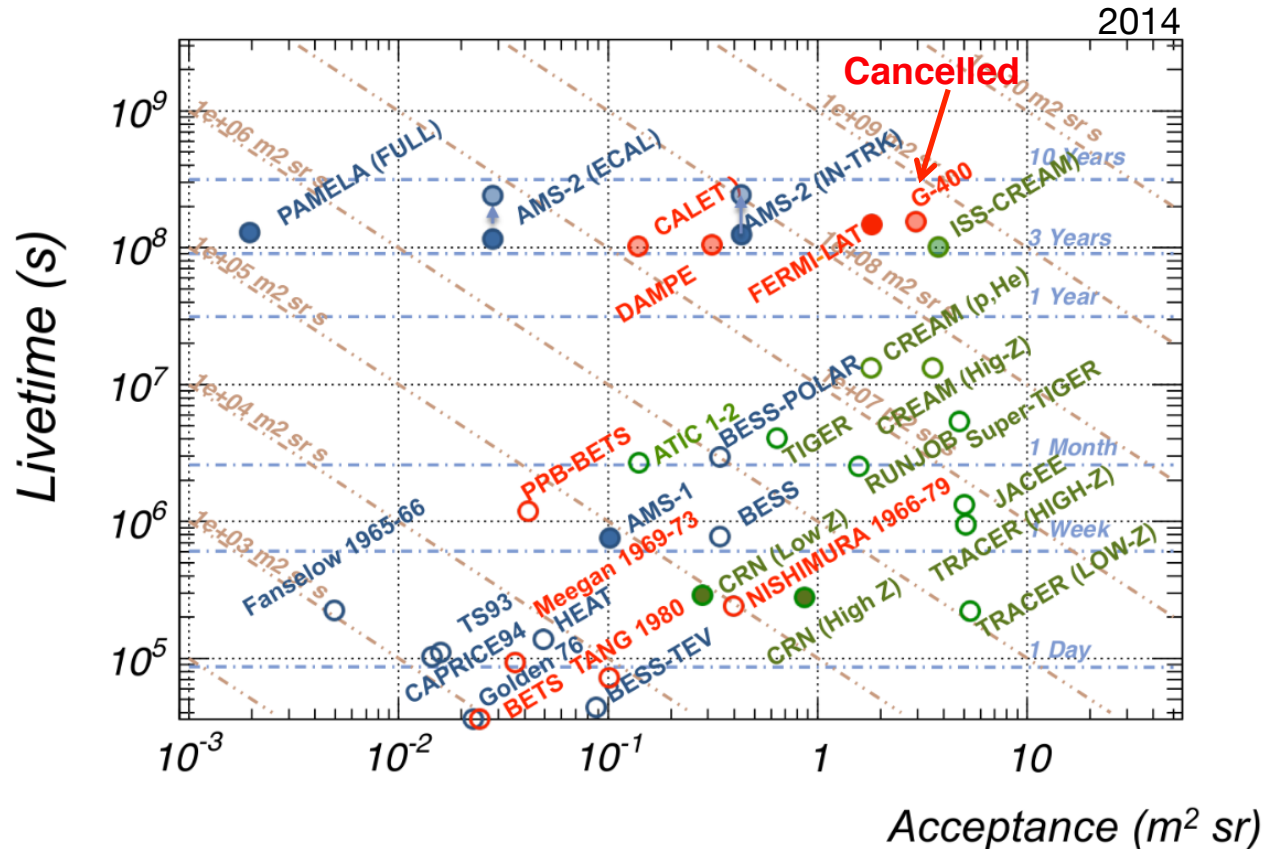
Secondary cosmic rays carry information about propagation of primaries, secondaries and the ISM.

Heavier Nuclei



Secondary/primary ratios are sensitive to propagation mechanisms.
AMS results are in agreement with Kolmogorov turbulence model of magnetized plasma

Future experiments



- No B field, different techniques with main focus on Z
- No B field, different techniques with main focus on e, γ
- Magnetic spectrometers

- Balloon
- Space
- ◐ Space (planned)

AMS-02 will be the unique magnetic spectrometer in space able to distinguish matter from antimatter for the next 10 years.



AMS is a unique, large acceptance, multipurpose magnetic spectrometer on the International Space Station.

There is no other magnetic spectrometer in space in the foreseeable decades.

The results from AMS to date are unexpected and contradict traditional understanding of cosmic rays.

We need to work closely with the theoretical community to develop a comprehensive model to explain all of our observations.

AMS will stay on ISS for the lifetime of the Station. By then (2024) we should be able to determine the origin of many of these unexpected phenomena.

Magnetic Spectrometers (the future?)

Basic Requirements to **extend anti-particle measurements** of at least one decade in energy

- **Acceptance** $O(m^2sr)$
- **MDR** x 20: either longer L or higher B
- **e/p separation**: independent Rigidity/Energy measurement
- **Z**: multiple charge measurement.....

Magnetic Spectrometers (the future?)

Basic Requirements to **extend anti-particle measurements** of at least one decade in energy

- **Acceptance** $O(m^2sr)$
- **MDR** x 20: either longer L or higher B
- **e/p separation**: independent Rigidity/Energy measurement
- **Z**: multiple charge measurement.....



Express a wish....

ALADINO will realize it.....

Antimatter Large Acceptance Detector IN Orbit



Proposal to ESA



Call for Science Ideas

Particle astrophysics in space

with an

Antimatter Large Acceptance Detector IN
Orbit (ALADINO)



INFN and/or Universities of
Bari, Bologna, Florence,
Genova, Lecce, Napoli,
Perugia, Trento, Trieste



CEA Saclay, Univ. Grenoble
and IN2P3 LSPC



KIT Karlsruhe



KTH Royal Institute of
Technology



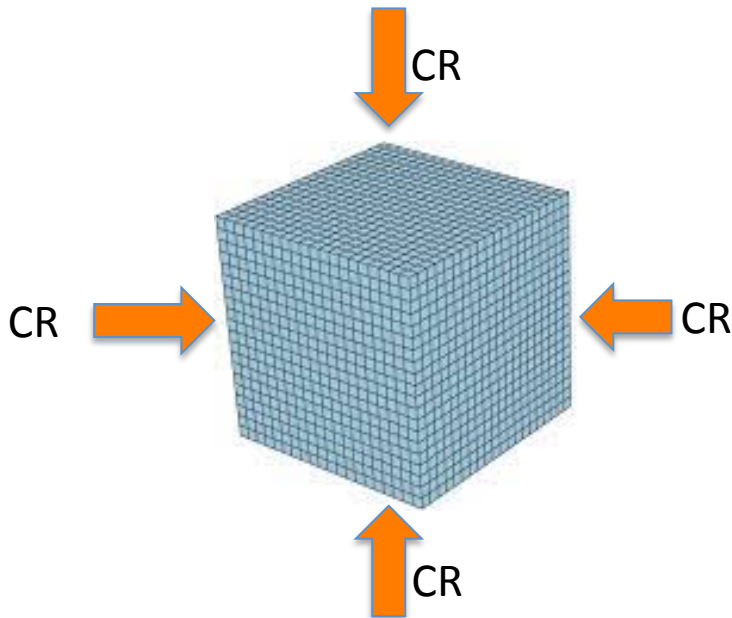
University of Geneva

Concepts

Novel ideas for a next generation cosmic ray experiment in space

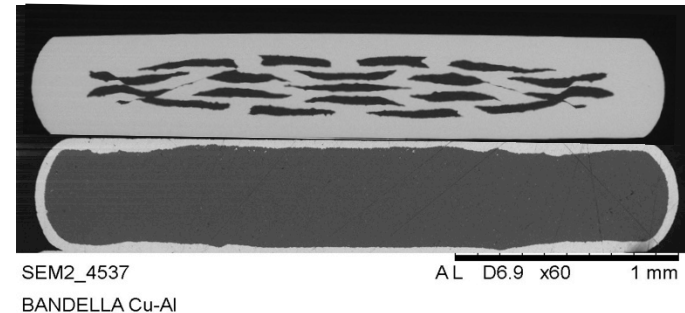
CaloCube (INFN)

- Exploit the CR isotropy to maximize the effective geometrical factor, by using all the surface of the detector (aiming to reach $\Omega = 4\pi$)
- The calorimeter should be highly isotropic and homogeneous



SR2S (INFN and UE)

- R&D of high temperature superconducting magnets (MgB_2) for space applications ($T \approx 10\div 20 \text{ }^\circ\text{K}$)



Materials percentages:

titanium: 40%

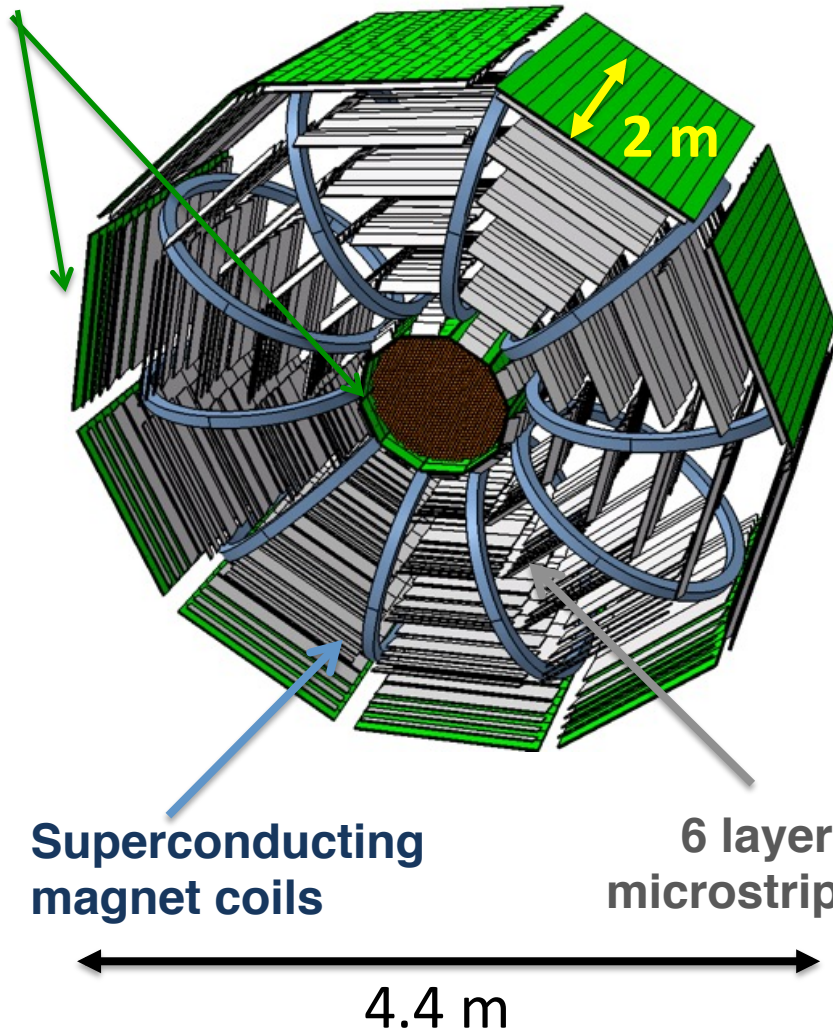
aluminium: 50%

MgB_2 : 10%

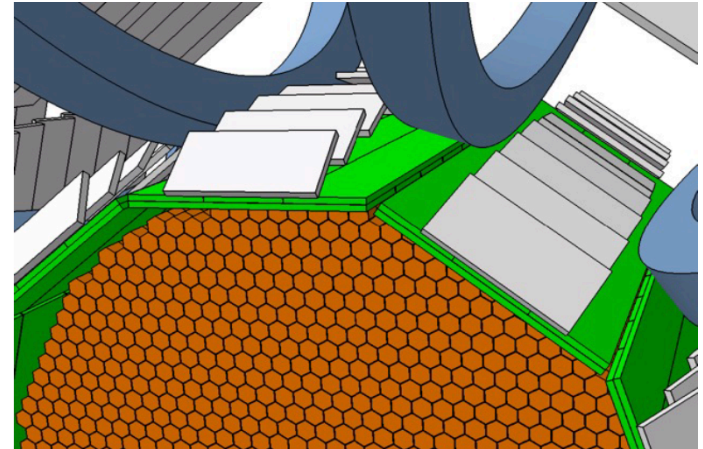
Quite small density: $\approx 3.4 \text{ g/cm}^3$

ALADINO

Time of Flight



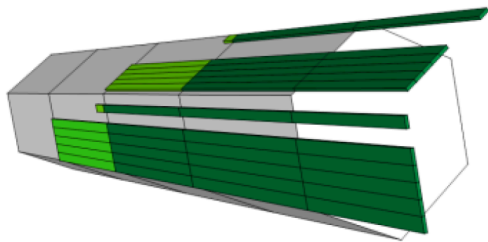
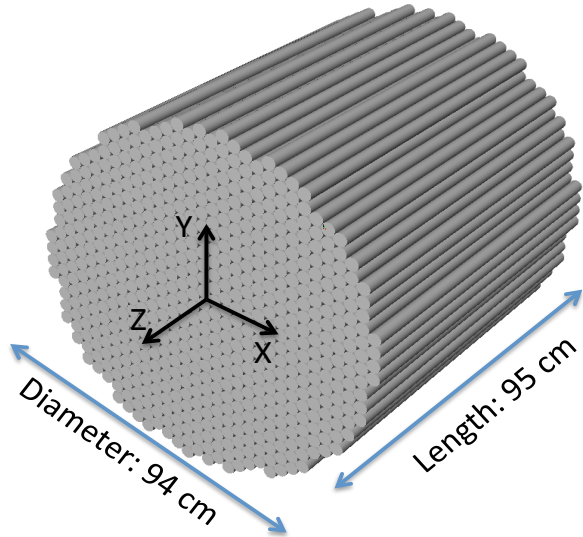
6 layers of double side
microstrip detectors ($\approx 68 \text{ m}^2$)



LYSO calorimeter
 $61 X_0$, $3.5 L_1$

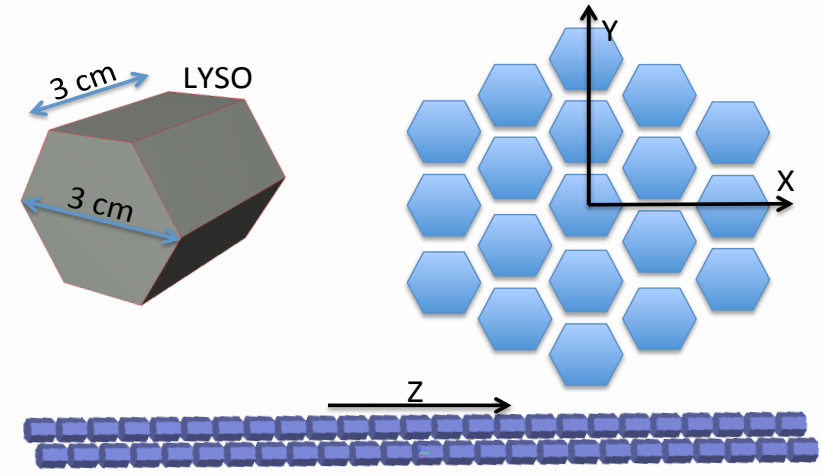
ALADINO: the calorimeter

~15k LYSO crystals on ~700 lines



Dual readout for high dynamic range
with WLS to SiPM/MAPMT

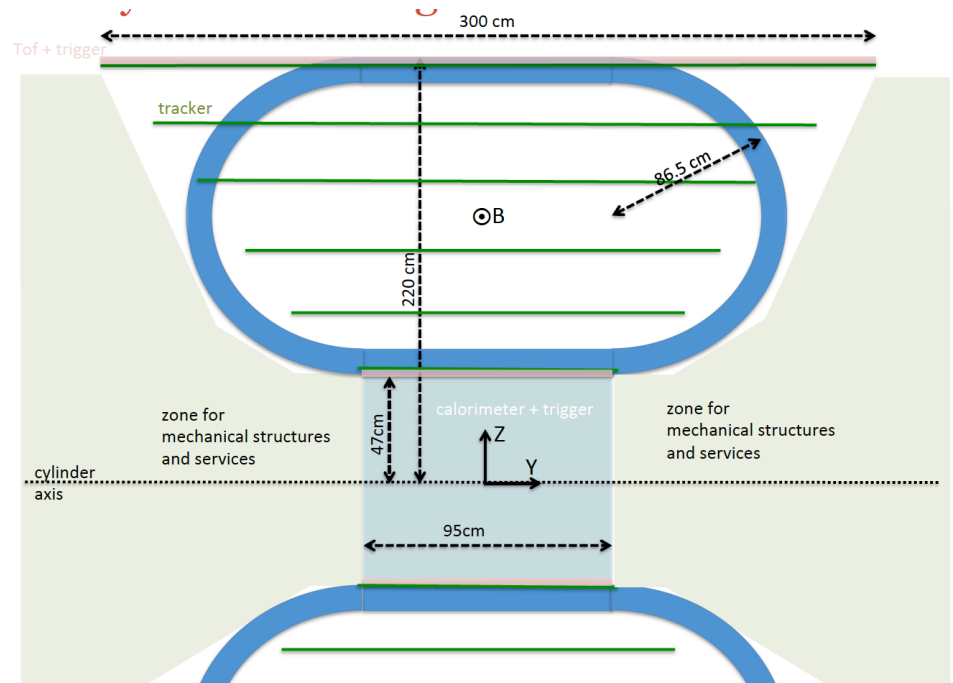
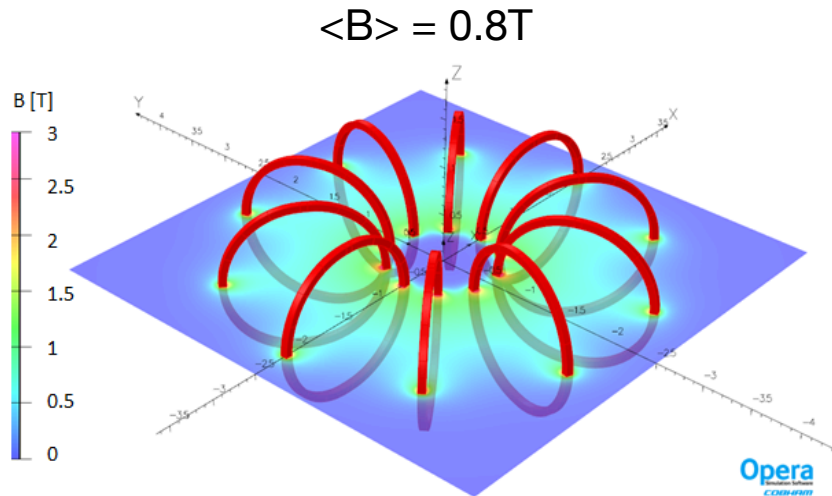
Staggered geometry to minimize deadspace



25 crystals along on line
8mm gap to accommodate mechanics and readout

61 X0, 3.5 λ
E res 2% for e^{\pm}
E res 24% - 35% for hadrons
e/p separation 10^6

ALADINO: the magnet



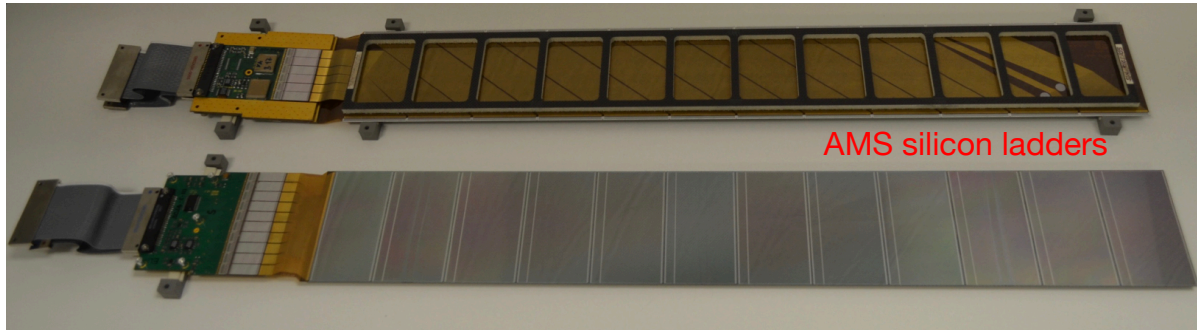
10 coils of MgB_2 in Titanium matrix operated at superconducting regime above 10K

No need of helium cryogenics

Lower quench probability (higher heat capacity)

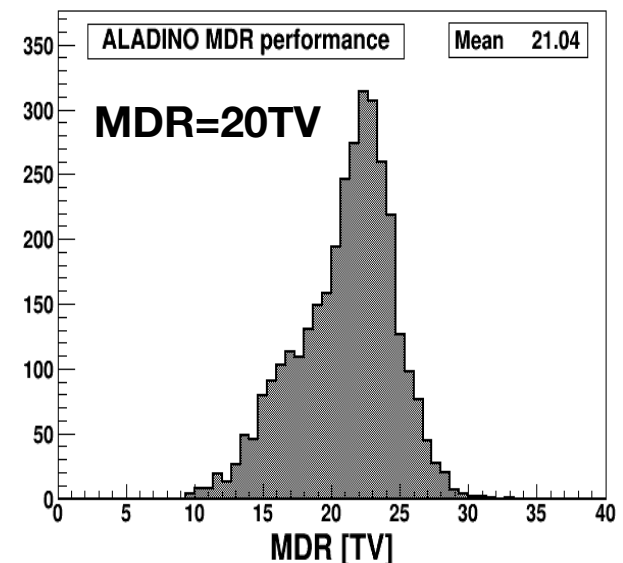
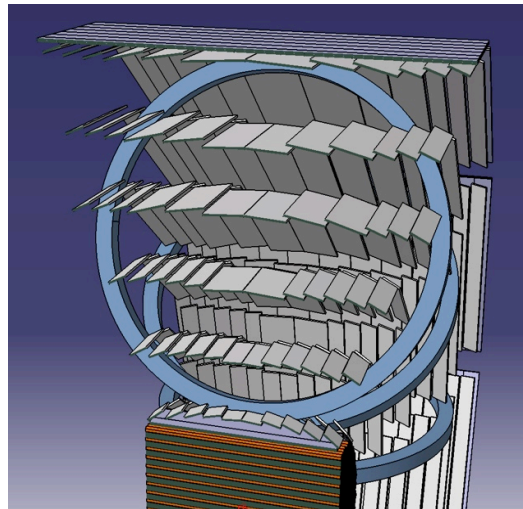
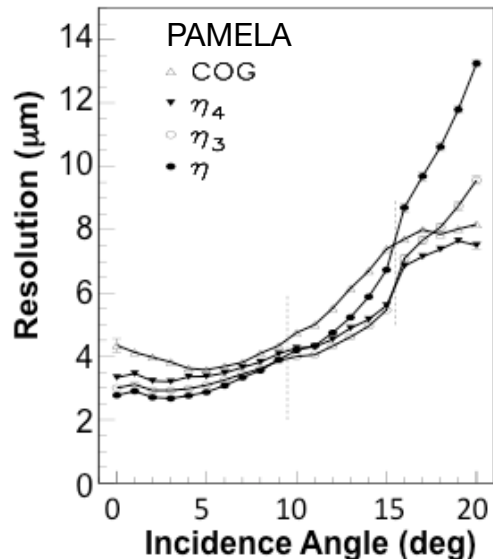
ALADINO: the spectrometer

Tracker based on PAMELA and AMS experience: double sided microstrip detectors



Strip pitch $25\mu\text{m}$,
Readout pitch $100\mu\text{m}$

Target resolution $3\mu\text{m}$
 0.3mW/channel



$95 \times 95 \text{mm}^2$ sensors, **Total active area 68m^2**

ALADINO: the spectrometer

Calorimeter acceptance	$\sim 9 \text{ m}^2 \text{ sr}$
Spectrometer acceptance	$\sim 3 \text{ m}^2 \text{ sr}$
Spectrometer Maximum Detectable Rigidity	$> 20 \text{ TV}$
Calorimeter energy resolution	24% ÷ 35% (for nuclei) 2% (for electrons and positrons)
Calorimeter e/p rejection power	$> 10^5$
Time of Flight measurement resolution	180 ps

Table 1: *main performance parameters of the ALADINO apparatus*

Total power budget: 2.8kW

- tracker: 1kW;
- calo: 200W;
- ToF: 400W;
- cryo: 1kW.

Total mass budget: 6.4 tons

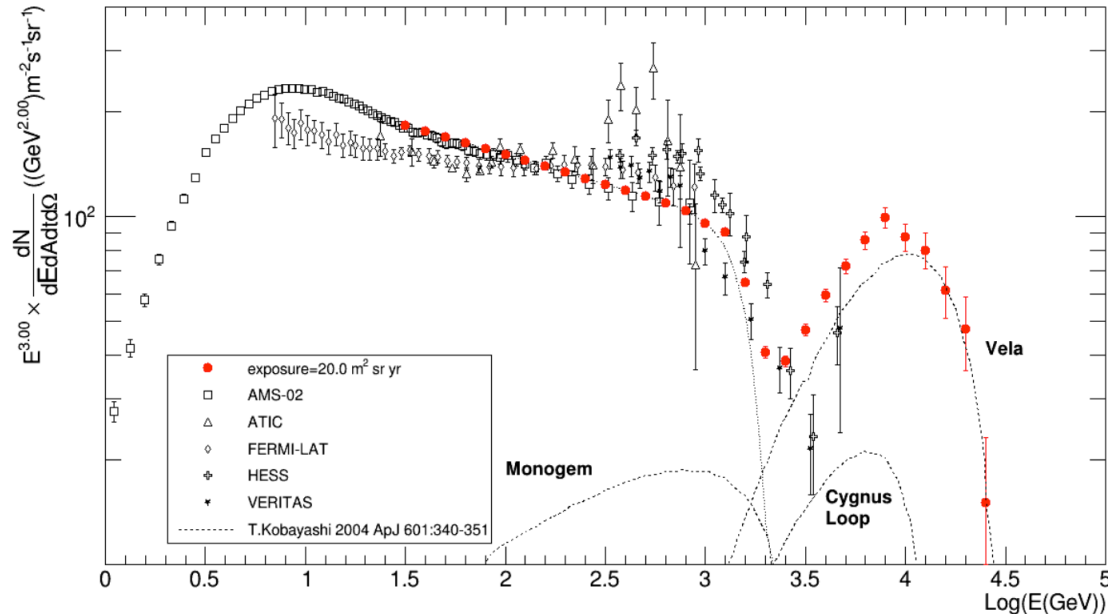
- tracker + tof: 1.5 tons;
- calo: 2.3 tons;
- magnet + cryo: 2 tons;
- power, modules: 0,5 tons.

5 years of operations on high-Earth orbit

Total collection factor $\sim 15\text{-}20 \text{ m}^2 \text{ sr y}$

ALADINO: electrons

Calorimetric measurement of $(e^+ + e^-)$ up to 50 TeV



2% uncertainty at TeV energies

Extends the measurement of current space calorimeters (DAMPE, CALET)

Overlaps with ground based experiments (CTA)

Measurement of separate e^+ and e^- up to 5 TeV (MDR/4)

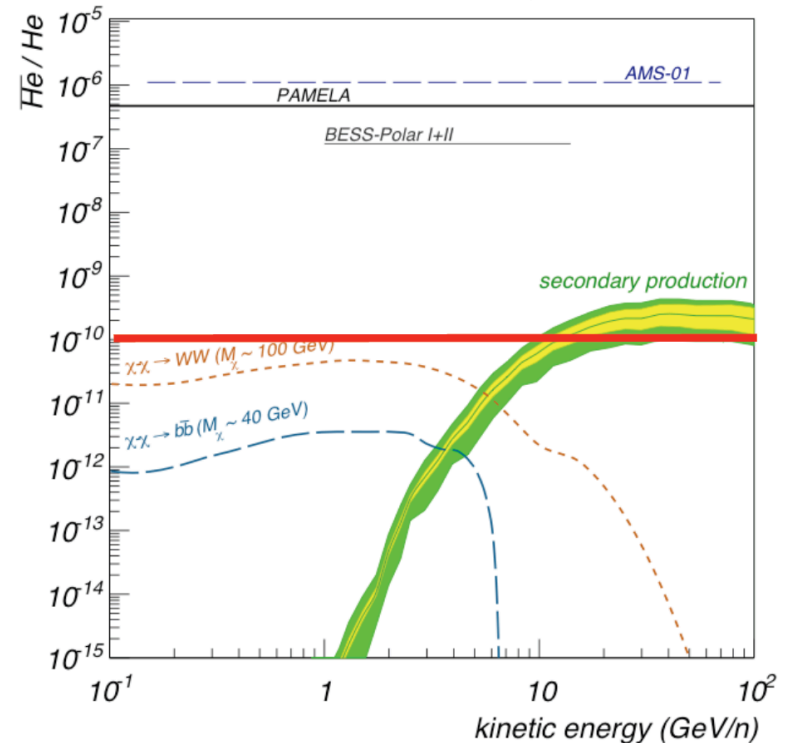
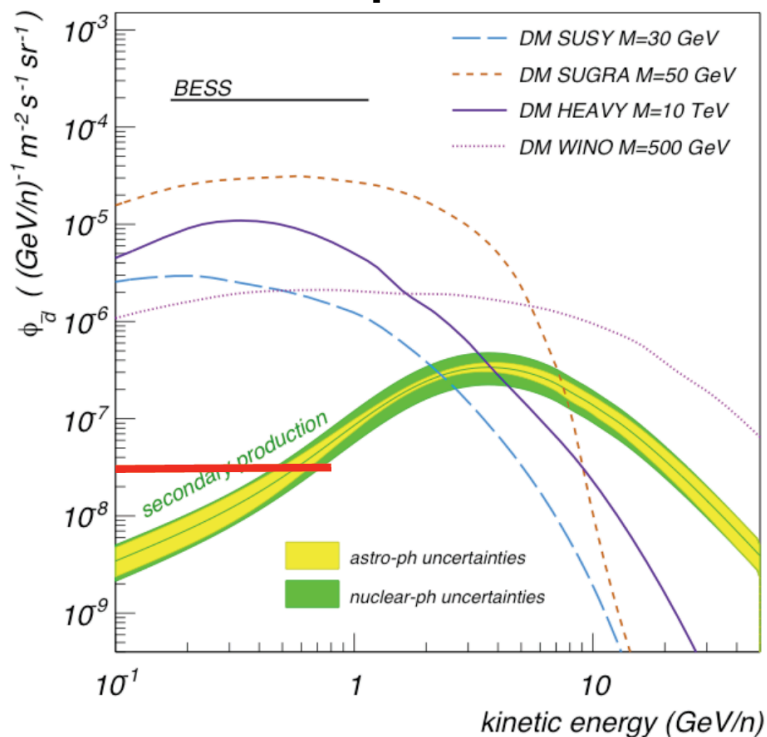
e^+ anisotropy at $O(0.1\%)$ for $E > 100$ GeV

(AMS limit will be 1% at the end of the mission)

ALADINO: antimatter

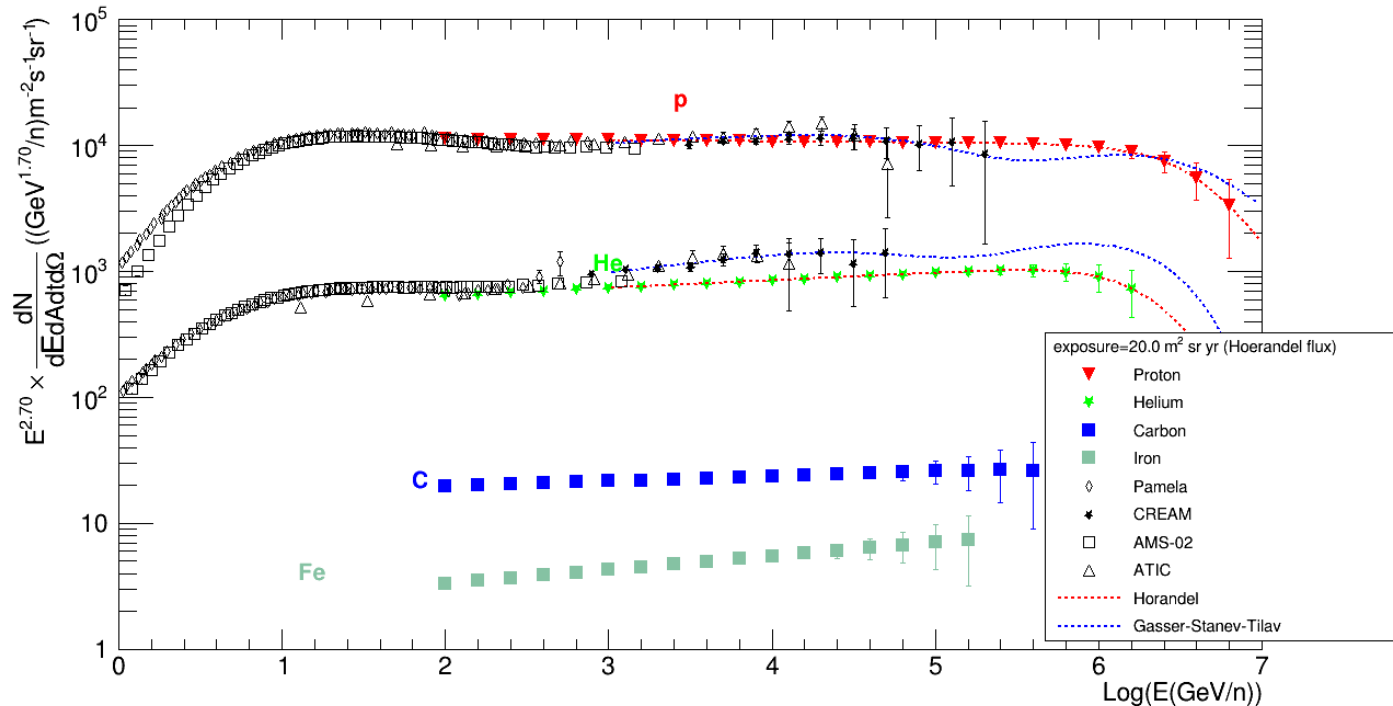
ALADINO will explore the TeV antiproton region
 to test the TeV scale DM annihilation models
 ~2000 really measurable antiprotons above 1 TeV
 ~100 really measurable antiprotons above 4 TeV

ALADINO will improve the current limits for antideuteron and $Z>1$ antinuclei



ALADINO: reaching the knee

Measurement of proton and He flux up to PeV energies



Few hundreds p and He events above 10^{15} eV

Overlaps with balloon and ground based experiments
Will resolve the CR composition below the knee

ALADINO

TIMESCALES:

- i. Preliminary Design Report: 1.5 years
- ii. R&D: 5 years
- iii. Construction, Tests and Integration: 6 years

With this giant, but not impossible, system, in 5 years of data taking we can reach:

- The **knee region** for direct CR measurement
- **Few hundreds p and He events above 10^{15} eV**
- The **multi TeV region** for charged antiparticles
- The multi TeV region for electrons and positrons separately

